**AES/RE/13-07** **Sensor based optimisation of eddy current separation in bottom ash recycling**

**13/05/2013** **Anwar Kasiemkhan**

| | | |
|---|---|---|
| Title | : | **Sensor based optimisation of eddy current separation in bottom ash recycling** |
| Author | : | Anwar Kasiemkhan |
| Date | : | May 2013 |
| Graduation committee | : | Resources & Recycling, Civil Engineering<br>Prof.dr. P.C. Rem<br>Dr.ir M.C.M. Bakker (MSc project supervisor)<br>Resource Engineering, Technical Geosciences<br>Dr. M.W.N. Buxton (MSc graduation supervisor)<br>Inashco B.V.<br>Ir. T. van de Winckel (industry supervisor) |
| TA Report number | : | AES/RE/13-07 |
| Postal Address | : | Section for Resource Engineering<br>Department of Geoscience & Engineering<br>Delft University of Technology<br>P.O. Box 5028<br>The Netherlands |
| Telephone | : | (31) 15 2781328 (secretary) |
| Telefax | : | (31) 15 2781189 |

# ABSTRACT

Non-ferrous (NF) metals in municipal solid waste incineration bottom ash are mostly recovered by an eddy current separator (ECS) to retrieve the positive economic value and to strongly improve the environmental quality of the mineral ash contents before reusing them in road foundations or other applications. The splitter in an ECS is a metal plate that splits the falling product stream of the ECS in a mineral product and a NF metal product. Variations such as moisture content in the feed of the ECS make it necessary to continuously make adjustments to the splitter position in order to achieve the highest possible value recovery. The main research idea in this work is to adjust the splitter continuously by means of a sensor that can count both the metal particles as well as all the particles in the falling materials stream into the metals product. In this work the gain in recovery and retrieved value provided by the sensor was investigated and a preferred strategy is proposed to control the splitter by means of the information generated by the sensor.

Particle trajectory tests were conducted to evaluate the changes in the trajectories due to variations in the bottom ash (BA) feed and to assess the possible consequences of these feed changes for metal recovery. The feed material used in the tests was the 1-6 mm size fraction, since ECS metal recovery from this fine fraction is the biggest challenge. The falling material stream from the ECS was intercepted by a 60 mm deep, flat container that was subdivided into multiple rectangular slots of 10 mm width. The material collected during 3 to 8 seconds of ECS processing was dried, weighted and classified and the NF metal particles in the different size fractions were analysed. Results from the ECS particle tests were used to simulate the system of ECS and sensor to assess how a sensor system would respond to variations in the BA.

Optimal economic value recovery in the metal product is achieved at 29-32% metal product grade, which complies with 6% sensor grade. This sensor grade is measured by the sensor as it samples the falling materials stream through a 30 mm tube at the position of the splitter. A special result is that this optimum holds for both feed with 12% moisture and feed with 14% moisture. The count ratio of metal particles to all particles (z) was z=0.12 for both feed with 12% moisture and feed with 14% moisture content and the average particle mass ratio of non-metal to metal (k) was k=1.3 for feed with 12% moisture and k=1.7 for feed with 14% moisture. A reduction in moisture content of 2% will require an adjustment of 25 mm of the splitter away from the ECS to maintain the optimal economic value of the metal product. Vice versa, a 2% increase in moisture will require an adjustment of 25 mm of the splitter towards the ECS. The sensor grade, metal product grade and the count ratio all showed a monotonically increasing behaviour with increasing splitter distance, giving the ideal conditions for reliable automated control of the splitter by a the desired value-optimizing criteria.

Simulations of ECS behaviour for different splitter positions showed that the sensor can add value to the metal product when compared to a human operator, who would adjust the splitter perhaps a few times per day, which is the common practice in industry. This conclusion holds for both feed with 12% and 14% moisture content, but the gain increases when the feed material becomes wetter. Moreover, control of the splitter as based on the sensor readings shows that the theoretical optimal value recovery in the metal product can be realized using the sensor.

# ACKNOWLEDGMENTS

This graduation thesis is the last part of my study at the Delft University of Technology. During my graduation I have enjoyed the kind help of many people for which I am grateful.
I would like to thank the following persons:

Thijs van de Winckel from Inashco, for offering me the opportunity to do this project, giving me feedback on a weekly basis and for being such an active mentor,

Maarten Bakker, for providing me with valuable feedback on writing, doing research and also for the fact that I could always knock on his door to ask questions,

Peter Rem, who taught me valuable lessons on data analysis and modelling during the many sessions I had with him,

Kees Hoek for the excellent work he did on manufacturing the container with slots,

Abdur Rahman for his time and explanation about the functionality of the sensor,

Ron Penners for his support and help during the laboratory experiments,

Finally, Peter Berkhout for his help in the lab, feedback and allowing me to use his card for coffee.

# TABLE OF CONTENTS

# 1. INTRODUCTION

The final goal of this work was to determine a strategy for automated control of the splitter in order to optimise the value recovery of the metal product from the eddy current separator (ECS). However the implementation of a sensor system that can set and control the splitter requires research about the ECS performance and behaviour under different BA conditions. Moreover, it should be founds out how the sensor should react to changing conditions to effectuate the optimum value recovery. The focus of this project therefore was to determine the trajectories of the non-ferrous metals, typically found in BA by doing experiments on an operating plant with a method that was first developed in the laboratory. This introduction will first describe the problem and the aim and objectives of the project.

## 1.1 Background and problem statement

### 1.1.1 Background

In the Netherlands household waste is collected, transported to a municipal solid waste incinerator (MSWI) and incinerated *(see Figure 2).* One of the incineration residues is bottom ash (BA), which is a heterogeneous particulate material (see Figure 1), consisting of sand, stone, glass, ceramics, metals and a small quantity of unburned material. The bottom ash contains 8-13% ferrous metal and 1.5-2% non-ferrous (NF) metals *(Muchova, 2010).* The metals represent a significant economic value and are therefore recovered for re-use.


**Figure 1: A raw bottom ash heap.**

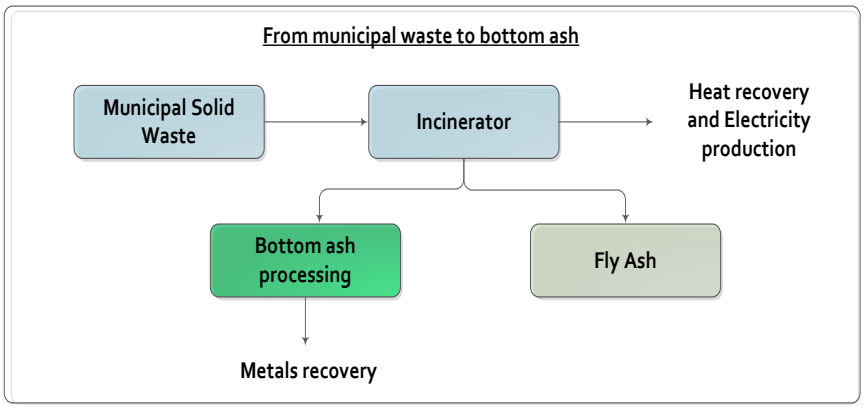


**Figure 2: From household waste to metals.**

The ferrous metal is separated by using magnetic separators. Magnetic separators are mounted with strong a magnet that attracts the ferrous metal. The NF metals are separated by using eddy current separators. In Figure 3 such an eddy current separators (ECS) is shown schematically. This machine is able to push the NF metals further away as result of a fast spinning rotor mounted with magnets. The non-metals in the case of BA called minerals falls naturally from the belt as can be seen in Figure 3. The exact separation principle is explained in *(Chapter 2.2).*The falling (product) stream from the ECS is split by a metal plate, called splitter, in a mineral product and a NF metal product. The position of this splitter influences the separation of the ECS. If the splitter is positioned too far to the right (away from the belt) then part of the NF metal particles will end in front of the splitter in the mineral product. And if the splitter is placed too close to the belt then part of minerals will end in the metal product resulting in a lower grade (metal content).

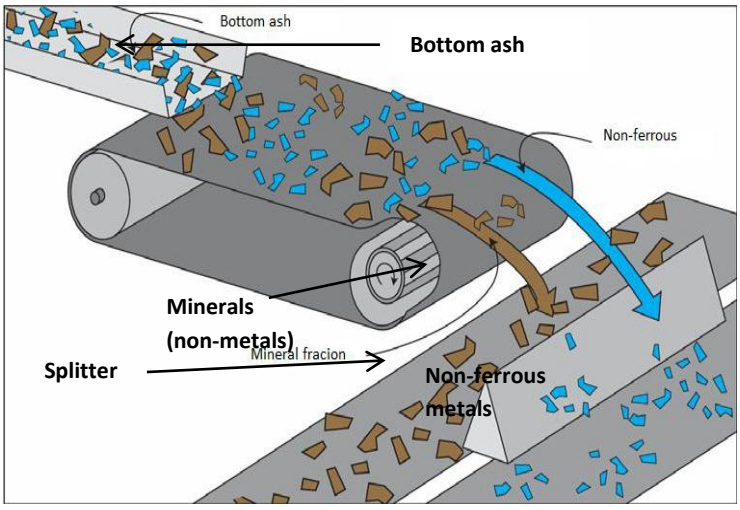


**Figure 3: Schematic diagram ECS**

### 1.1.2 Problem statement

Variations in BA composition, such as different moisture contents, influence the behaviour of the ECS as changes occur in the particle trajectories of the material (*See Figure 4).* These variations of the BA (moisture, metals content) and the feed rate during the 12 hours operation per day, require a regular adjustment of the splitter for the optimum position of the splitter to achieve the highest value recovery, which is a function of both the metals grade and the metals recovery in the metals product. In present day operations the splitter is adjusted every now and then by an operator, who estimates the best position from experience and just visual inspection. However, human observation can be flawed and lead to a poor separation performance. An alternative is to take samples regularly and analysing them in a laboratory, but this is too time-consuming and costly for large-scale operations as explained in the paper of *(Berkhout et al., 2010)*. Moreover, few processing sites are equipped with a laboratory, which makes the option even less feasible.

A much better way of controlling the splitter would be by means of a sensor, which objective is in determining optimum splitter position, not limited by human observation and error, and which can adjust the splitter continuously. However before implementing a sensor system that can adjust the splitter position continuously research about the ECS performance and behaviour under different BA conditions is required. Moreover, it should be founds out how the sensor should react to changing conditions to effectuate the optimum value recovery.

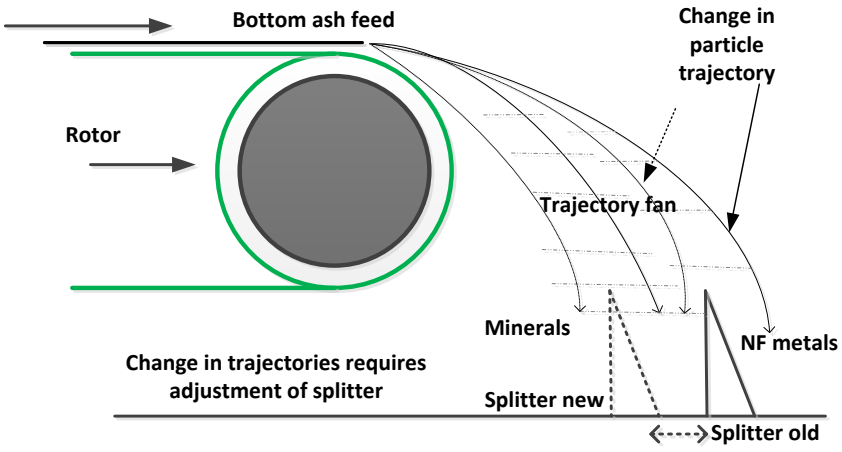


**Figure 4: Illustration of particles trajectories and the results of particle trajectory change.**

## 1.2 Aim and objectives

Online quality inspection of the metals product and control of the splitter distance aided by a sensor was investigated by *(Rahman and Bakker, 2012; 2013).* They introduced a hybrid sensor that can count metal particles and all the particles in a falling particles stream such as BA. This project is a continuation of the work done by Rahman and Bakker.

***The aim of this graduation work is to determine a strategy for sensor based control of the splitter position in real-time by doing in-situ ECS experiments and by simulating fixed and moving splitter positions.***

In order to achieve this aim, first the material distribution discharged from the ECS *(see Figure 4)* was investigated by a method that was developed by doing tests in the laboratory. The main objectives in this work are:

1. Develop a method for the determination of the ECS particle trajectories;
2. Evaluate and interpret the changes in ECS particle trajectories;
3. Assess the possible consequences of feed changes for value recovery;
4. Model and simulate how a sensor system should react to changes in BA feed in order to obtain a maximal value recovery of the metal product.

First the laboratory, ECS tests were done do develop and method that could be used for the collection and analysis of the material discharged from the ECS for the determination of the particle trajectories. Subsequently, in-situ ECS tests were done to obtain data and to create a better understanding of the material behaviour. Finally by modelling and simulating fixed and moving splitter positions at different feed conditions a sensor system that counts particles was evaluated. To obtain sensor parameters for possible control of the splitter position, sensor tests in the laboratory were done as well. The objectives are structured in Figure 5.

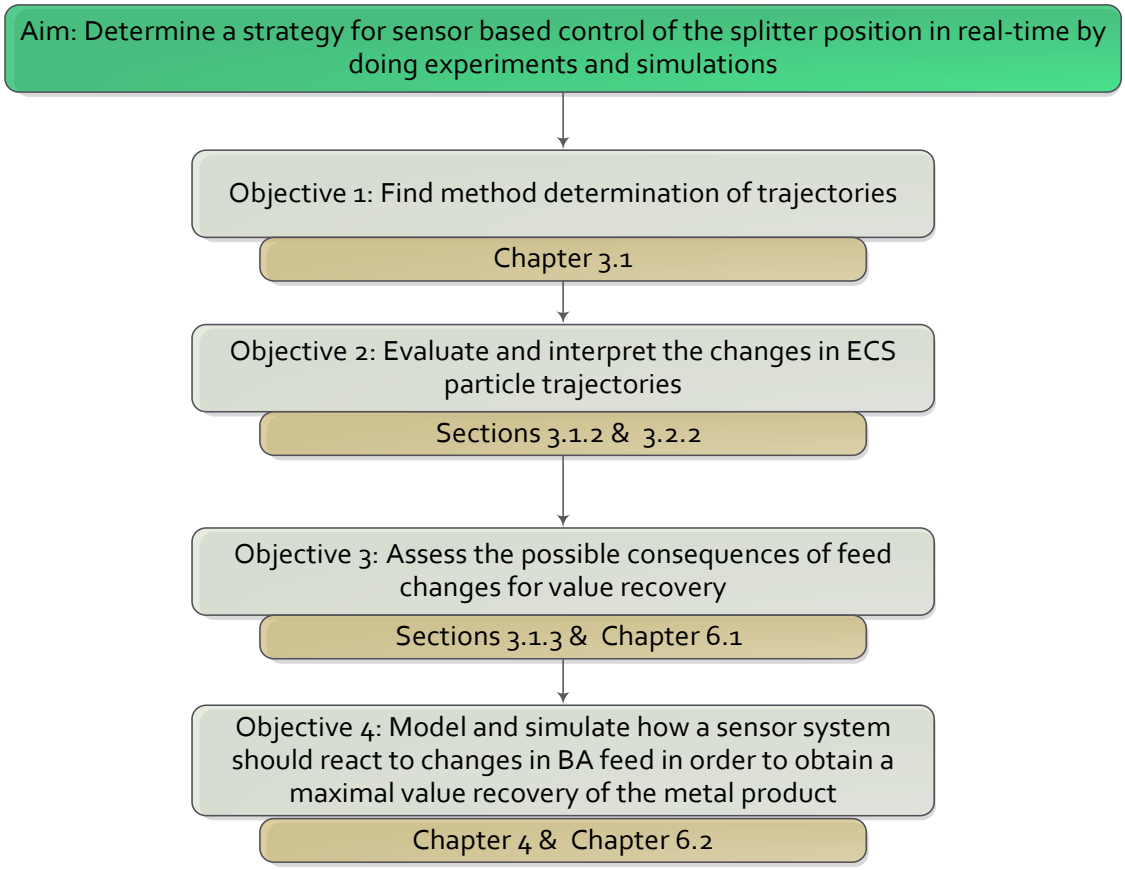


**Figure 5: Aim and objectives.**

## 1.3 Research methodology

In this chapter the methodology used to achieve the final goal will be introduced, more details of the setup and apparatus are explained in *Chapter 3*. First trial particle trajectory tests were conducted in the laboratory of the TU Delft, in order to develop a suitable method for the collection of the particles from a falling stream and to analyse the collected material. The method that was found satisfactory and fulfilled the requirements was a container containing multiple slots, which were filled with water to avoid bouncing of particles. The container with slots was placed in the falling product stream of the ECS to provide a classification according to distance and to determine the particles trajectories, see *Section 3.1* for the details of the setup.

To evaluate the changes in the particle trajectories, in-situ ECS particle trajectory tests were done with the method developed in the laboratory. The weight, size distribution and metal content of the accumulated material in each slot were analysed. The NF metals per sieve size was handpicked and sorted on aluminium, copper, lead and zinc particles after which the number and mass per metal type were recorded. In this way the distribution per metal type as function of the horizontal distance could be determined and by applying curve fitting techniques the particle trajectories of each metal type was modelled. The results from the modelling and the data from the particle trajectory tests in combination with the sensor tests in the lab resulted in how the sensor should react to changes in the BA ECS feed.

## 1.4 Thesis outline

The thesis can be divided into three phases:

| | |
|---|---|
| Phase 1 | Background information |
| Phase 2 | Particle trajectory tests (obtaining data) |
| Phase 3 | Modelling and simulations (analysing data) |

Before starting a new phase an indication with an arrow will be shown on top of the page. In Figure 6 the main topics of these phases are illustrated by a flow chart. Between the brackets the section is given in which the subject is described. The phases can be than subdivided into the following chapters and appendices:

| | |
|---|---|
| Chapter 1 | Introduction |
| Chapter 2 | Theoretical background |
| Chapter 3 | ECS particles trajectory tests |
| Chapter 4 | Particle trajectory modelling |
| Chapter 5 | Hybrid sensor |
| Chapter 6 | Economical optimum splitter position and simulations |
| Chapter 7 | Conclusions |
| Chapter 8 | Recommendations for sensor installation |

| | |
|---|---|
| Appendix A | Eddy current forces |
| Appendix B | Parameters alpha, mean, sigma and free for the metal particle distribution |
| Appendix C | Principle IR and EM sensor |
| Appendix D | Sensor count data |

After the introduction, the necessary background information is given in *Chapter 2*. First bottom ash origin and processing is explained followed by the principle of the eddy current separator and the forces playing a role in the particle trajectories.

In *chapter 3* the method development in the laboratory for the particle trajectory tests is first explained in *Section 3.1*. The results from the in-situ tests are presented in *Section 3.2*. The obtained data from the tests was further used in *Chapter 4* for modelling of the trajectories. In order to simulate the ECS splitter, relations/formulas for the calculation of the material and metal mass as function of the distance was derived in *Chapter 4*.

For the counting of the mineral particles and for the determination of possible parameters for automated control sensor measurements were done. The laboratory sensor experiments and background of the sensor is explained in *Chapter 5*. In *Chapter 6* a fixed and moving splitter was simulated with varying feed conditions. Before the simulations could be done, the optimal splitter position was determined first by using the data obtained during the in-situ tests. The conclusions are presented in bullet point in *Chapter 7*. The recommendations for sensor installations are given in *Chapter 8*.

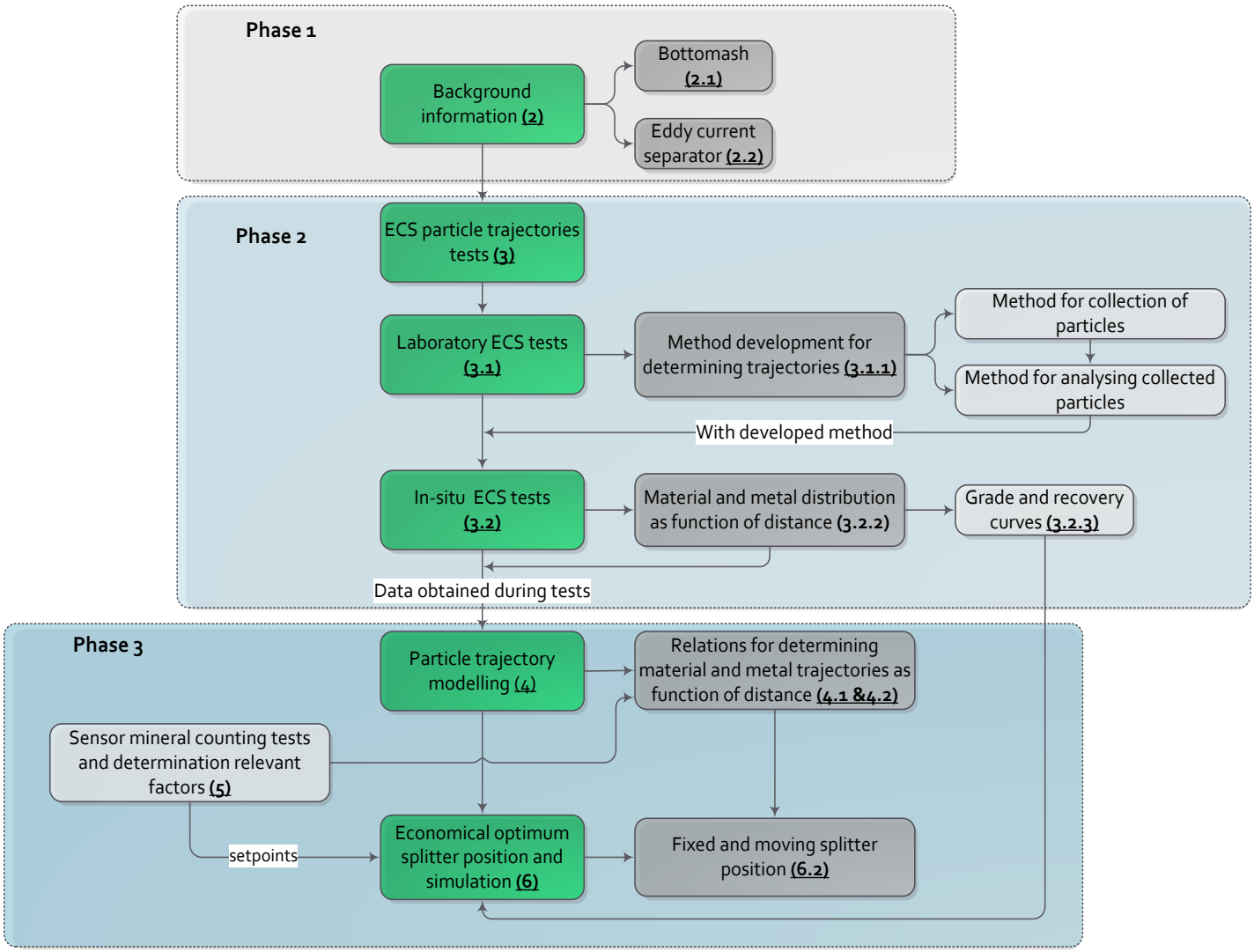


**Figure 6: Flow chart of the main sections in this thesis.**

## 1.5 Research scope and limitations

In this chapter the scope of the research and the limitations will be given by using a table. In the table the subjects that are in scope and out scope are given.

**Table 1: Scope of this work**

| ***Subjects*** | ***Included*** | ***Excluded*** |
|---|---|---|
| *Feed material* | - 1-6 mm BA fraction after removal of fines by ADR[1]<br>- Analysis of feed properties such as moisture content, particle size distribution and metal content | - + 6 mm fraction<br>- Oxidation levels of aluminium particles |
| *ECS particle trajectory tests* | - Size of particle<br>- Non-ferrous metals determination (AL, Cu, Pb, Zn and Brass) | - Other NF metals and alloys such as Sn.<br>- Analysis of glass, BA slag, ceramic and stone particles<br>- Analysis of magnetic material (Ferrous particles.<br>- Orientation of particle on belt<br>- Shape |
| *Sensor measurements* | - Counting of minerals in the lab with material from the in-situ tests | - Metal counts<br>- Signal processing |
| *Modelling and simulation* | - Model for metal mass and particles distribution<br>- Model for the number of mineral particles and mass of material as function of distance | - ECS and ballistic model to calculate the trajectory by analytical formulas<br>- Variable feed grade |

[1] ADR: Advance Dry Recovery a machine that separates the fines(0-2mm) out of BA

# 2 THEORETICAL BACKGROUND

In order to understand and interpret the changes in the ECS particle trajectories, this chapter provides the necessary background information about the properties and composition of bottom ash and the principle behind eddy current separation.

## 2.1 Bottom ash origin, composition and processing

In order to create a better understating of bottom ash this chapter will give the origin, composition and the processing steps before bottom ash is separated by eddy current separators.

### 2.1.1 Origin

Municipal household waste collected by trucks from curb containers or from underground collection bunkers are transported to a municipal waste incinerator where it is incinerated. A residual product of these municipal waste incinerators is bottom ash (BA). The waste is incinerated in order to reduce the volume of the waste. Moreover the heat of incineration is nowadays utilized to produce electricity and/or hot water (70-90˚C) or warm water (30-50˚C) for domestic heating or agricultural purposes such as greenhouse heating. State-of-the-art MSWI plants produce typically between 200 and 350 kg bottom ashes per tonne of input household waste. In the Netherlands around 1.5 million tonnes of bottom ash is produced annually *(Vereniging afvalbedrijven, 2012)*.

### 2.1.2 Composition

BA consists of inert and post-combustion products, such as sand, stone, glass, porcelain and metals. The average composition of BA from the Netherlands is shown in Table 1. Some characteristics of the BA are subject to regulation, such as the total organic content (TOC) that should stay below 5 wt. %.

**Table 1: Composition of BA from Netherlands, Amsterdam *(Muchova, 2010)*.**

| Materials | Mass percentage (%) |
|---|---|
| **Minerals (stone, glass, ceramics, slag)** | ± 80% |
| **Iron scrap (Ferrous metal)** | 8-13% |
| **Non-ferrous metals (Al, Cu, Pb, Zn and brass)** | 2.3% |
| **Precious metals** | 0.001% |
| **Organics (paper, plastics, bones)** | 1-5% |

The materials that are typically found in BA are shown in Figure 7 . In the first three pictures on the left, the minerals are shown and the right three pictures the metals. In this figure however, the metals and alloys such as lead (Pb), zinc (Zn), tin (Sn) and brass are not shown as these metals are not dominantly present in BA.


Figure 7: Examples of materials that are typically found in bottom ash.

### 2.1.3 Aging

After the incineration the raw bottom ash is quenched in water, which is the cause of the water content of BA. The moisture content of the 2-6 mm BA fraction is 12-18% *(Muchova, 2010).* The moisture content varies depending on the season of the year and size fraction. After quenching the bottom ash is stored for aging, typically from a few weeks to a few months. Ageing has a beneficial effect on the quality of BA as it lowers the pH value from pH=10-11 to pH=4-5 due to $CO_2$ absorption, which decreases leaching of metals, while microbial activity (bacteria, fungi) seem to be beneficial for the organic contents of the BA. However, a drawback of ageing is shown by a Dutch BA processing plant, which came to the conclusion that 10 weeks ageing reduced the recoverable content of metallic aluminium by some 6 kg/tonne *(Berkhout et al., 2010)*.

### 2.1.4 Processing

The aim of processing the BA, is to separate the metals. The first step in the processing is to classify the BA in different size fraction to render the following separation processes more effective such as eddy current separation, which performance is limited to size ranges. Ferrous metal may be removed prior to eddy current separation as the ferrous particles can damage the head pulley of the ECS. The ferrous metal is removed by using magnetic separators. Magnetic separators are machines that utilize strong magnets to attracted ferrous metal and separate them. The NF metals are separated by using eddy current separators. In the next chapter the operating principle of the ECS is explained in details.

## 2.2 Eddy current separator (ECS)

The ECS plays a key role in this work since the final goal is to optimize this machine by first investigating the particle trajectories, therefore knowledge about the operating principle of the ECS is essential in order to understand the particle trajectories. This chapter explains how non-metals and metals are separated by the ECS. Moreover the forces that may affect the separation and the thus the particles trajectories are also reviewed.

### 2.2.1 Construction and operating principle of a ECS

Eddy current separators, also known as NF metal separators, are machines which were developed for applications in solid waste recycling processes for the selective separation of NF metals. Some applications are: municipal solid waste, solid waste incinerator ash, shredder residue, electronic scrap and plastic waste. The ECS consists of a conveyor belt, rotor on which the magnets are mounted, head pulley, vibrating feeder and the splitter, these parts are shown in Figure 8. Typical ECS machines settings are 10-12 tonnes per hour feed capacity, 1.5-2 m/s belt speed and the frequency of the rotor is 2000-3000 rpm *(Maraspin et al., 2004).* The rotor of the ECS can spin pro-grade (clockwise) mode or retrograde (counter clockwise).

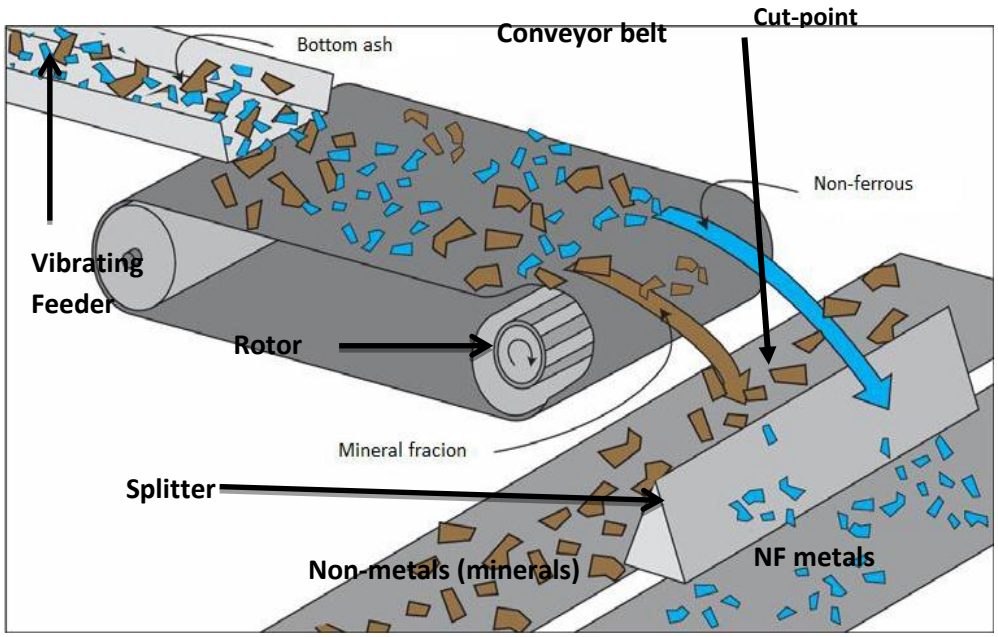


**Figure 8: Schematic diagram of an ECS.**
***Source: European Commission, Joint Research Centre, 2006.***

Separation principle

The permanents magnets with changing polarity are attached on the periphery of the rotor. During rotation an alternating magnetic field with a frequency of up to approx. 1000 Hz (dependent on the number of pole pairs and the speed) is formed *(Rem, 1999).* Permanent magnets with particularly high remanence (neodymium and iron boron) and their special arrangement on the rotor generate a strong alternating magnetic field. Within the zone of the alternating magnetic field, electric currents are induced only in the metal particles since the metal particles are electrical conductive. These so called eddy currents generate its own magnetic field which is in the opposite direction of the field generated by the spinning rotor of the ECS. The repulsive force of the two magnetic fields results in a deflection of the metal (conducting) particles. Due to this deflection metal particles have longer trajectories than the non-conductors/non-metals. In bottom ash the non-conductors are the minerals. The minerals fall off the belt due to gravity and have shorter trajectories compared with the metal particles *(Pretz, 2012)*. More information about the forces influencing the separation is given in the *Sections 2.2.3 and 2.2.4.* Particles that are magnetic such as the slag particles in BA will be attracted to the to the head pulley due to the magnetic field of the rotor. These slag particles are discharged beneath the head pulley (see Figure 10).

Splitter

A metal plate called splitter separates the falling product stream in a mineral and metal product (see Figure 5b). The horizontal distance of splitter can be adjusted during operation if for example the properties such as moisture content of the feed changes which affects the trajectories. The splitter determines the cut-point (point at which the falling stream is split) and thus the quality of the metal product and also the recovery of metal in the metals product. The quality of the metal product is often called grade and the recovery is how much metal is recovered relative to the amount of metal in the feed. If the splitter is placed too much to the left (close to the head pulley) mineral particles will end up in the metal product reducing the quality of the product and if the splitter is placed too much to the right (far away from the head pulley) metal particles will end up in the minerals product which is also not in favour. So there is an optimal splitter position that will result in the highest value recovery of the metal product.

Feeding

The material is usually fed by a vibrating feeder in order to spread the particles evenly and in monolayer. The material is fed in monolayer in order achieve an efficient separation as the strength of the magnetic field reduces with distance.

Figure 9a shows an example of a vibrating feeder in BA recycling and in

Figure 9b the head pulley, splitter and the two products bins are shown. The left figure shows an operating ECS that is fed in a monolayer. The right figure illustrates how the splitter separates the falling stream in a metal and mineral product. Notice that the majority of the particles are mineral particles and fall in front of the splitter close to the head pulley.


**Figure 9: (a): Left an example of an ECS for the 1-6 mm fraction with the vibrating feeder. (b) The right picture shows the product discharge area. *Source: Inashco, 2013.***

### 2.2.2 Concentric and eccentric rotor

The rotor in the head pulley can be mounted concentrically or eccentrically. For the ECS particle trajectory tests, both types were used. And since the way the rotor is mounted can influence the particle trajectories, this section will explain the differences between these two configurations by using Figure 10. Figure 10a shows the configuration of the concentric rotor and Figure 10b the eccentric one. By placing the rotor eccentrically in the head pulley the effect of the magnetic force is concentrated exactly on an area where the material leaves the belt. Moreover in the eccentric system the angle of the rotor with respect to centre can be varied from 0-30 degrees. The position of rotor angle influences the metal trajectories *(Rem, 1999*).

In a concentric system the magnetic field is acting just above the head pulley before the material leaves the belt. Some manufactures of the eccentric type e.g. Steinert, claim on their website *(Steinert, 2013)* that the NF metals are therefore not adequately deflected, mainly the smaller NF metal particles. Another claim is that ferrous (magnetic) particles that are attracted on the periphery of the head pulley of the concentric rotor, are getting heated up by the eddy currents and can burn holes into the pulley which is fabricated from glass fibre reinforced plastic while this does not occur if an eccentric rotor is used, also claimed by *(Pretz, 2012).* During this project both types were used, for the laboratory tests a concentric system and in-situ tests the eccentric type.

(a)

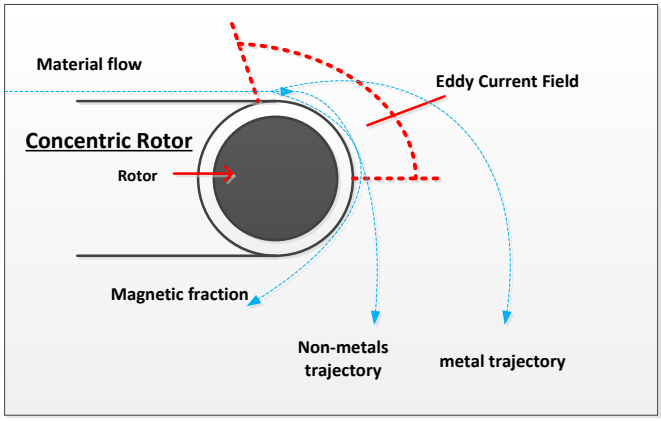


(b)

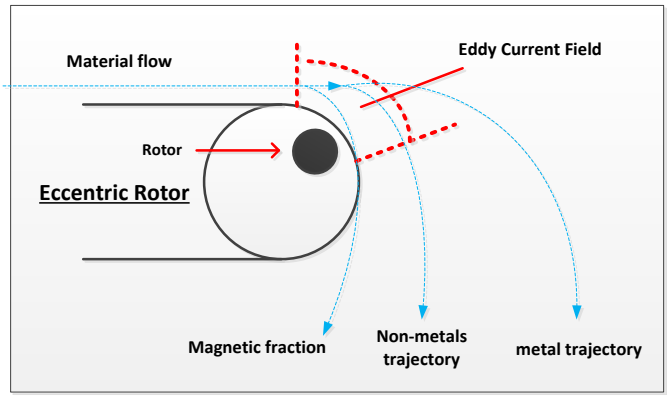


**Figure 10: (a) Configuration of a concentric type ECS. (b) ECS with an eccentric rotor. *Source: (Pretz, 2012)***

### 2.2.3 Eddy current deflection force

Now it is known how the separation between metals and non-metals is achieved, it is also important to understand which properties affect the separation and thus the particle trajectories. The exact version of the eddy current forces affecting the separation is quite complex due the alternating magnetic field and shape and orientation factors. The model for the derivation of the eddy current forces due to an alternating magnetic field is based on the dipole model and is explained in the book of Rem *(1999).* In order to understand the parameters that affect the particle trajectories a simplified version of the eddy current forces is enough. The deflection force according to *(Zhang, 1998)* can be expressed as follows:

$$F_d = KB_e^2 fm\frac{\sigma}{\rho}p \qquad [2.1]$$

K : coefficient related to the magnetic rotor of the ECS
$B_e$ : effective magnetic induction
f : oscillation frequency of the magnetic field
m : mass of the conducting particle
σ : electrical conductivity
ρ : mass density of the particle
p : (complex) particle factor related to the dimension and shape as well as orientation of the particle in the magnetic field.

In coefficient K the size, radius of the particle is incorporated with a factor. A more expanded version of the ECS forces is shown in *Appendix A* there the coefficient K is written in terms of the radius of the particle and relations related to the magnetic rotor. Judging from the formula the deflection force is influenced by the type of ECS, speed of the rotor and metal particle properties such as size, density, electrical conductivity and shape. Each NF metal type has their own mass density and electrical conductivity, which causes the different metals to follow different trajectories.

The ratio of the electrical conductivity and the mass density (σ/ρ), and the particle size are the two dominant variables affecting the trajectory of a particle *(Zhang et al., 1999).* The greater the σ/ρ ratio the greater the deflection force the longer the particle trajectory. Aluminium particles for example have the longest trajectories, due the biggest σ/ρ ratio. Also the shape influences the trajectory though the affect is minimal, cylinder shaped particles have the shortest trajectory and spherical the longest *(Zhang et al., 1999).* In *Appendix A* the σ/ρ ratios for pure aluminium (Al), copper (Cu), zinc (Zn) and lead (Pb) are shown. In BA however the metals found are not in pure form, due to the incineration process were some metals melts and oxidation during the aging process *(see Section 2.1.3).*

### 2.2.4 Frictional, adhesive and drag forces

Frictional forces occur between the particle and the conveyor belt of the ECS. These frictional forces have a significant effect on the trajectory of a small particle < 5 mm, in which case the eddy current forces are not strong enough to dominate the competing forces *(Zhang et al., 1998)*. The frictional force, in particular the dynamic friction coefficient is causing randomness of the particles trajectories, since the dynamic friction coefficient show strong variation *(Zhang et al., 1998).*

The adhesive forces let the wet particles stick to the conveyor belt of the ECS. It was found that the moisture content of 12-15% have a positive effect on the recovery of non-ferrous metal particles in the range from 2 to 6 mm *(Settimo et al., 2004).* Since the torque of the magnet rotor applies selectively to metal particles, only these are liberated from the belt and are collected in front of the rotor. Non-metal particles remain stuck to the belt and are released below the conveyor. According to *(Settimo et al., 2004),* if the water layer between the particle and the belt is approached by a cylinder shape, the adhesive force can be written as follows:

$$F_{adhesive} = 2\pi\gamma\sqrt{d\delta} \qquad [2.2]$$

| | | |
|---|---|---|
| γ | : surface tension for water and air | [J/m$^2$] |
| δ | : thickness of the water layer | [m] |
| d | : diameter of the particle | [m] |

Well conducting non-ferrous metal particles are able to break loose if the electromagnetic torque is of the order Fd/2, which is achieved for well conducting particle if d > 2 mm at typical ECS settings *(Settimo et al., 2004)*. The drag forces may play a role once the particles are in flight. The drag force can be calculated as follows *(Bird, Stewart and Lightfoot, 2001)*:

$$F_{drag} = \frac{1}{2}\rho_{air} v^2 C_d A \qquad [2.3]$$

| | | |
|---|---|---|
| $F_{dragg}$ | : drag force | [N] |
| ρ | : density of the air | [[kg/m$^3$] |
| v | : speed of the object relative to the air | [ m/s] |
| A | : cross-sectional area of the particle | [m$^2$] |
| $C_D$ | : drag coefficient | |

# 3 ECS PARTICLE TRAJECTORY TESTS

The objective of these following experiments was to determine the distribution of the different materials in BA as a result of their trajectories, where the emphasis is on the NF metal distributions. Knowledge about the distribution may be correlated with the sensor performance and lead to an optimal strategy for sensor based control. The focus of this project therefore was to determine the distribution of the different materials in BA by doing experiments on an operating plant. Before doing experiments on an operating plant, where the opportunities and time of doing experiments are limited and to avoid disturbance of the processes, the methodology for the determination of the ECS particles trajectories was developed and improved in the laboratory first.

The method development and evaluation of the method is described in the section laboratory particles trajectory tests. The particle trajectory tests done in-situ, from which the data will be used further for the modelling of the trajectories, is described in the in-situ ECS particles trajectory tests.

## 3.1 Laboratory ECS tests

The aim of the laboratory tests was to develop a method for the collection of particles in order provides a classification according to distance from which the trajectories could be determined. For the determination of the trajectories after collection of the particles it was necessary to separate them in metals and minerals. A method for the separation of metal and minerals was also developed and evaluated during the laboratory experiments and will be explained in this chapter. Moreover since the laboratory particles trajectories tests also generated some results that can improve the understanding of the trajectories and indicate where to focus during the in-situ tests, these results are presented in this chapter.

Two laboratory tests were conducted each with 1200 g BA, size fraction 1-6 mm. The first test was conducted with BA containing 9% moisture and the second test with material containing 4% moisture, the material of the second test was dried beforehand. These two tests were done to develop a method and to make sure the method can applied in-situ. A third test was performed with 1000 g material (9% moisture) with the focus to visually inspect whether the particles bounce of the lamellae, and end in another slot and to obtain a generic mass balance.

### 3.1.1 Materials and methods

**Method development**

The idea in order to determine the particle trajectories was to place a container in the falling stream of the ECS to collect the particles in intervals of 10 mm. In this was way the distribution of the material as function of the distance could be obtained. Since the particles fall from a conveyor belt they have a certain speed that will cause the particles to bounce if landed on a flat surface such as a wooden box. Bouncing of the particles would have resulted in uncontrolled and biased trajectory measurements as particles would have ended at other horizontal distances. The challenge therefore was to find a method that can collect and damp the impact of the falling particles and thus prevents them from jumping. Moreover once the particles were collected, the method should also allow for easy removal and analysis of the particles. And finally it should be applicable on an operation plant.

Three materials were tried in the lab that could prevent the particles from bouncing. The materials used were:

- *Agar-Agar*[2]
  The agar-agar gave unsatisfactory results because it became stiff rapidly. Moreover it was not suitable for an in-situ test as boiling/heating was necessary. Also removal of the particles would have been a real challenge.
- *Wheat flour*
  Flour was a disaster because it was sticking to the particles. Also not suitable for in-situ tests if it would have started to rain or to snow which was often the case.
- *Fine sand*
  Sand could not prevent the particles from bouncing. In Figure 11the bouncing of particles is shown by the empty holes in the sand. These holes indicate that particles bounced or rolled away after touching the sand.

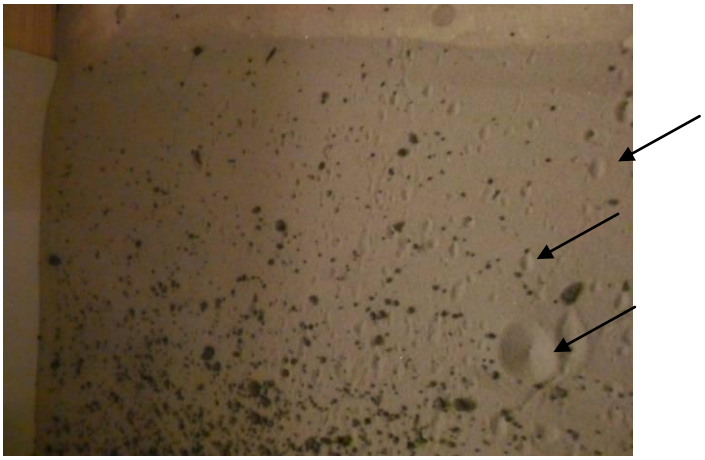

Figure 11: Empty holes in the sand.

[2] Agar-Agar a gelatinous substance derived by boiling a polysaccharide in red algae.

- *Container*

  A stainless steel container was produced which contained another bin with a steel wire mesh bottom. The inner bin was subdivided into slots (10 mm wide, 40 mm deep) using thin lamellae (0.5 mm thick). The set of slots was filled up with water until the lamellae of the inner bin were about 5 mm under water to prevent the particles from bouncing. Since the inner bin was perforated it may be conveniently lifted out of the outer bin while simultaneously removing all the water. This inner bin was placed in an oven to dry it out completely, after which the contents of the slots was analysed further. A few trials confirmed that this method is suitable for its purpose and by making a video of the falling particles it was observed that the particles were not bouncing once landed on the water surface if the water is filled slightly above the lamellae. Based on the tests and video it was concluded that particles were not bouncing once they touch the water surface and thus was this method selected for the in-situ tests. The setup of this method is explained in the next section.

**Setup**

The container with slots was positioned in the trajectory paths of the particles from the ECS in order to collect them and provide a classification according to distance. The experimental setup is shown in the Figures 12 and 13. The dimensions and the settings used during the trials are shown in Figure 12 and the positioning of the container is shown in Figure 13.This position was marked so it could be replaced accurately at each new test. After the container was positioned in place a vibrating feeder was used to evenly distribute the bottom ash in a 250 mm wide monolayer on the conveyor belt. The effective mass feed rate was 576 kg/h per meter width of the feed belt during 60 seconds. For the laboratory tests a concentric type Bakker Magnetics (type BM 29.713/118) ECS was used. The belt width was 800 mm and its speed was set to 1.7 m/s. The rotation of the rotor was set to 3000 RPM, but it measured a bit lower at 2987 RPM.

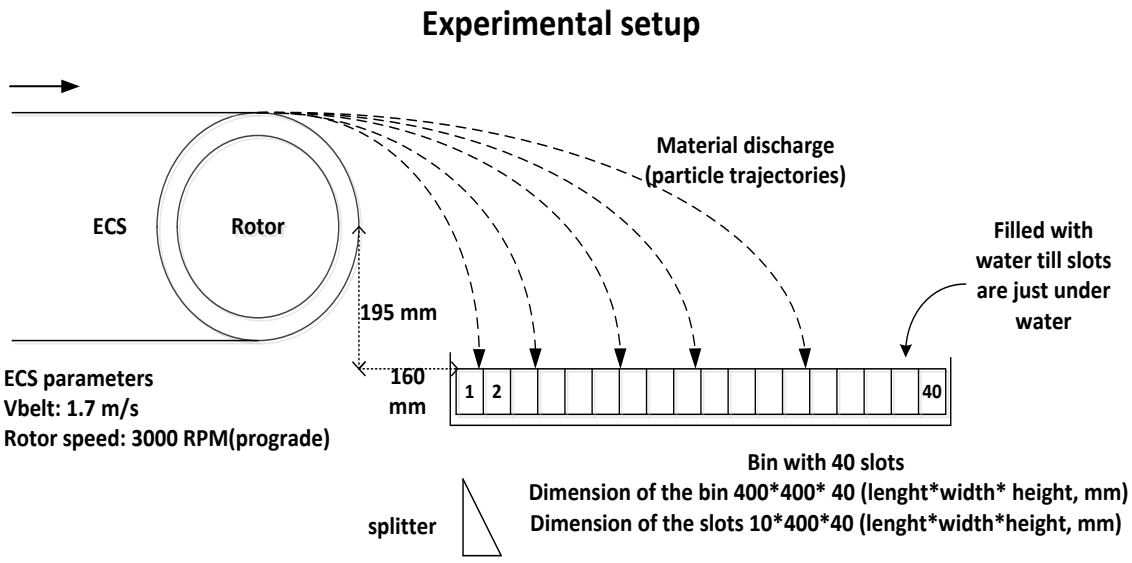


Figure 12: Setup of the experimental trajectory measurement in the laboratory.

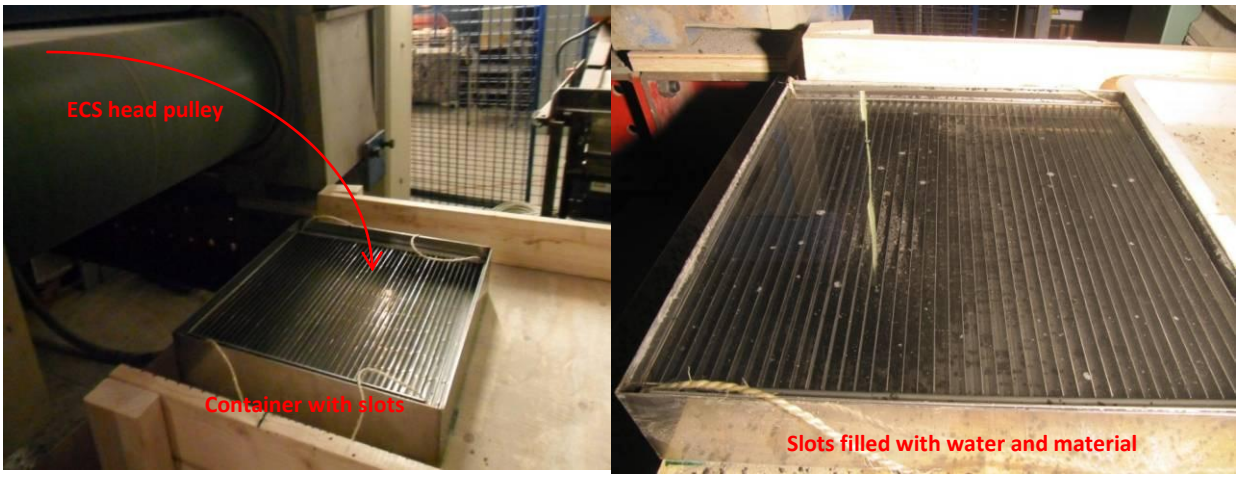


(a) (b)

Figure 13: (a) Experimental setup, material flow indicated with arrow. (b) After a test, the water-filled slots contain the BA.

### Material analysis

Beside the development of the method for the collection of the particles, a reliable method to analyse the collected particles per slot was also required. The goal was to obtain the different types of NF metal particles typically found in BA by first separating them from the minerals. In order to separate the minerals and metals, trials with a metal detector, Magnetic Density Separation *(Berkhout et al., 2010),* dense fluid separation was performed however without success. The metal detector, Magnetic Density Separation and dense fluids proved to work

unsatisfactory for small particle < 2mm or were too time consuming. Finally by using a laboratory ECS on a special way as described further in Figure 16 a workable method for analysing the material was found. The steps for the material analysis are presented in Figure 14.

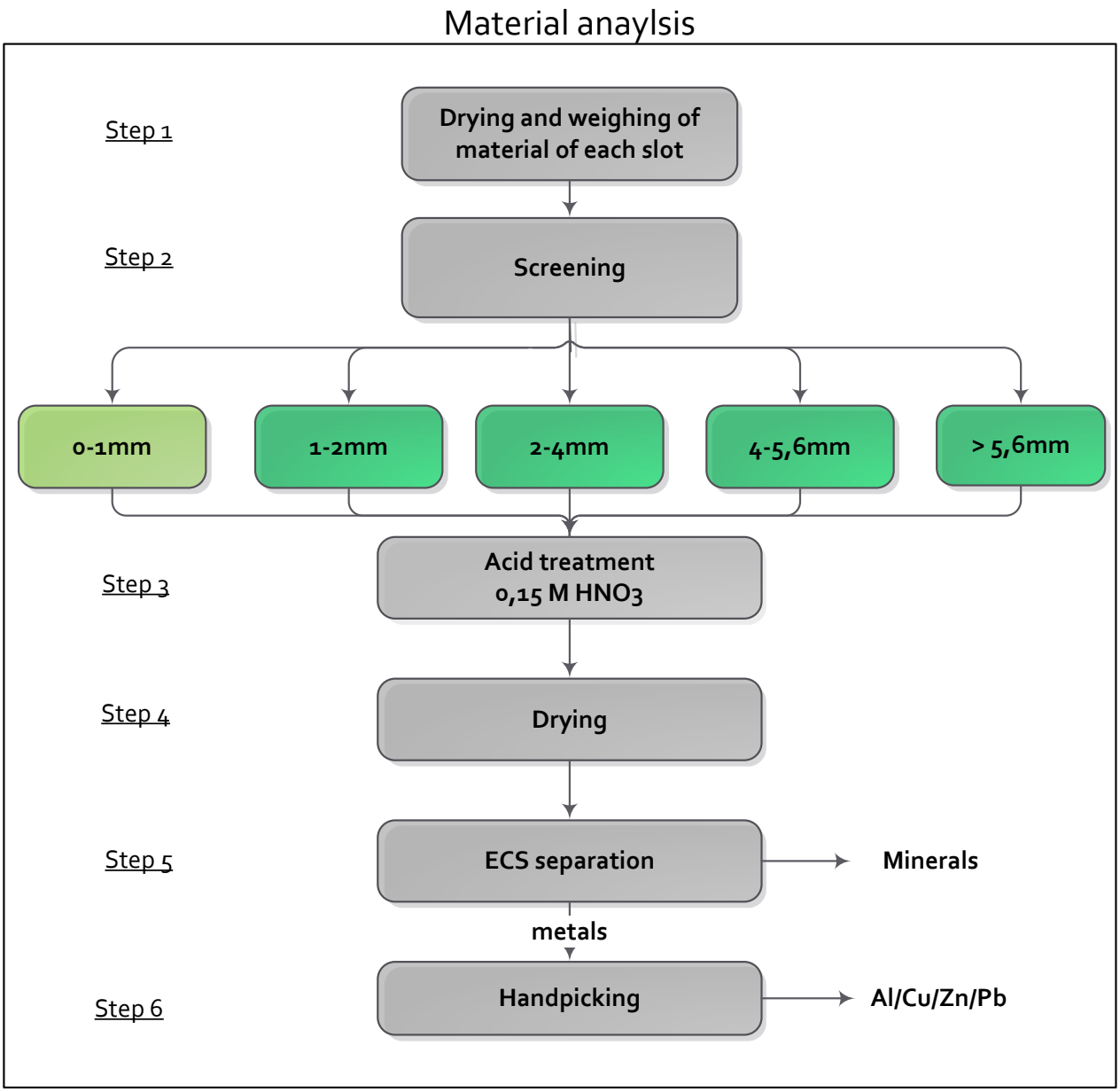


Figure 14: The followed steps to obtain metal particles of certain size.

The collected material per slots was analysed as follows:

- Step 1: After each test the accumulated material was placed in an oven for 24 hours on 105 °C as it was wet due to the water in the slots. It was also possible to dry the material while the material was still in the slots. Removal of the particles after drying in the slots proved less time consuming and thus more efficient.
- Step 2: Not only the type of metal but also the size of the metal particle affects the trajectory. Measuring the particle sizes individually would have cost a lot of time. Therefore the material was sieved to still have a certain size range. The 0-1 mm was not analysed further as it was to fine do so.

- Step 3: In order to make the particles visible for the handpicking step later, the particles were treated with diluted nitric acid ($HNO_3$) and washed with water. In Figure 15 three pictures are shown. In the first picture (a) the bottom ash is shown before treatment and in the last (c) bottom ash after treated with acid. Now the particles are better visible.

(a) (b) (c)

**Figure 15: (a) Dried BA 1-6mm, (b) Nitric acid treated BA, (c) After acid treatment and washing.**

- Step 4: To separate the material with an ECS, it was dried again. Moreover during handpicking the weight of the metal particle was recorded.

- Step 5: Separation of the metal particles was a real challenge. To solve this, the following was invented. Particles were placed on top of the rotor of a small laboratory scale ECS, in the range of the magnetic field. By only turning on the rotor of the ECS, rolling of the metal particles due to the electromagnetic force could be achieved while the mineral particles remained at their original position. In Figure 16 separation of the minerals and metals is shown. The use of the ECS in such a clever way was invented during this graduation work and might be used in the laboratory for the metal analysis of the 1-6 mm BA fraction.

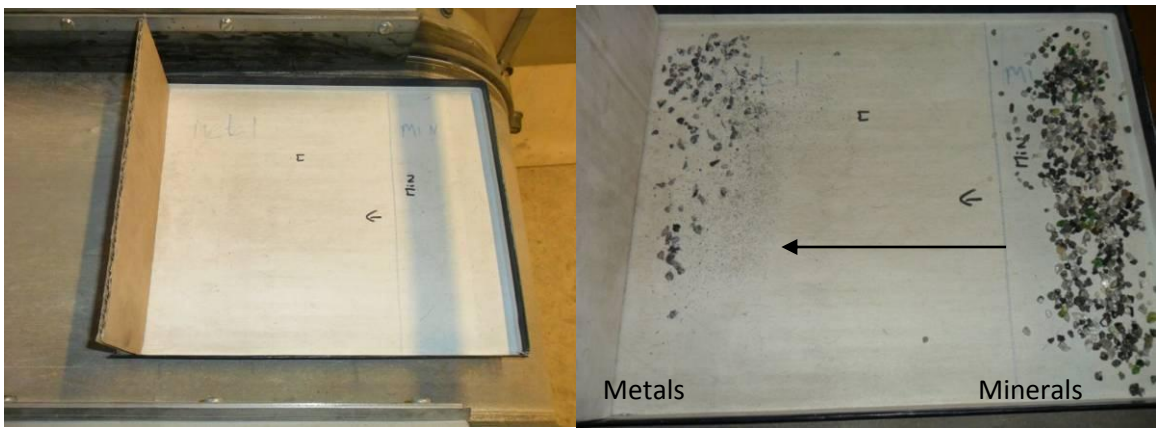


**(a)** **(b)**

**Figure 16: (a) Setup of the metal seperation with laboratory ECS. (b) Separation minerals and metals.**

- Step 6: To obtain each metal type separately, handpicking of the individual metal types were done. Four metal types were distinguished namely: Al, Cu, Pb, and Zn. BA however also contains other metals such as Sn, stainless steel and alloys, those were classified as other. These metals however were scarce. After acid treatment brass may look similar (red in colour) to copper, therefore brass and copper were taken together. Brass particles however were also scarce. Shape too may affect has an effect on the trajectory and therefore the shape of the Cu particles were noted down. Three shapes were distinguished, spherical, cylindrical and else classified as other. Metal particles found in BA can be oxidised, partly melted and not look like a metal particle making handpicking a time consuming task.

### 3.1.2 Results

In this section the results obtained during the three tests will be discussed. These results will show the type of data that can be generated with the developed model. Moreover it also allowed for extra information about the particle trajectories. The material distribution will show the repeatability, and metal and shape distributions will try to give more insight in the particle trajectories. In the last section the material and metal distributions are combined to show that part of metal particle particles is barely deflected.

**Material mass distribution**

In order to evaluate how the material, discharged from the ECS is distributed, the material mass per slot was plotted against the horizontal distance. First a general overview of the material distribution will be discussed where after material mass per slot will be presented.

During the two tests it was observed that only half of the material accumulated in the 40 slots. The other half was falling beneath the ECS belt. Therefore during the third test, bins were placed beneath the ECS to capture all the metals and to verify whether the material accumulation in the slots can be justified. The material accumulated in the bins around the ECS was dried and weighted. The material collected in the slots was also weighted. It was found that 50% of the feed fell in the 40 slots and the other 50% between the rotor and the container and also beneath the rotor as the ferrous particles are attracted to the head pulley due to the magnetic force of the rotor. These particles are discharged beneath the ECS. In Figure 17 an illustration the material distribution is shown. It was also found that up to slot 12-13 (280-290 mm from the rotor axis) about 30% of the particles were magnetic and attracted by a ferrite block magnet. In most of BA recycling facilities the ferrous particles are removed prior to ECS separation to avoid damages to the ECS belt and head pulley. However the ECS in this processing plant was mounted with an eccentric rotor, which is not affected due to the ferrous particles *(see Section 2.2.2)*. An observation was that from the slots 15 till 20, dominantly glass and ceramic/stone type of particles were found rather than magnetic slag particles. An explanation could be that slag particles are magnetic and thus attracted by the rotor resulting shorter trajectories compared with glass and ceramic/stone particles that are not magnetic.

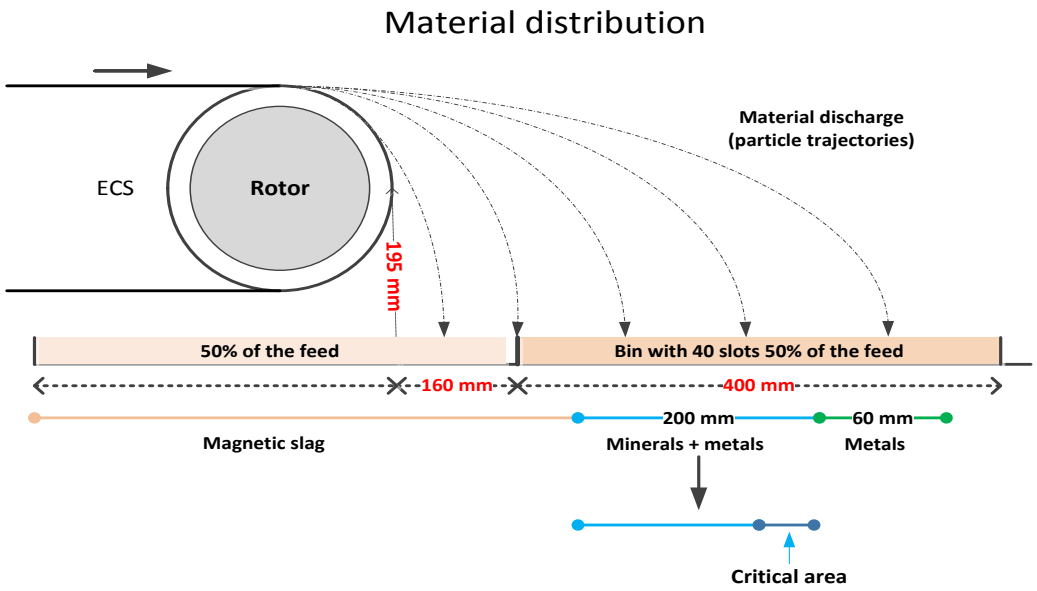


Figure 17: Illustration of the feed material distribution.

The third test was conducted in order to verify whether particles bounce and fall in another slot. During test 3 the water level above the slots was kept 1-5 mm above the lamellae while at test 1 and 2 the water level was about 8-10 mm. The hypothesis was that if the particles did not bounce at 1-2 mm water level they will not do so at few mm higher water levels. From Figure 18 it can be observed that the material mass distribution of the 3 tests is almost identical from which it was concluded that bouncing of the particles is not occurring. Moreover it can also be concluded that the results are quite repeatable.

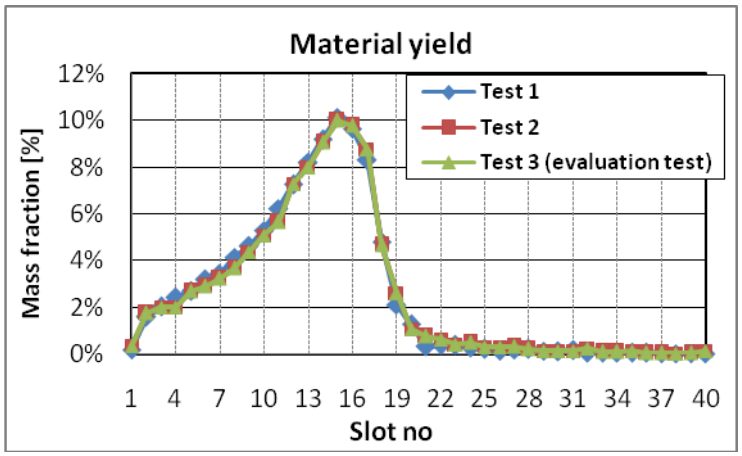


Figure 18: Material yield plotted as mass fraction.

**Size distribution of the material**

Sieve analysis was done in order to see whether particle trajectories are affected by the size of the particles. Figure 19 shows the cumulative particle size distribution curves. From the graphs it can be observed that smaller particles have shorter trajectories and the larger particles longer. This means that the average particle mass will increase with increasing slot number. The size distribution of the feed affects the performance of the ECS, the narrower (closely sized) the distribution the better the separation *(Pretz, 2012)*.

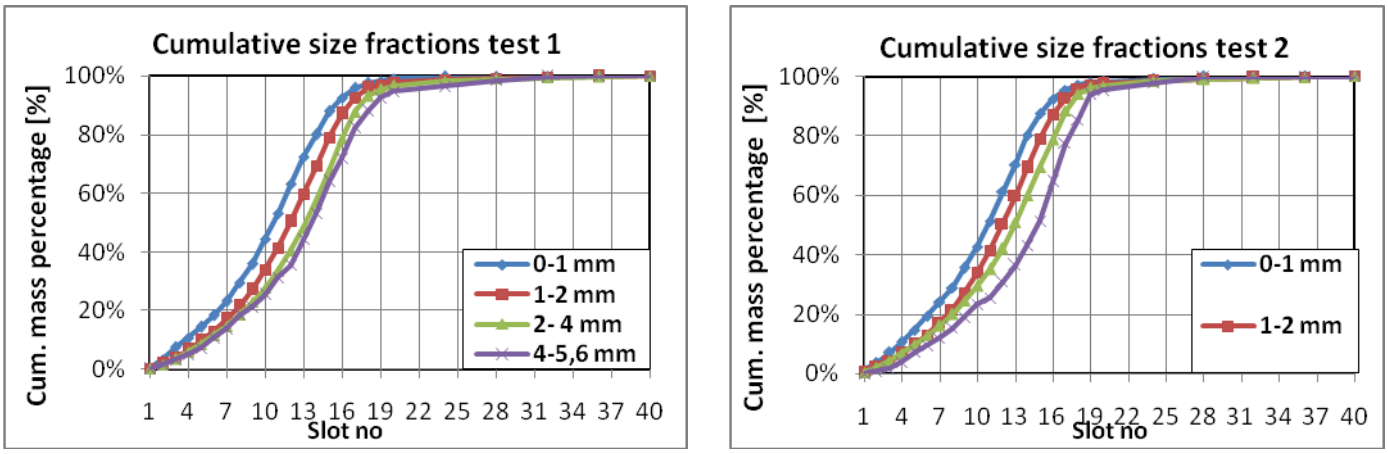


Figure 19: Size distribution of the material in the slots. Left test 1 and on the right side test 2

**Non-ferrous metal distribution**

In order to determine the trajectories of the different metal particles the masses and number of particles were plotted cumulatively. The plots are shown below.

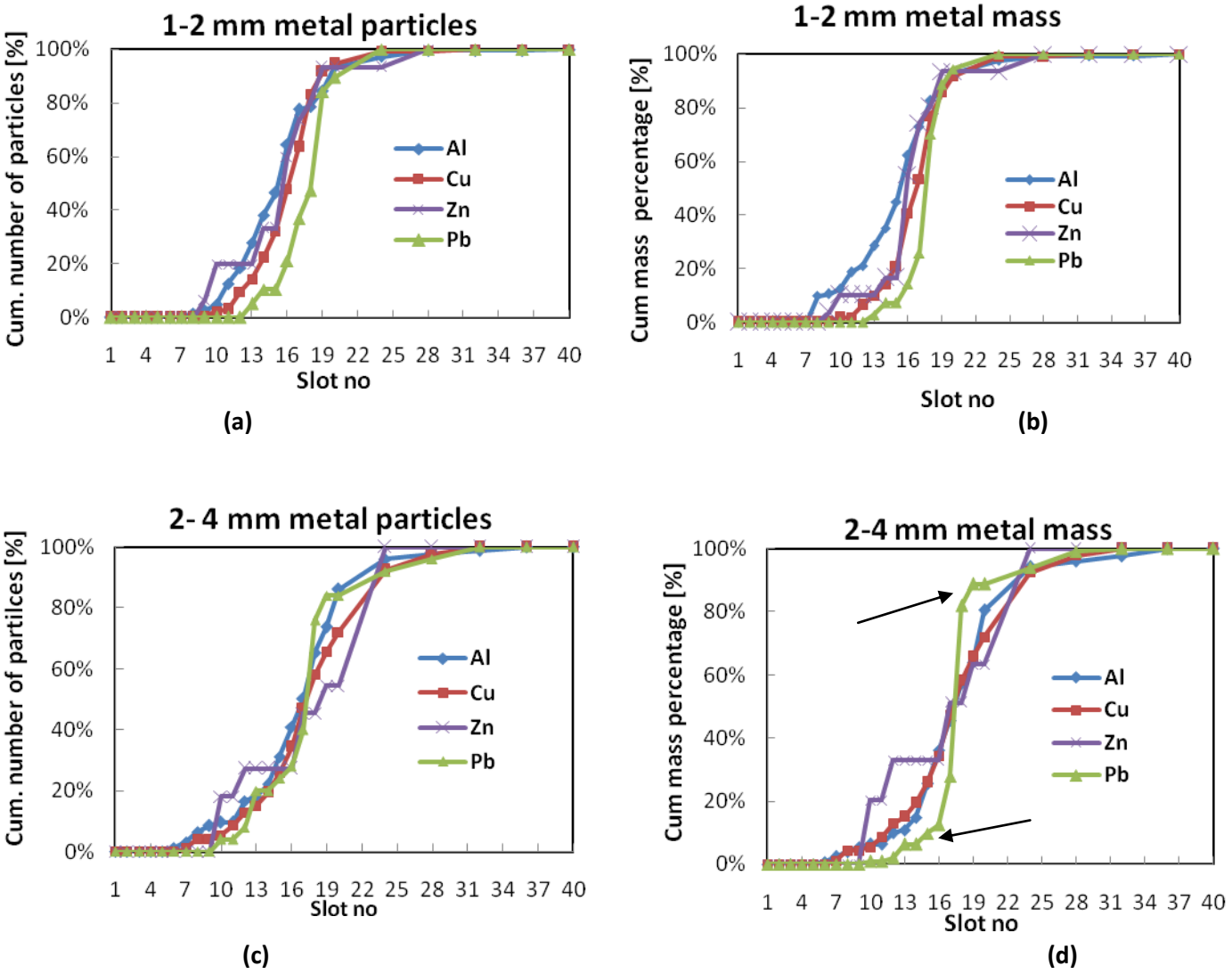


**Figure 20: NF metal mass and particle distribution per metal type and per size fraction. (a) and (c) show the particles. (b) and (d) show the mass distribution.**

The results showed that in the 1-2 mm fraction, Pb particles had the longest trajectories followed by Cu, Zn and Al as shown in Figure 20a and 20b. It was expected based on the σ/ρ ratio that Al particles would had have the longest trajectories as a results of greatest deflection force. That the other metals have the longer trajectories that Al indicates the effect of the deflection force is negligible small for 1-2 mm particles, they are barely deflected. And that the

1-2 mm particles fall of the belt as a result of inertia forces, which is bigger for particles with greater mass such as Pb.

Comparing the graphs (a) and (c) or (b) and (d) it can said that the 2-4 mm particles have longer trajectories than the 1-2 mm particles. And now focus on the green line of graph (d). On the bottom arrow the green line farther away from the head pulley and on the arrow on top it is the closed to the head pulley. It seems like there is a mix of two events. The first one bottom arrow were the flection force is not playing a role and the second (top arrow) where the deflection force may start to play a role since Pb particles there has the shorts trajectory. The + 4mm fraction is not plotted due to the poor statistics as number of + 4mm particles was scarce.

**Shape distribution of Cu particles**

The shape of a metal particle influences the eddy current forces and thus the trajectory of a particle. Therefore the shape of the Cu particles was recorded in order to evaluate whether the effect of the shape will have a significant effect on the particle trajectories. In Figure 21 the cumulative shape distribution of Cu particles is shown. The 2-4 mm Cu particles show, however not explicitly that cylinder shaped particles are having slightly shorter trajectories than spherical particles. For the 1-2 mm particles the lines are almost identical, meaning that the trajectories were not affected by the shape. The curves of the 2-4 mm particles is flatter (more spreading) compared with the 1-2 mm particles from which it can be said that with increasing particle size the shape may play an role on the length the particle trajectory.

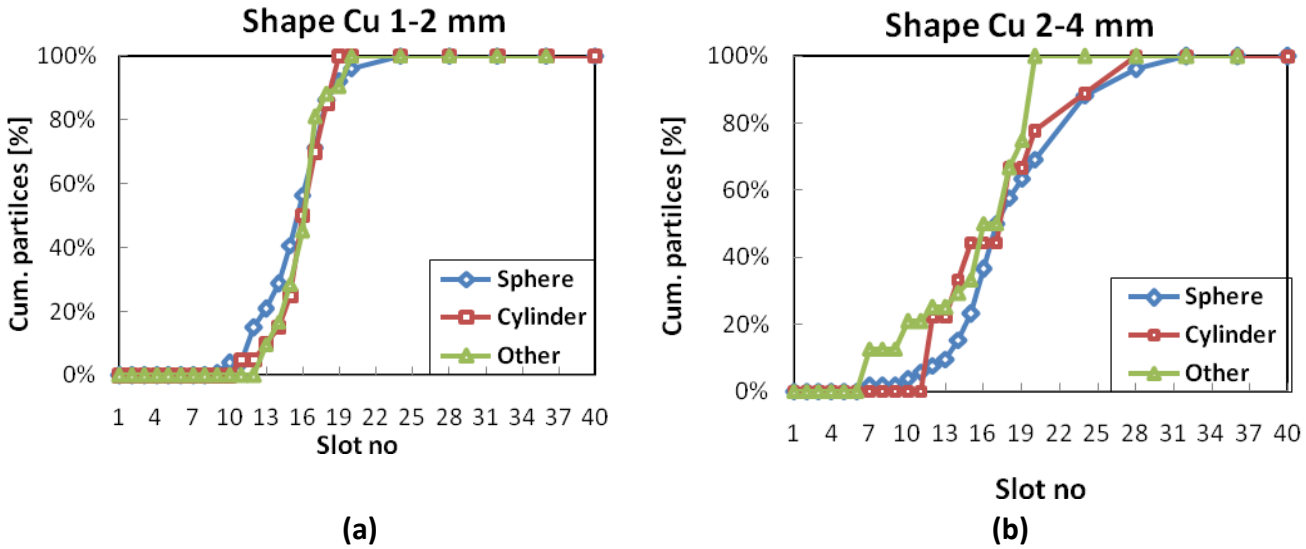


Figure 21: Shape distribution of the Cu particles. (a) Left: 1-2 mm particles, (b) 2-4 mm particles.

**Material and metal combined**

In order to show that that majority of the 1-2 mm and part of the 2-4 mm particles are poorly deflected by the ECS, the material and metal mass are plotted in one graph, shown in Figure 22. Observe in graph (a) that slot 15 has the highest material yield. Therefore it can be said that the main material stream fell in slots 15-16, about 460-470 mm from the rotor. To avoid this main mineral stream, the splitter would have certainly placed after slots 15-16. This than would have resulted in that minimal 44 % of the 1-2 mm and 27 % of the 2-4 mm particles would have not been recovered in the metal product. Notice also from graph (a) that close to the peak of the material the metal also show a peak. This could indicate that part of the metal particles that are not deflected may dragged into the main material stream. Adjustment of the splitter to recover these metals would result in a low product grade which is undesirable.

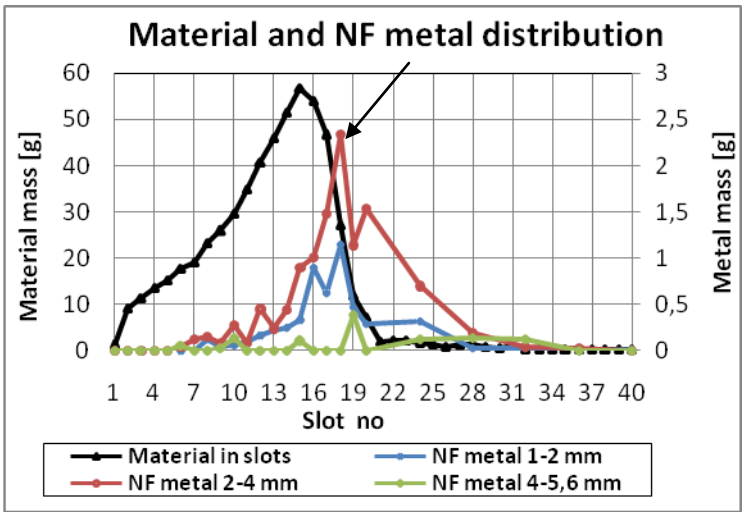


(a)

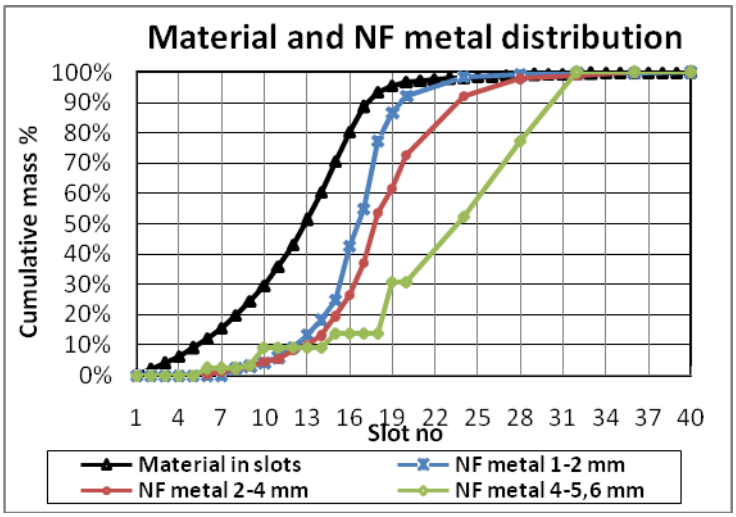


(b)

**Figure 22: (a) Material and metal measured mass per slot. (b) Cumulative material and metal mass per slot.**

**Summary**

The laboratory results showed that with the developed method, particles from a falling stream can be collected, analysed and from which the particles trajectories can be determined. Material distributions showed that the results are reproducible and metal distributions indicated where to focus on the in-situ particle trajectory tests. Moreover by doing the laboratory tests understating of the particle trajectories has also increased that may help during the in-situ tests.

## 3.2 In-situ ECS tests

After developing and improving the methodology for the particle trajectory tests in the lab, three in-situ tests were done in two batches at BA separation plant. The objective of the in-situ tests was to determine the particle trajectories at different feed conditions such as moisture content in order to evaluate its effect on the trajectories. Changes in the trajectories as a result of changes in the BA feed can require adjustment of the splitter position to achieve the highest value recovery of the metal product. The data obtained from the in-situ test was further used in *Chapter 4* for the modelling of the trajectories.

Two tests were conducted at two different moisture contents. An additional third test was performed in order to have backup material. This chapter first describes the setup and the feed material properties. Subsequently, the results of the tests are presented in two phases. First the material and metal mass distributions are presented and secondly the grade and recoveries are shown. The setup of the in-situ tests was different than the laboratory setup and therefore described again. The material analysis steps were the same and therefore not described again in this chapter.

### 3.2.1 Setup

For the collection of the material during the three tests the same methodology was used as in the laboratory tests, however with some few modifications. In the laboratory the amount of material fed could be adjusted to meet the capacity of the slots. In-situ, this could not be done since the ECS was operating continuously. Moreover the ECS in-situ was a lot bigger than the one used in the laboratory. For the in-situ tests more capacity was required and therefore the container was scaled up. The capacity of the slot was to accumulate about 325 g of BA. Since the ECS is now operating continuously and thus placing the container with slots in the stream would have resulted in an uncontrolled accumulation of the material, a triplex plate was placed, that functioned as a curtain in order to prevent particles from falling in the slots unintentionally. During the tests the triplex plate was lifted vertically, then material started to accumulate in the slots and after seconds the triplex plate was placed again to stop the collection. An illustration of the experimental setup in-situ is shown in Figure 23 .The scale of the figure is inconsistent, however the objective of this picture is to only illustrate the setup. The dimensions and settings of the ECS are also shown in the figure. The figures (c) and (d) give an impression of how the container was placed in the falling stream. In Table 2 the collection times and positions of where the container was placed is given. Test 1 was measured slightly farther away from the head pulley deeper in the metal product, while test 2 and 3 close to the head pulley covering both the mineral and metal products.

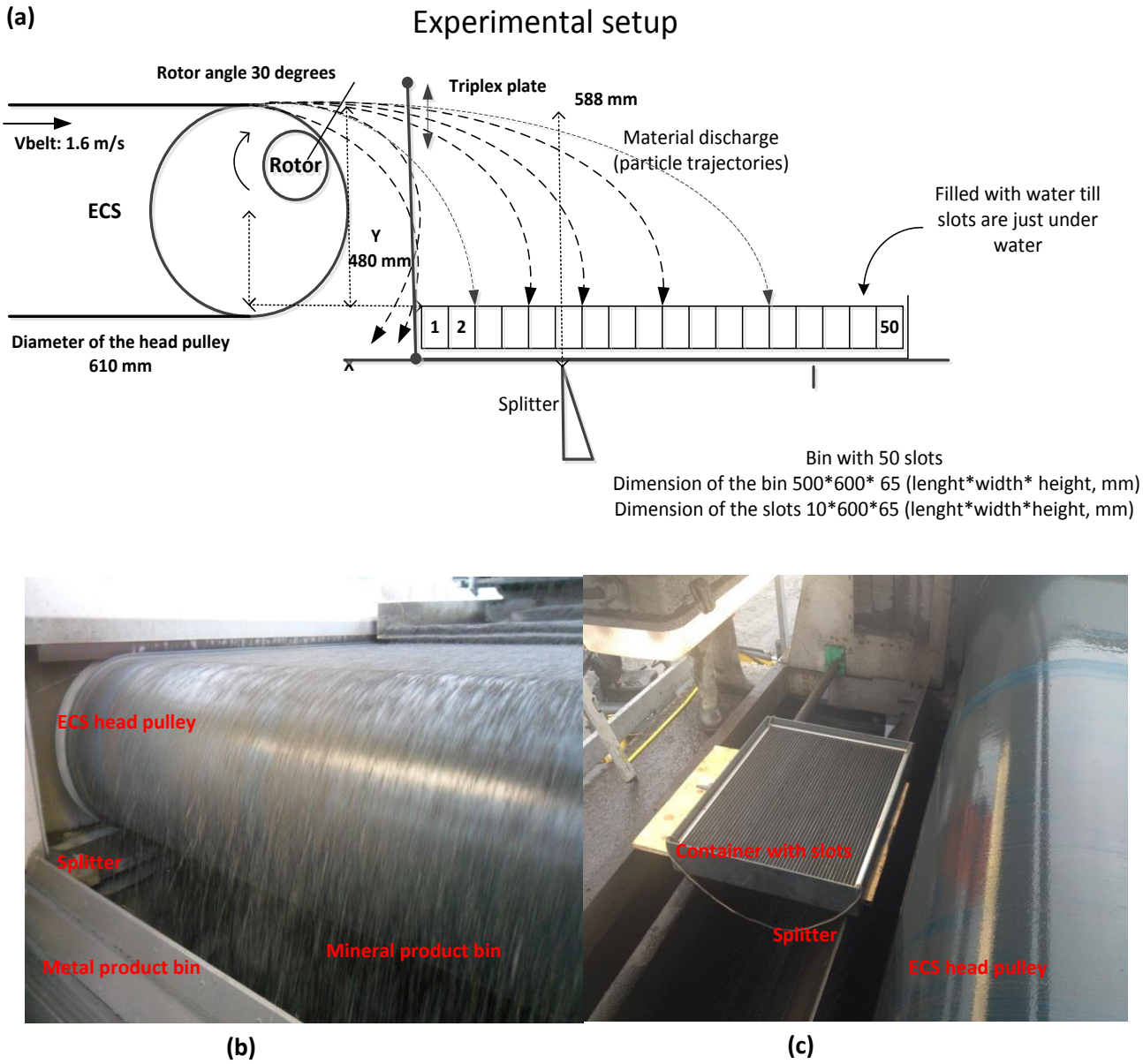


**Figure 23: (a) Experimental trajectory measurement in-situ. (b) ECS falling product stream. (c) Experimental setup**

Table 2: Distance and collection time of tests 1, 2 and 3.

| | Test 1 | Test 2 | Test 3 |
|---|---|---|---|
| **Horizontal distance from the centre of head pulley till centre of the first slot [mm]** | 459 | 355 | 359 |
| **Distance from top belt till water level [mm]** | 480 | 480 | 480 |
| **Collection time [s]** | 8 | 3 | 3 |

**Throughput and properties ECS feed**

Prior to every test the throughput through the ECS was determined. This was done by collecting the two output products (minerals and metals) in big bags simultaneously for a certain interval time. The big bags were placed at the discharge point of mineral and metal conveyor belts as can be seen in Figure 24. After every test a sample of the ECS feed was collected in order to analyse the moisture content, the particle size distribution. These properties and the throughput were determined in order to use that data further for the modelling part and also to compare the test which each other. The results of these measurements are given below.

Figure 24: Collection of the mineral product in a big-bag in order to determine the throughput.

In Table 3 the moisture content and throughputs are shown. During test 2 and 3 the feed going into the plant was higher than test 1, while the throughput measured through the ECS during test 2 and 3 was smaller than test 1. It was observed that during test 2 the material was finer in comparison with test 1. This might be the result of sieving with clogged screen apertures, caused by the wet feed (14% moisture). In laboratory, a sieve analysis of the feed was conducted to verify the observation. In Figure 25 this sieve analysis done in the laboratory of the feed is shown. It was found that the ECS feed of tests 2 and 3 was indeed slightly finer. It is however hard to quantify the effect of this difference. Therefore it is further assumed that the effect of this difference can be neglected. The NF metals grade of the feed material was around 2.3%.

**Table 3: Material properties of the ECS feed**

| ***Material properties of the ECS feed*** | | |
|---|---|---|
| | **Test 1 (Batch 1)** | **Test 2&3 (Batch 2)** |
| **Moisture content [%]** | **12.4** | **14.2** |
| **Throughput ECS [t/h]** | **12** | **9.2** |
| **Indication throughput plant [t/h]** ***(according to the operator)*** | 60 | 62 |
| **Sampling point: Vibrating feeder after ADR treatment and flip-flow screen** | | |

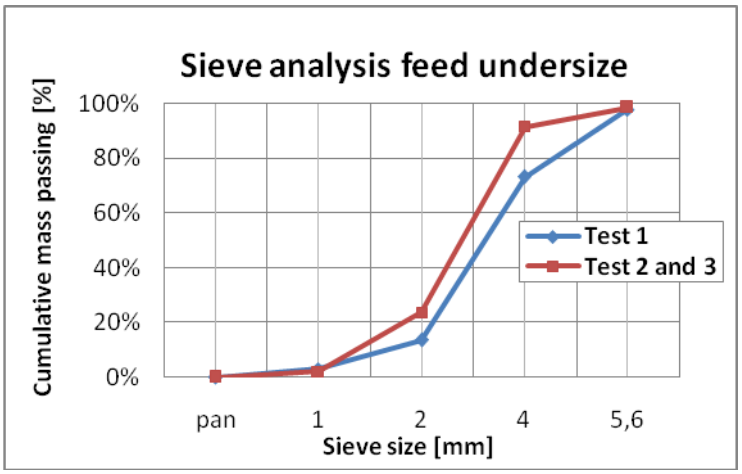


**Figure 25: Particle size distribution of the ECS feed.**

### 3.2.2 Results

This section will present the results obtained during the in-situ tests. First the material mass distributions will be presented to show the general trend and to compare the three tests. Then the metal mass and particle distributions will be shown of tests 1 and test 2. Finally the grade and recoveries of the tests 1 and 2 will be compared, and general trends will be discussed.

**Material mass distribution (yield)**

The material mass distribution was plotted to evaluate how the material was distributed as function of the distance and to compare the tests which each other. In this way the trajectories of the particles could be determined and evaluated. In Figure 26 the accumulated mass/s as function of the distance is shown. The mass distribution of the three tests shows a monotonic increasing function towards the head pulley, $m_{x-1} > m_x$. Between test 1 and tests 2 and 3 there is an offset of 30 mm. A possible explanation for this offset is the increase in the moisture content. During test 1 the feed contained 12% moisture and test 2 and 3 14% moisture. From the literature *(Settimo et al., 2004)* it was found that particles tend to stick to belt surface at higher moisture content depending on the type and size of the material.

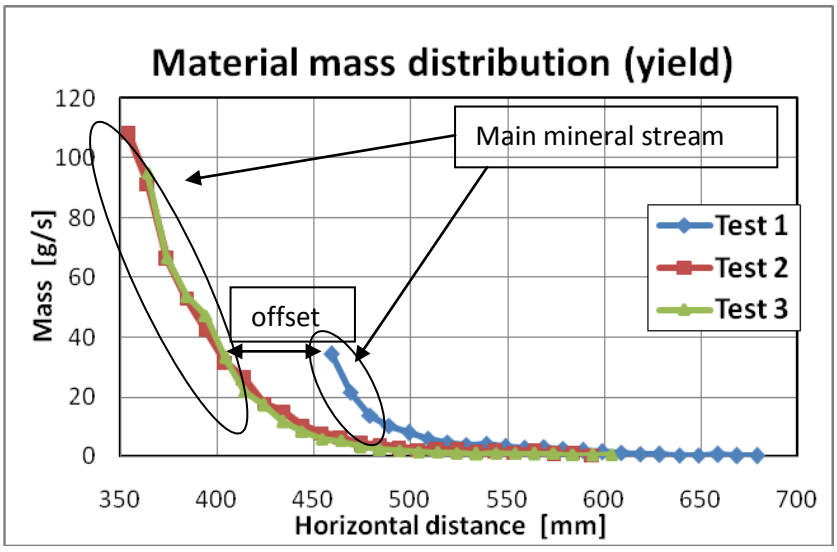


Figure 26: Material mass distribution (yield).

**Metal distribution tests 1 and 2**

The metal mass and particle distribution was plotted as function of the distance to determine and evaluate the different trajectories of the metal particles. Since test 1 contained 12 % moisture and test 2 14 % moisture, the effect of variable moisture could be evaluated.

Metal distribution test 1

In Figure 287a the mass of 1-2 mm NF metal found per slot of test 1 is plotted against the horizontal distance. On average the Cu 1-2 mm fell around 535 mm and Al 1-2mm around 515 mm. In Figure 287b the metal masses of the 2-4 mm and 4-5.6 mm fractions are shown, the maximum metal mass for Cu about 539 mm lies farther away from the head pulley in comparison with Al about 509 mm from which it was concluded that Cu particles have longer trajectories than Al particles. Judging from figures (a) and (b) the Cu 2-4 mm (peak at 520 mm) particles seem to have longer trajectories compared with the Cu 1-2 mm (peak at 510 mm) particles from which it was concluded that increasing particles size may lead to longer particle trajectories if the particle is deflected by the ECS. This result is in line with the theory of the eddy current deflection force.

**(a)**

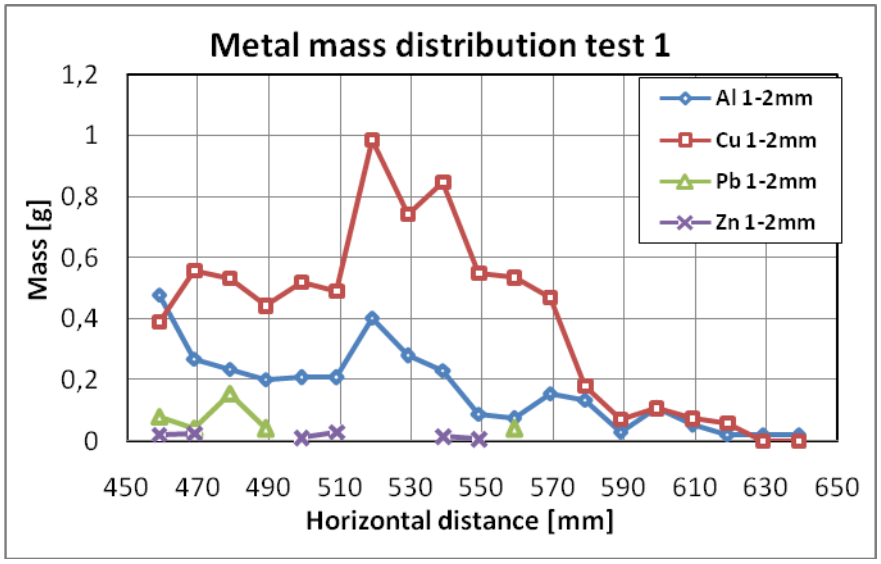

(b)

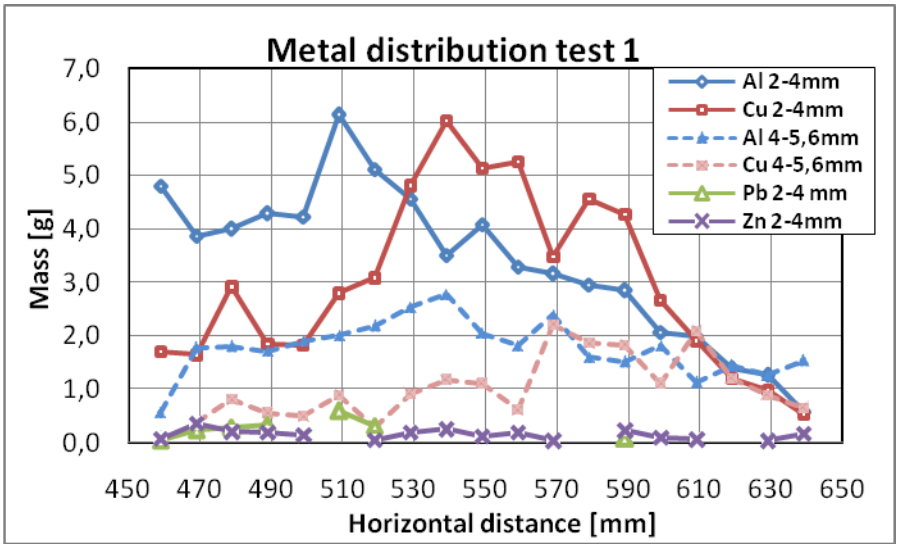


Figure 27: (a) Metal mass per slot, 1-2 mm fraction, (b) Metal mass per slot, 2-5.6 mm fraction.

*Particles*

The number of metal particles is plotted to again evaluate the trends. Trends in the metal particle distribution will be used in the modelling part to simulate a sensor system that can count particles. The Al, Cu, Pb and Zn particles per size fraction are shown in Figure 28. It was found that towards the head pulley the 1-2 mm, Al and Cu particles increases, indicating that part of the 1-2 mm metal particles are dragged into the mineral stream (from 460-480 mm) and thus probably fall before the ECS splitter plate. Figure 28b shows the metal particle distributions of the 2-4 mm and the 4-5.6 mm fractions. A peak around 510 mm was found for 2-4 mm Al particles followed by a declining trend. The maximum number of 2-4 mm Cu particles was around 540 mm. The number of 4-5.6 mm particles was almost constant with a slight increase around 540 mm.

(a)

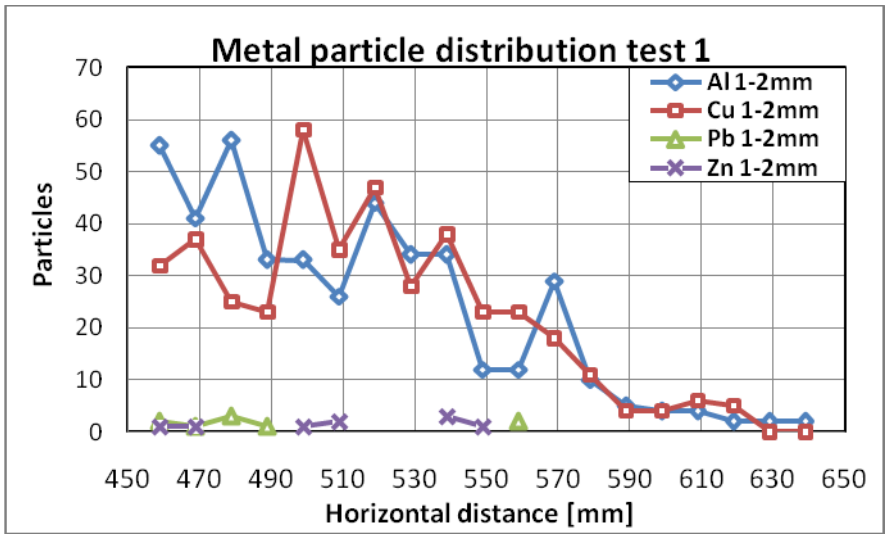

(b)

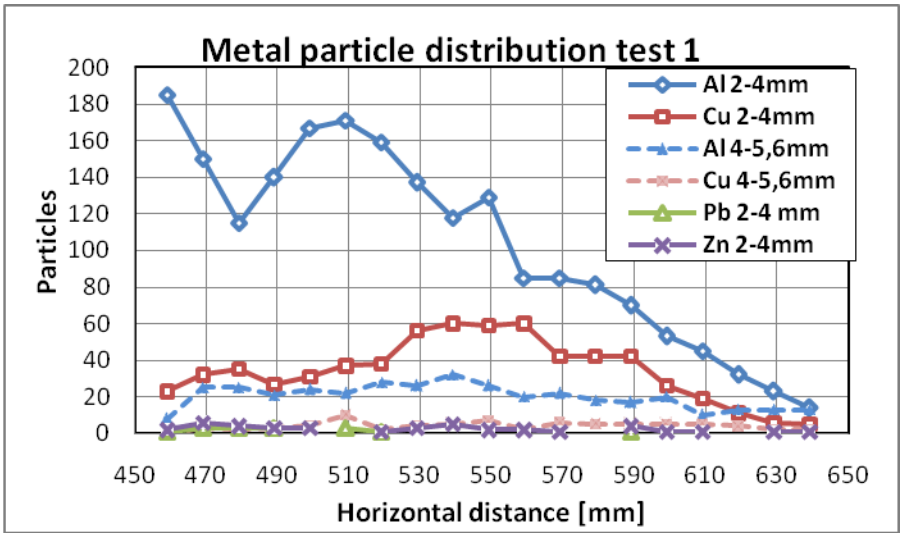


Figure 28: (a) 1-2mm metal particle per slot, (b) 2-5.6 mm metal particles distribution per slot.

**Metal distribution test 2**

It was found that close to the head pulley indicated with arrows (see Figures 29 and 30) the number of metal particles and mass increases. And in Figure 29 the 2-4 mm Al particles show an increase towards the head pulley indicated with and arrow and a peak indicated with the dashed arrow at about 515 mm. Cu 2-4 mm particles show a peak at 530 mm and a slight increase from 350-370 mm. Notice this slight increase for Cu 1-2 mm particles in greater than the 2-4 mm Cu particles. Indicating that part of the 1-2mm particles may be dragged with main mineral stream which is was somewhere between 350-370 mm judging from Figure 26. From these two observations it was concluded that part of the metals particles, mainly Al is again is dragged with the main mineral stream (at 350-370 mm) and that this affect is stronger for the 1-2 mm particles. As the test 2 was done closer to the head pulley where the number of particles increases, the collection time was only 3 s till the first few slots were full. Therefore the metal particles > 4mm were under sampled and could be presented in these graphs.

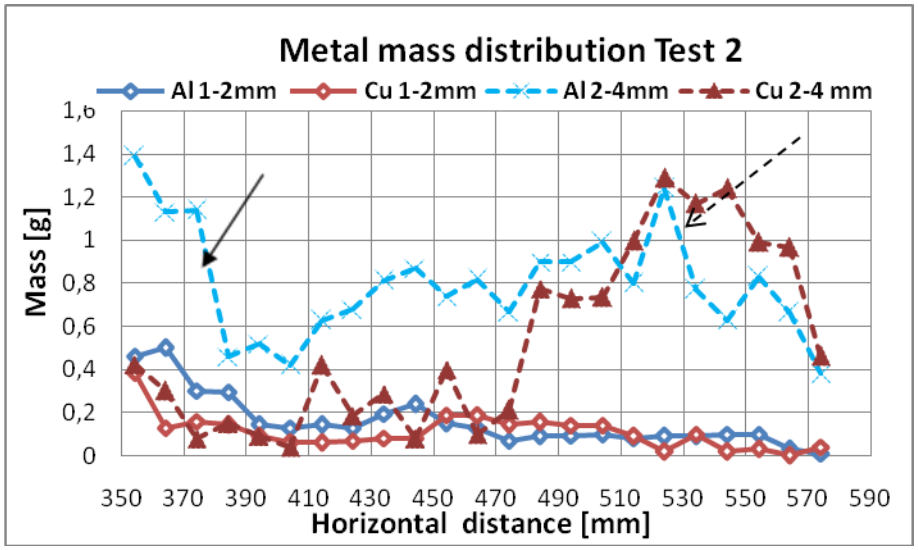


**Figure 29: Metal mass per slot per type metal of the 1-2 mm and 2-4 mm fractions, test 2.**

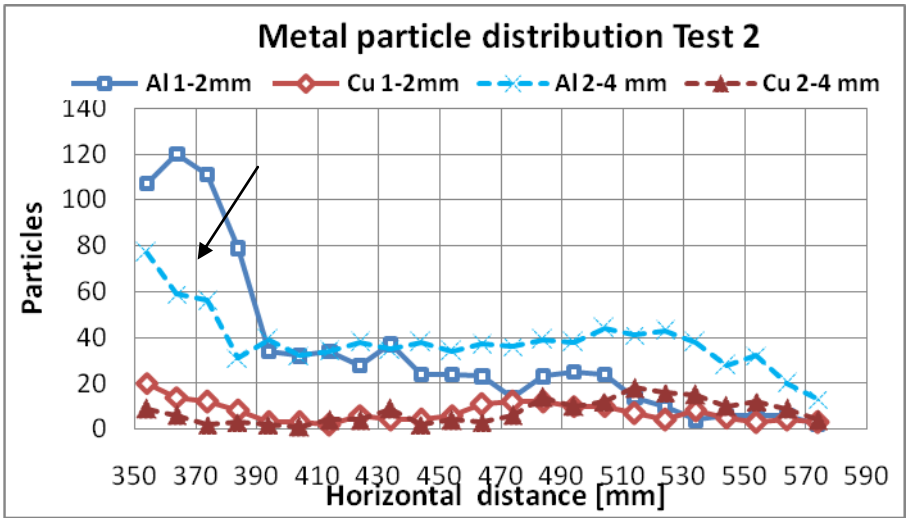


**Figure 30: Number of metal particles per slot per type of the 1-2 mm and 2-4 mm fractions, test 2.**

### 3.2.3 Grade and recovery

With the developed hybrid sensor described in *chapter 5* for the control of the splitter the grade can be obtained from the measured data. Therefore trends about the grade can be used to develop the strategy for the control of the splitter. In this paragraph the grade both the slot and product grade as well as the recoveries will be discussed first. Then the relation between slot and product grade will be shown.

**Slot grade**

The metal grade or metal concentration is a function of horizontal distance as result of the differentiation in particle trajectories. Close to the splitter for example the grade will be lower in comparison with the grade of the ECS metal product. The grade per slot (10 mm) was calculated to determine how the grade changes with distance and to assess the influence of the moisture content. The grade per slots was calculated as follows:

$$Slot\ grade = \frac{metal\ mass\ per\ slot}{material\ mass\ per\ slot} \qquad [3.1]$$

It was found that the slot grade increases after 450 mm with increasing horizontal distance for all the three tests as can be seen in Figure 31, in which the slot grade of tests 1, 2 and 3 is shown. In general it can be said that a shift of 10 mm in distance will cause the slot grade to increase with 15% for distances greater than 450 mm. The increase in grade for test 1 (12% moisture) is lower than the increase in tests 2 and 3. Considering the feed material of test 1 was less moist in comparison with the material from test 2 and 3, the mineral particles in that test had slightly longer trajectories as they were not sticking on the belt and therefore ending up in the metals product causing a lower product grade. The grade of test 2 increases almost up to

100% while the other two tests do not show this trend. During the material analysis of test 2, relative heavy metal particles were found resulting high grades. This can also be seen in Figure 43 where the average metal particle mass of test 2 is plotted against distance. Another point that should be mentioned is that that at the edges the grade less reliable to compare as results of the relatively poor statics.

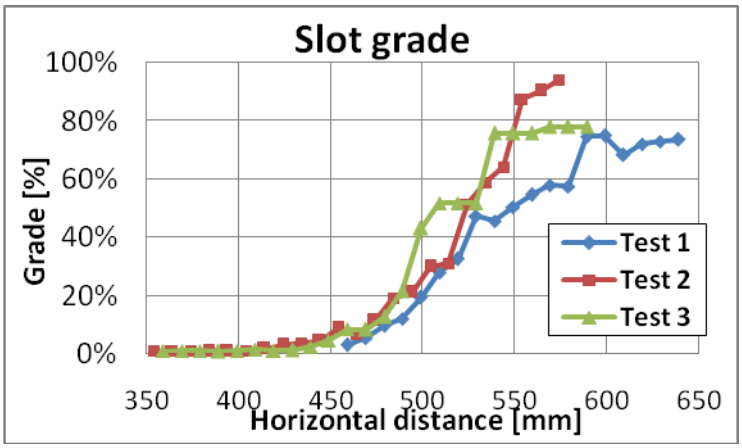


Figure 31: Slot grade as function of the distance.

**Product grade and recovery**

In order to optimise the value extraction of the metal product by using a sensor system the relation between the product grade and recoveries should be known first. More interesting even is to evaluate how the grade and recoveries changes as a result of changes in moisture content for example. This is shown in this section.

The product grade was calculated by taking the cumulative metal and material mass form the slots, with the first slot as starting position. Notice that the recovery or metal yield will be 100% for the first slot as it was assumed that all the metal falls behind this point. Figure 32 shows the grades and recoveries of tests 1 and 2 as function of the horizontal distance. Test 1 was measured relative far away from the head pulley and therefore starts from 20% product grade. The results show that at drier feed material the product grade is lower for the same splitter distance.

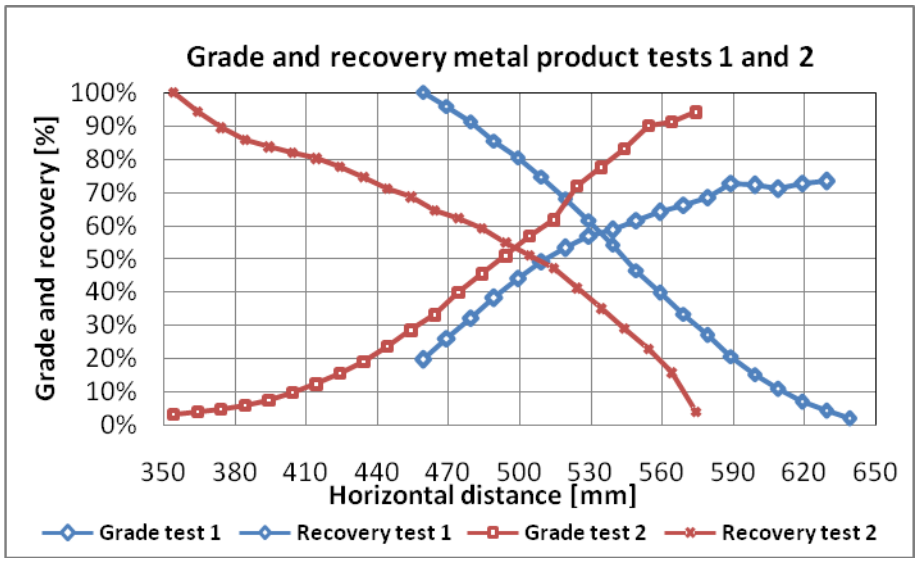


Figure 32: Product grade and recovery (yield), tests 1 and 2.

The economic value of the ECS metal product of metal concentrate is calculated by the prizes of Al and Cu. The grade and recoveries of these two metals therefore are important for the adjustment of the splitter position. In the next graph the grade and recovery as function of the distance is shown.

Figure 33 shows the grade and recovery of Al and Cu of test 2. For the same horizontal distance the recovery of Cu is roughly 20% higher than the Al recovery as a result of the longer Cu

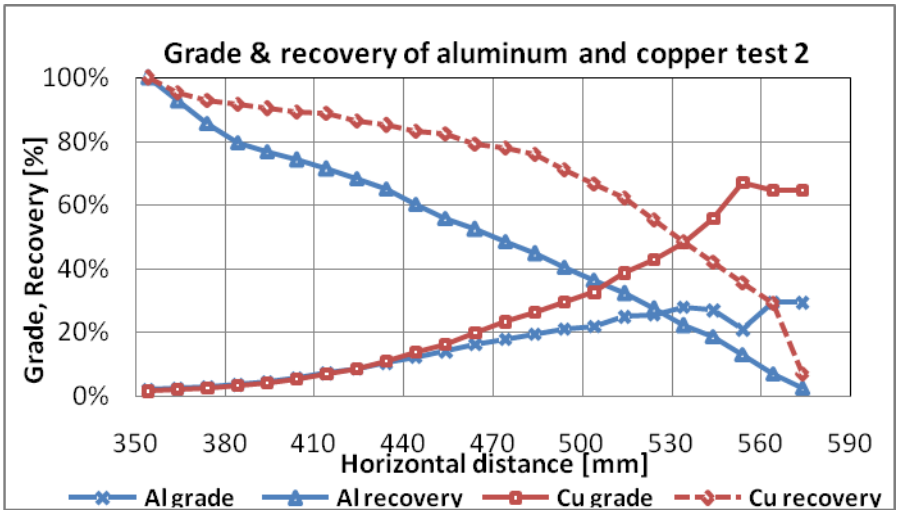


Figure 33: Grade and recovery of aluminium and copper.

trajectories.

**Relation local and product grade**

The grade measured at a certain horizontal distance will be different than the product grade. In order to investigate how the slot grade is related to the product grade these two were plotted against each other. In Figure 34 the slot (a) and the sensor (b) grade against the product grade is shown. It can be observed that a change of 10% in the slot grade will result in a 10-15% change in the product grade in the range of 30 to 50 % product grade.

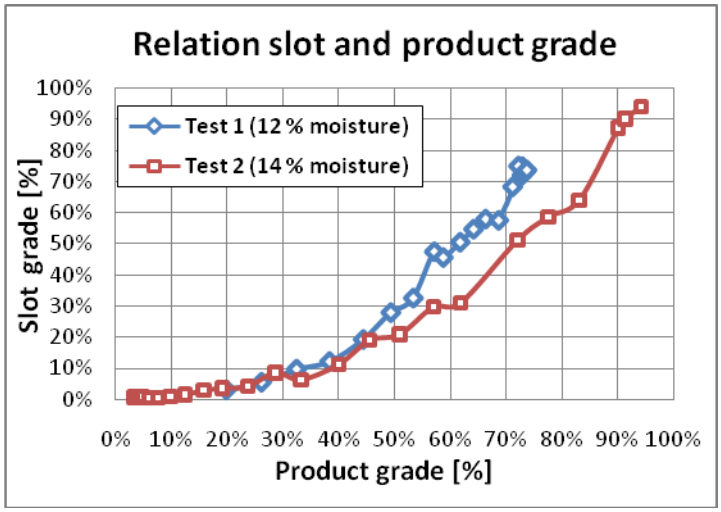


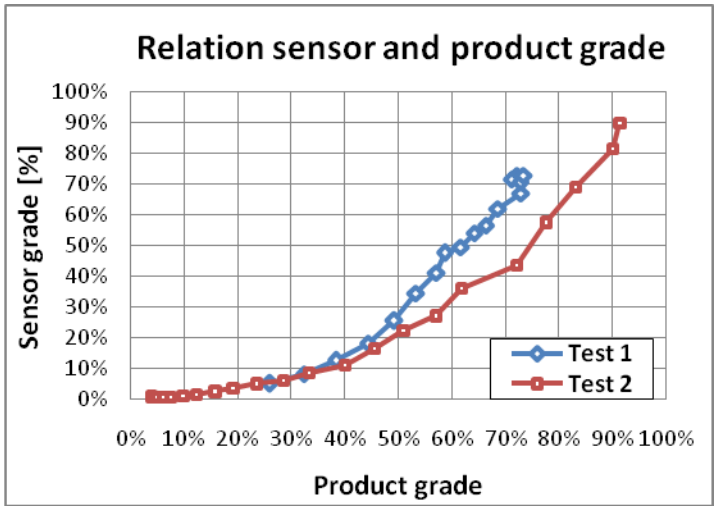


Figure 34: (a) Slot grade of the wet and the dry case and the product grade, (b) Calculated sensor grade and the product grade.

# 4 PARTICLE TRAJECTORY MODELLING

After obtaining data from the in-situ tests, the next phase in this work was to use that data and to find relations for the material and metal mass distribution as function of the horizontal distance. And to simulate a sensor system which principle is based on counting metal and all particles in a falling stream, relations to calculate the number of participles as function of the distance was required. In this chapter the derivation of the relations for number of mineral and material distribution will be presented first. Subsequently, the model or relations for metal mass and particle distribution will be explained.

## 4.1 Curve fitting mineral particles and material mass estimation

The objective of the curve fitting was to obtain formulas to determine the mass as function of distance and since the intended sensor for automated control of splitter counts particles the a relation for the number of mineral particles was also obtained. In this section a relation for the determination of the number of mineral particles as function of the distance will be derived and explained. So far only metal particles were counted. In order to count the mineral particles a hybrid sensor was used. These sensor mineral counting tests are explained in *Chapter 5.*

The number of mineral particles as function of the horizontal distance x was estimated by a power law function that was fit on the number of mineral particles. These mineral particles were counted by using the hybrid sensor described in *Chapter 5.* The formula of this trend line can be written as follows:

$$trend\ \ line(x) = \left(\frac{x_0}{x}\right)^{16,51}$$ , with $x_0$ equal to 430 mm [4.1]

The data used for the fit was measured at an ECS throughput of 9.2 t/h and a moisture content of 14%. In order to estimate the number of mineral particles for different moisture contents and throughputs the formula should be adjusted with respect to the measured throughput and moisture content. A change in moisture content will cause a shift (see Figure 26) in distance, these shift was about 15 mm for 1% change in moisture content. The adjusted formula can now be expressed as:

$$N^{minerals}(x) = \left(\frac{x_{0-}(moist - moist_{ref}) \times c}{x}\right) \times \left(\frac{T}{T_{ref}}\right)$$ , [4.2]

for the estimation of the number of mineral particles per second between a certain horizontal distance $x_1$ and $x_2$, called Δx, with width (w) the formula becomes;

$$N^{minerals}(\Delta x) = \left( \frac{x_0 - (moist - moist_{ref}) \times c}{x_1} \right)^{16,51} - \left( \frac{x_0 - (moist - moist_{ref}) \times c}{x_2} \right)^{16,51} \times \left( \frac{T}{T_{ref}} \right) \times \left( \frac{w}{w_{ref}} \right) \times total\ particles \quad , \qquad [4.3]$$

where:

| | | |
|---|---|---|
| moist | moisture content | [%] |
| $moist_{ref}$ | reference moisture content (14%) | [%] |
| T | throughput ECS | [t/h] |
| $T_{ref}$ | reference throughput (9.2 t/h) | [t/h] |
| w | width of opening 'tube' | [mm] |
| $w_{ref}$ | width of a slot (600 mm) | [mm] |
| c | a constant, 15 (shift due to moisture) | [mm] |

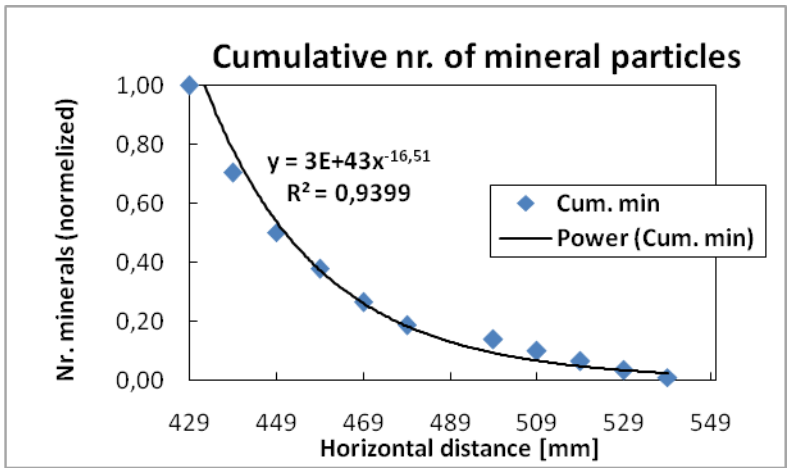


Figure 35: Trend line mineral counts.

In order to evaluate the formula and obtain data for the feed containing 12% moisture, the material from test 1 was also measured by the sensor. Test 1 contained 12% moisture and the throughput was 12 t/h. The number of mineral particles were both estimated by Eq. [4.3] and also measured in the lab.

Figure 36 (left panel) shows the measured and estimated number of mineral particles per slots per second of test 1. It can be observed that the approximation is quite close to the measured data. Figure 37 shows the estimated number of mineral particles per second for a 30 mm opening (square) at variable moisture contents and throughputs as functions of the horizontal distance. The idea was to estimate the number of mineral particles for a sensor tube of 30 mm at various conditions such as moisture content and throughput. Notice that the number of counts at a horizontal distance can be used as an indication for the moisture content of the feed. So indirectly the sensor is able to indicate the moisture content of the feed.

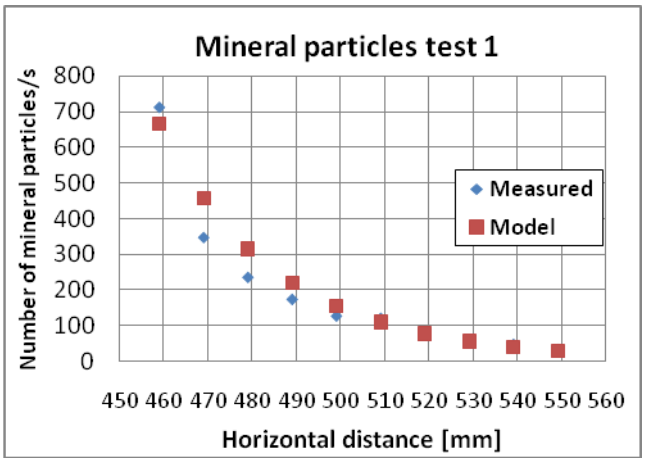


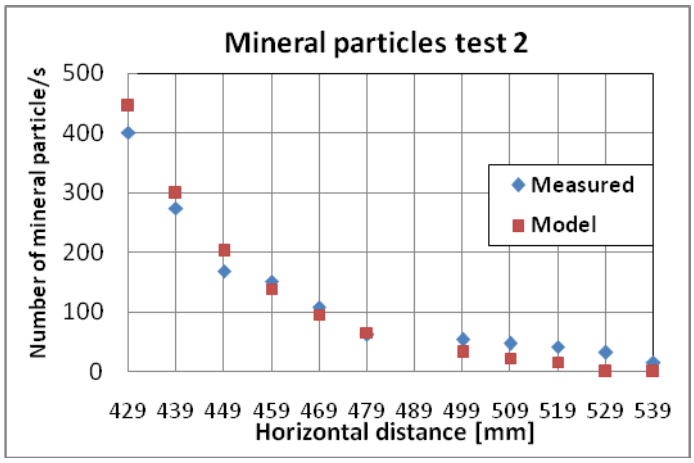


Figure 36: Experimental and modelled number of min particles, left test 1 and right test 2

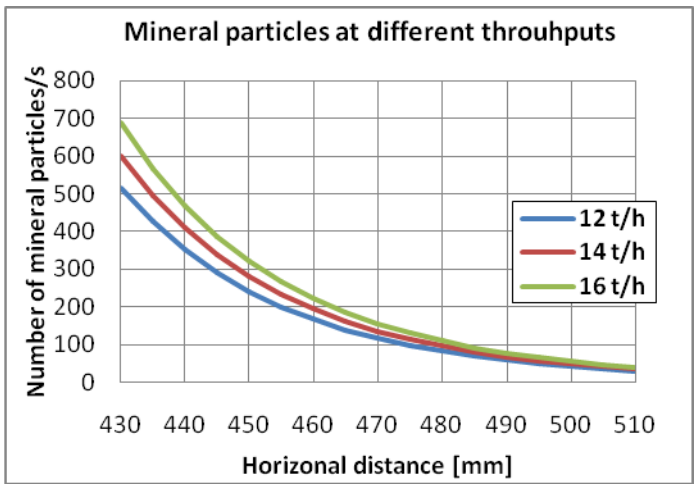


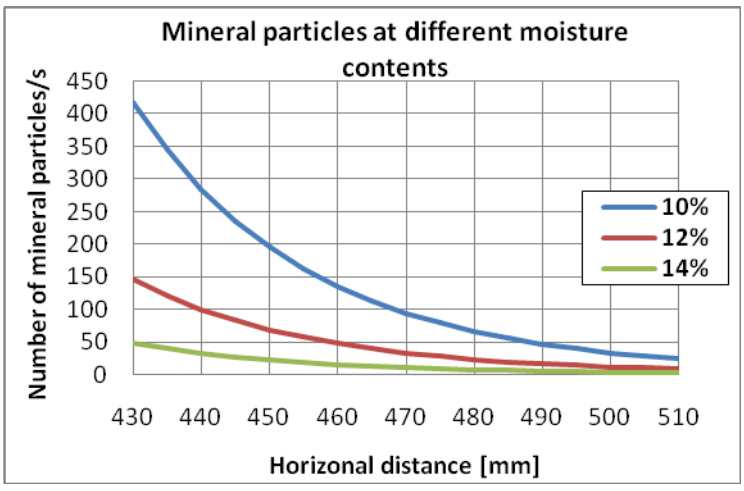


Figure 37: Modelled number of mineral particles at different throughputs and moisture contents for 30 mm tube.

**Material mass estimation**

In order to estimate the mass of the material that falls after a horizontal distance x, a power law function was fitted on the (measured) material mass per slot of test 2. It was assumed that 100 % of the material, non-magnetic fraction fell after $x_0$ which now is 349 mm. Figure 38 shows the fit and measured results. The formula of the trend line for the material mass distribution as function of the horizontal distance can be written as follows:

$$Cum.\ material\ mass(x) = \left(\frac{x_0}{x}\right)^{10} \qquad [4.4]$$

Again taking into account the shift in horizontal distance as a result of the moisture content the formula becomes:

$$Cum.\ material\ mass(x) = \left(\frac{x_0 - (moist - moist_{ref}) \times 15}{x}\right)^{10}, \qquad [4.5]$$

where

| | | |
|---|---|---|
| $x_0$ | 349 mm | |
| x | horizontal distance | [mm] |
| moist | moisture content | [%] |
| $moist_{ref}$ | reference moisture content is 14% | [%] |

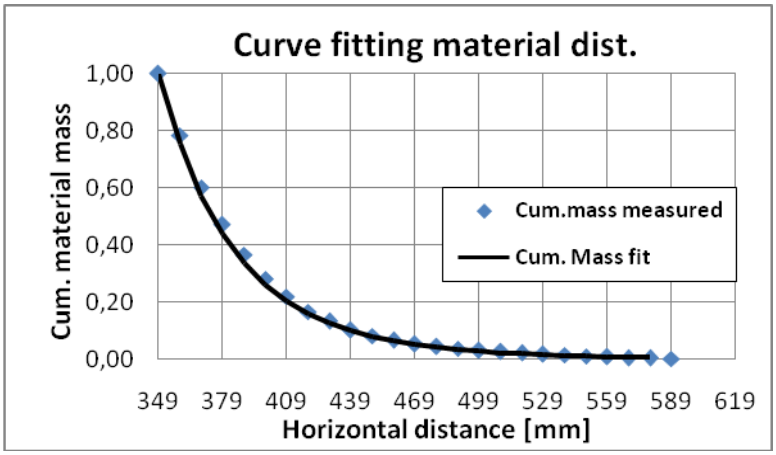


Figure 38: Trend line material mass distribution.

## 4.2 Model for metal distribution

In this section the metal mass and particle distributions that were obtained during the in-situ tests were further fitted. From these fits a formula was derived that calculates the metal mass as function of the distance. And also a formula was derived that calculates metal particles as function of the distance in order to simulate the hybrid sensor that counts particles. The objective of obtaining these relations was to use it for the simulating the hybrid sensor described in *Chapter 5.1.*

### 4.2.1 Formula metal mass

The metal mass can be distinguished in two populations. The first population particles were deflected by the ECS, the so called free metal particles. And the second population of particles were dragged in the main mineral stream *(see Section 3.2.2)*.The population of particles that is deflected by the ECS can be estimated by a normal distribution which is expressed as:

$$Deflected\ metal(x) = \alpha \times normcdf(x, \mu, \sigma), \qquad [4.6]$$

In which the constant Ω is a correction factor for the metal particles that were not accumulated in the slots, μ and σ are the mean and standard deviation in mm and x is the horizontal distance in mm. Notice that the cumulative normal distribution is used indicated with cdf. If now the particles that are dragged into the main mineral stream and the metal particles that are deflected by the ECS are combined, a model for the metal mass distribution is obtained for each metal type and size fraction. The formula as function of the horizontal distance can now be expressed as:

$$Dist.\ metal(x) = f \times defl.\ metal + (1-f) \times rel.material\ mass\ , \qquad [4.7]$$

In which f, called the free factor, is a constant that represents the fraction that is deflected by the ECS. The difference between the measured and estimated metal mass is calculated as follows:

$$Difference = \frac{(rel.mass - model)^2}{model}, \qquad [4.8]$$

The difference was calculated in order to minimize the sum of the differences by using the solver function of Excel.

Example of 2-4 mm Al particles

To explain the idea and the method an example of Al 2-4 mm particles will be worked out by the help of Table 4. The measured mass of Al 2-4 mm particles is shown in column (a) and the normalised mass in column (b). In columns (c) and (d) the same is done for the material mass. In order to construct column (e), formula [4.6] was used.

The values given in column (f) are calculated with formula [4.7] and is called model in Figure 39. This so called model gives the metal mass distribution as function of the horizontal distance and taking into account that part of the metal particles are dragged in the main mineral stream. However in order to obtain the best fit, the sum of the differences between measured and model was minimized by changing the parameters: alpha (α), mean (μ), sigma (σ) and free and by constraining the sum of the model (f) to one. This procedure was done for all the metal types per size fraction of test 1 (12% moisture) and test 2 (14% moisture), for the metal mass and the number of metal particles. One remark is that the 4-5.6 mm particles could not be fitted and was therefore estimated by looking at the results of *Section 3.2.2*.

**Table 4: Estimated mass distribution Al 2-4 mm.**

| | | x1 | x2 | (a) | (b) |
|---|---|---|---|---|---|
| **Slot no** | **x [mm]** | **x left [mm]** | **x right [mm]** | **Al 2- 4 mm measured mass [g]** | **Normalised to 1** |
| **1** | 354 | 349 | 359 | 1.39 | 0.08 |
| **2** | 364 | 359 | 369 | 1.13 | 0.06 |
| **3** | 374 | 369 | 379 | 1.14 | 0.06 |
| **4** | 384 | 379 | 389 | 0.46 | 0.03 |
| **5** | 394 | 389 | 399 | 0.52 | 0.03 |
| **6** | 404 | 399 | 409 | 0.42 | 0.02 |
| **7** | 414 | 409 | 419 | 0.63 | 0.03 |
| **8** | 424 | 419 | 429 | 0.68 | 0.04 |
| **9** | 434 | 429 | 439 | 0.813 | 0.04 |
| **10** | 444 | 439 | 449 | 0.87 | 0.05 |
| **11** | 454 | 449 | 459 | 0.74 | 0.04 |
| **12** | 464 | 459 | 469 | 0.82 | 0.04 |
| **13** | 474 | 469 | 479 | 0.668 | 0.04 |
| **14** | 484 | 479 | 489 | 0.9 | 0.05 |
| **15** | 494 | 489 | 499 | 0.9 | 0.05 |
| **16** | 504 | 499 | 509 | 0.99 | 0.05 |
| **17** | 514 | 509 | 519 | 0.801 | 0.04 |
| **18** | 524 | 519 | 529 | 1.24 | 0.07 |
| **19** | 534 | 529 | 539 | 0.77 | 0.04 |
| **20** | 544 | 539 | 549 | 0.63 | 0.03 |
| **21** | 554 | 549 | 559 | 0.83 | 0.05 |
| **22** | 564 | 559 | 569 | 0.663 | 0.04 |
| **23** | 574 | 569 | 579 | 0.381 | 0.02 |
| | | | Total mass | 18.386 | 1 |

| (c) | (d) | (e) | (f) | (g) |
|---|---|---|---|---|
| **Total material mass** | **Normalised to 1** | **Free metal deflected metal** | **Model** | **Difference (measured –model )$^2$/model** |
| **324.32** | 0.218 | 0.003504 | 0.150327 | 0.00032529 |
| **273.79** | 0.184 | 0.005199 | 0.12761 | 3.8095E-07 |
| **198.05** | 0.133 | 0.007505 | 0.093485 | 0.00485299 |
| **158.45** | 0.106 | 0.010542 | 0.076219 | 0.00600802 |
| **127.85** | 0.086 | 0.014411 | 0.063356 | 0.00198999 |
| **91.93** | 0.062 | 0.019169 | 0.048324 | 0.00288558 |
| **76.08** | 0.051 | 0.024812 | 0.042804 | 4.4003E-05 |
| **50.07** | 0.034 | 0.031252 | 0.032861 | 0.00077996 |
| **43.05** | 0.029 | 0.038305 | 0.031847 | 0.00222768 |
| **30.04** | 0.020 | 0.045686 | 0.028181 | 0.00247587 |
| **22.06** | 0.015 | 0.053022 | 0.026815 | 1.4156E-05 |
| **19.01** | 0.013 | 0.059881 | 0.027567 | 4.9175E-06 |
| **12.28** | 0.008 | 0.065808 | 0.026334 | 0.00271531 |
| **10.73** | 0.007 | 0.070375 | 0.027056 | 4.8722E-05 |
| **8.86** | 0.006 | 0.073234 | 0.027094 | 0.00018868 |
| **6.57** | 0.004 | 0.074158 | 0.026331 | 4.9573E-05 |
| **9.33** | 0.006 | 0.073074 | 0.02726 | 0.00139031 |
| **5.84** | 0.004 | 0.070068 | 0.024709 | 0.00669647 |
| **4.97** | 0.003 | 0.065377 | 0.022835 | 0.00034838 |
| **4.6** | 0.003 | 0.059360 | 0.020773 | 0.00131684 |
| **3.96** | 0.003 | 0.052445 | 0.018306 | 0.00189294 |
| **6.28** | 0.004 | 0.045090 | 0.017061 | 0.00045196 |
| **2.15** | 0.001 | 0.037723 | 0.012845 | 0.00119052 |
| **1490.27** | 1 | 1.000000 | 1.000000 | 0.03789854 |

| | |
|---|---|
| **Free factor** | 0.69 |
| **Alpha** | 1.12 |
| **Mean** | 503.60 |
| **Standard deviation** | 60.5 |

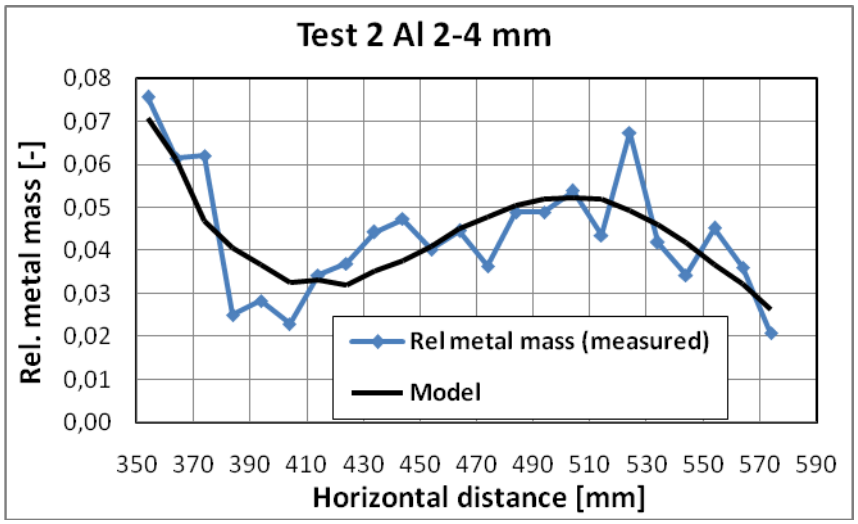


**Figure 39: Example of the model for the Al 2-4 mm fraction.**

Collecting the four parameters of each metal type per fraction per test resulted in the Table 5 (test 1) and Table 6 (test 2).The mean increases with increasing particles size which means that the particles have longer particle trajectories with increasing particle size. Increasing particle size also shows an increasing trend of the standard deviation meaning that the bigger particles were widely distributed. And an increase in moisture content will result in more particles being dragged in the main mineral resulting in smaller free factors as observed in the two tables. The four parameters based on the number of metal particles found per slot are shown in *Appendix C*. In order to estimate the number of metal particles going through the sensor tube, the four parameters based on fitting with the number of metal particles were used. And for estimation of the metal mass the four parameters based on fitting with the metal mass were used.

**Table 5: The parameters alpha, mean, standard deviation and free for test 1**

| Test 1 | Alpha | Mean [mm] | Standard dev. [mm] | Free |
|---|---|---|---|---|
| **Cu 1-2 mm** | 1.03 | 534 | 30.00 | 0.66 |
| **Cu 2-4 mm** | 1.05 | 546 | 47.17 | 0.95 |
| **Cu 4-5.6 mm** | 1.30 | 579 | 62.14 | 1.00 |
| **Al 1-2 mm** | 1.04 | 500 | 41.06 | 0.6 |
| **Al 2-4 mm** | 1.24 | 517 | 65.82 | 0.92 |
| **Al 4-5.6 mm** | 1.36 | 544 | 82.03 | 1.00 |

**Table 6: The parameters alpha, mean, standard deviation and free for test2**

| Test 2 | Alpha | Mean [mm] | Standard dev. [mm] | Free |
|---|---|---|---|---|
| **Cu 1-2 mm** | 1.03 | 495 | 50.00 | 0.54 |
| **Cu 2-4 mm** | 1.26 | 535 | 52.83 | 0.86 |
| **Al 1-2 mm** | 1.11 | 475 | 33.68 | 0.44 |
| **Al 2-4 mm** | 1.13 | 504 | 60.48 | 0.68 |
| **Al 4-5.6 mm** | 1.20 | 544 | 72.71 | 1.00 |

### 4.2.2 Formula for number of metal particles

The number of metal particles can be estimated as function of the horizontal distance with the derived model for metal distribution and using the four parameters based on the fits with the number of metal particles. The four parameters are not only a function of metal type and size but also moisture content. It was found that the four parameters between the two tests were different from each other. To obtain the four parameters for moisture contents different than 12% and 14%, linear interpolation was used. The formulas for the four parameters in than expressed as:

$$
\begin{aligned}
free &= free_{12} + \frac{(moist - moist_{12})}{2}(free_{14} - free_{12}) \\
\alpha &= \alpha_{12} + \frac{(moist - moist_{12})}{2}(\alpha_{14} - \alpha_{12}) \\
\mu &= \mu_{12} + \frac{(moist - moist_{12})}{2}(\mu_{14} - \mu_{12}) \\
\sigma &= \sigma_{12} + \frac{(moist - moist_{12})}{2}(\sigma_{14} - \sigma_{12})
\end{aligned}
\qquad [4.9]
$$

In which the 12 and 14 stands for moisture content in percentage. Now two relations can be made by using the Eq.[4.7], one for metal mass distribution, a formula that can estimate the metal mass after a horizontal distance x, and the second formula that can estimate the number of metal particles through an opening between a distance of $x_1$ and $x_2$. In the two relations Eq. [4.7] will be indicated as model and not rewritten again to avoid long formulas. However it should be noticed the normal distribution function calculates the fraction before a point x not after, therefore for the metal mass after a distance x, it should subtracted from one. Also notice that x is a variable in the model. The formula for the metal mass as function of the horizontal distance is now written as:

$$Metal\ mass(x) = T \times 1000 \times \frac{\tau}{3600} \sum_{metal\ type} [1 - (model\ dist.metal) \times conc._{metal}], \qquad [4.10]$$

In which the Al and Cu metal masses is estimated in kg, that will fall after a horizontal distance x. With this relation for a fixed splitter position the metal yield can be estimated. However for the simulation of the hybrid sensor not the metal mass but the number of particles was required since the hybrid sensor counts particles. So the number of metal particles through an opening as function of the distance x can be expressed as:

$$N_{metal}(\Delta x) = \left(\frac{T}{T_{ref.}}\right) \times \left(\frac{w}{w_{ref}}\right) \times \left(\frac{\tau}{t_{ref}}\right) \times \sum_{metal\ type} [(model\ dist.metal)_{\Delta x} \times meas._{nr.metal}], \qquad [4.11]$$

where

| | | |
|---|---|---|
| T | throughput ECS | [t/h] |
| τ | integration time | [s] |
| conc. | concentration per metal type in feed | [kg] |
| $t_{ref}$ | collection time test | [s] |
| w | opening | [mm] |
| $w_{ref}$ | width of a slot (600 mm) | [mm] |
| $meas._{nr\ metal}$ | nr of metal particles measured | |

Now the metal, material and the number of mineral particles can be estimated as function of the horizontal distance. In the next section an ECS operating with a fixed and moving splitter is simulated based on the formulas derived in this section.

# 5 HYBRID SENSOR

For the automated control of the splitter and online quality inspection, a hybrid sensor was developed and tested by *(Rahman and Bakker, 2012).* They introduced a hybrid sensor that can count metal particles and all the particles in a falling fine particles stream such as BA from an ECS. The aim of this work was to present a strategy for the control of the splitter distance for maximal value recovery by using this developed hybrid sensor. Therefore this section will explain the purpose and principle of the sensor first. After which results from mineral counting tests done with sensor will be presented.

## 5.1 Description of the hybrid sensor

In order to understand the how the splitter can be controlled by using the developed hybrid sensor, knowledge about its functionality and what can be measured by use of the hybrid sensor in a falling stream of fine particles is essential. In this section the purpose and principle of the sensor will be explained. Moreover this chapter also explains the sensor parameters.

### 5.1.1 Purpose and principle

The purpose of the sensor is to place it in the ECS falling stream (trajectory fan). In this falling stream the hybrid sensor should count the metal particles and all the particles. In this way online quality inspection of the ECS metal product can be done. It even allows for control of the splitter by using a controlling unit with certain settings.

The hybrid sensor consists of two sensor units, an infrared sensor (IRS) and an electromagnetic sensor (EMS). The IRS is meant to detect all the particles passing through it, while the EMS solely counts the metal particles. In Figure 40 the setup of the hybrid sensor and the data processing unit are illustrated. The particles passes through a tube, called sampling tube which guides the particles to central compartment. In the top section of the central compartment the IRS is mounted that detects all the passing particles and on the bottom section the EMS is mounted that detects the metal particles. The raw data in form of signals is send to a signal processing unit. In the signal processing unit the signals are amplified and processed resulting in particles counts. In order to depress noise interferences special arrangements were taken The EMS detects metals and in order to obtain counts of the NF metals of BA also special measures were taken *(Rahman and Bakker, 2012)*. The principle of the individual sensors IRS and EMS is explained in more detail in *Appendix C.* And for the sensor specialists the paper by *(Rahman and Bakker, 2012)* is recommended in which the hybrid sensor is described in more detail.

From the counts, the ratio of the metal and all the particles counts can be obtained called count ratio z. And in order to calculate the grade for online quality inspection a calibrated factor called k-value, the ratio of average mineral particle mass and average metal particles is needed.

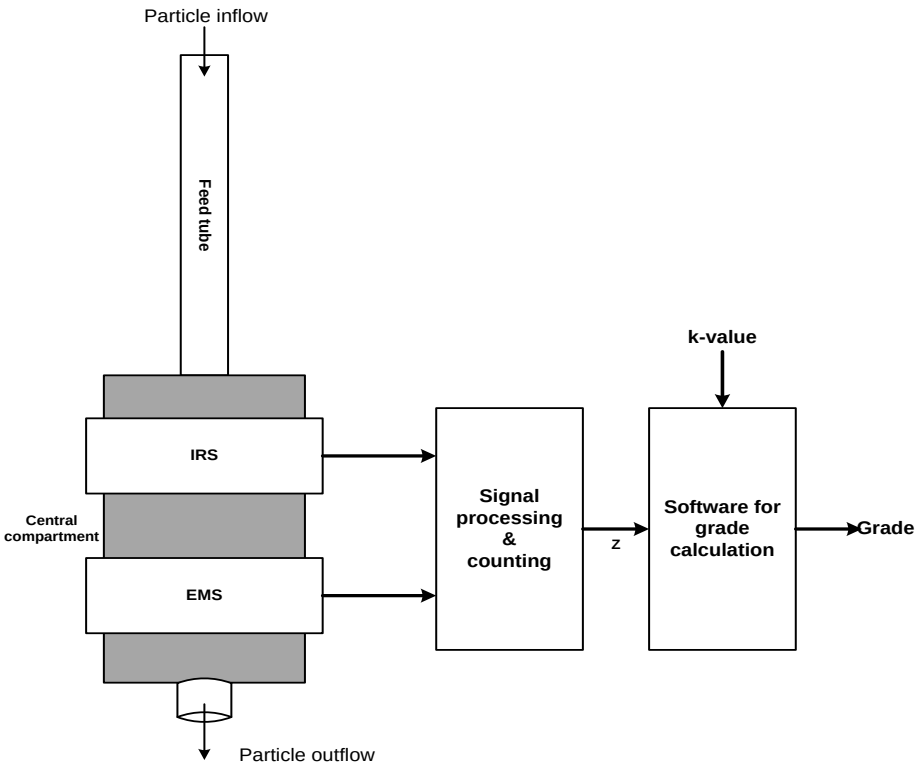


**Figure 40: Schematic diagram of the hybrid sensor system with the necessary hardware.** ***Source: personal notes during communications with Rahman, 2012.***

### 5.1.2 Parameters and grade calculation

The quality inspection of the sensor in the ECS falling stream is based on the grade. This measured grade can be even used for controlling the splitter. In this section the hybrid sensor parameters that lead to the grade calculation will be explained.

In order to calculate the grade two factors are important, the count ratio z and the k-value and correction factor for if the sensor misses particles due to simultaneously falling particles. The formulas for z, k and C can be expressed as follows:

$$z = \frac{N^{EMS}}{N^{IRS}} \qquad k = \frac{m^{non\text{-}metal}}{m^{metal}} \qquad C = \frac{C^{IRS}}{C^{EMS}} \qquad [2.9]$$

The metal grade G is related to the sensor measurements as follows *(Rahman and Bakker, 2012.)*

$$Grade = \frac{z}{(C - z)k + z} \qquad [2.8]$$

In which G is the metal grade, z (0<z<1) is the count ratio of sensor counts, C is the ratio of sensor count correction factors $C^{IRS}$ and $C^{EMS}$ .

**Correction factor**

As a result of particles falling simultaneously the sensor may count more than one particle as a single count. The chance of particles falling simultaneously increases with increasing feed rates. However it was found by *(Rahman and Bakker, 2012)* that the number of misses was (quite) repeatable for a known feet rate giving the ability to introduce correction factors $C^{IRS}$ and $C^{EMS}$. If however the correction factors for both sensors are almost equal, the correction ratio C would be one, and no correction will be required. In *Appendix C* the graphs in which the correction factor of each individual sensor as function of the feed rate is presented.

**k-value**

The k-value is required for the calculation of the grade and should be known prior to the online quality inspection. And since the grade might be used as one of the criteria's for automated control of the splitter, the trend of the k-value will be evaluated in the next section.

## 5.2 Laboratory sensor tests

After removal of the metal particles the minerals were counted with the sensor to obtain possible control parameters such as the count ratio z and the grade for which the number of the mineral particles was required. Also the will the k-value be presented and evaluated.

### 5.2.1 Material and method

After removal of the metal particles, the material per slots was fed through the sensor in order to count the mineral particles. For test 1 the first 10 slots (459-549 mm) were selected and for test 2 slots 9 till 20 (934-544 mm). The objective of these tests was to count the mineral particles after which the average particle mass, k-value and the count ratio z could be determined. The setup of the experiment is shown Figure 40. The material was slowly fed via a vibrating feeder with a v-shaped end in order to feed the sensor particle by particle. In the bottom, a bucket was placed to collect the falling particles and store them afterwards. Due to an accident the number of mineral particles in slot 15 of test 2 could not be measured.

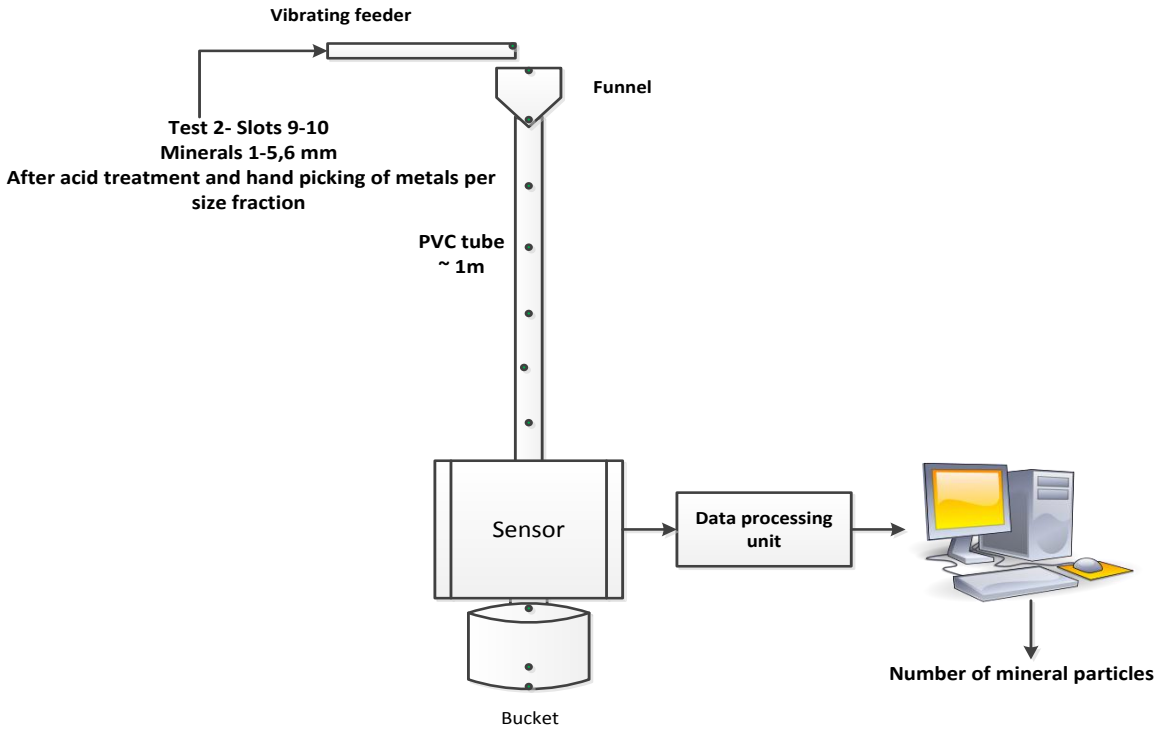


Figure 41: Setup sensor test in the lab, counting the mineral particles.

### 5.2.2 Results

In this section the number and masses of the mineral and metal particles will be discussed. Subsequently, the k-value and count ratio z of the tests 1 and 2 will be compared.

**Number of particles**

In Figure 42 the mineral and metal particle counts of test 1 (12% moisture) and test 2 (14% moisture) are shown, including the count ratio of the metal and total number of particles, the so called count ratio z. The number of mineral particles shows a monotonic increasing function towards the head pulley (decreasing distance).

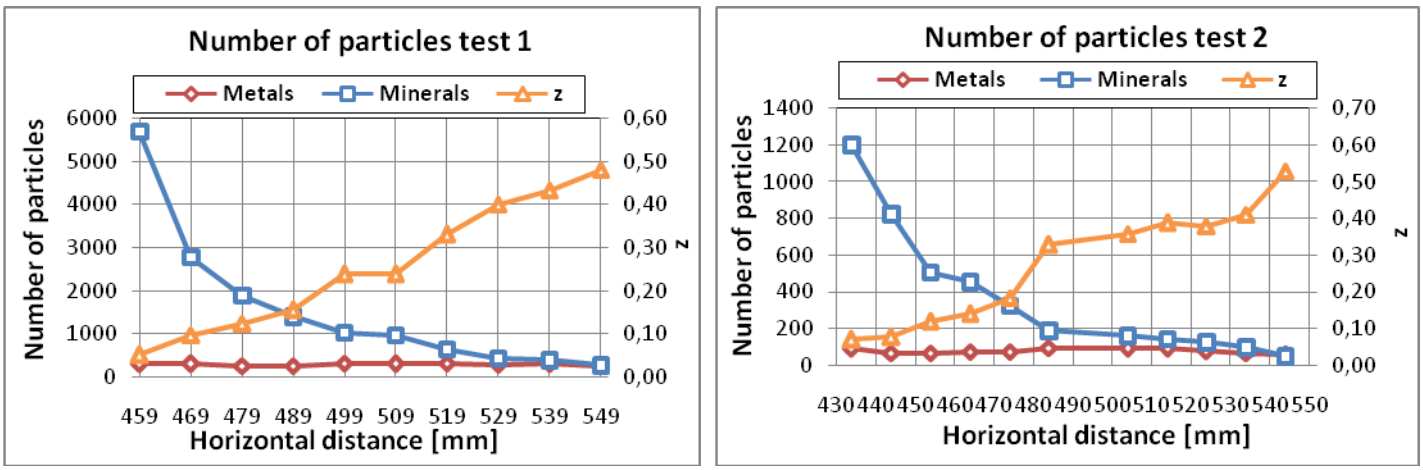


Figure 42: Number of particles and count ratio z. Left test 1 and right test 2

**Average mineral and metal particle mass**

The average mineral and metal mass is presented to show how the mass varied with distance. Figure 43 gives the average mineral and metal particle mass. For test 1 the average particle masses are relatively constant while for test 2 the metal particle mass increases rapidly from 505 mm, namely due to the Cu particle mass.

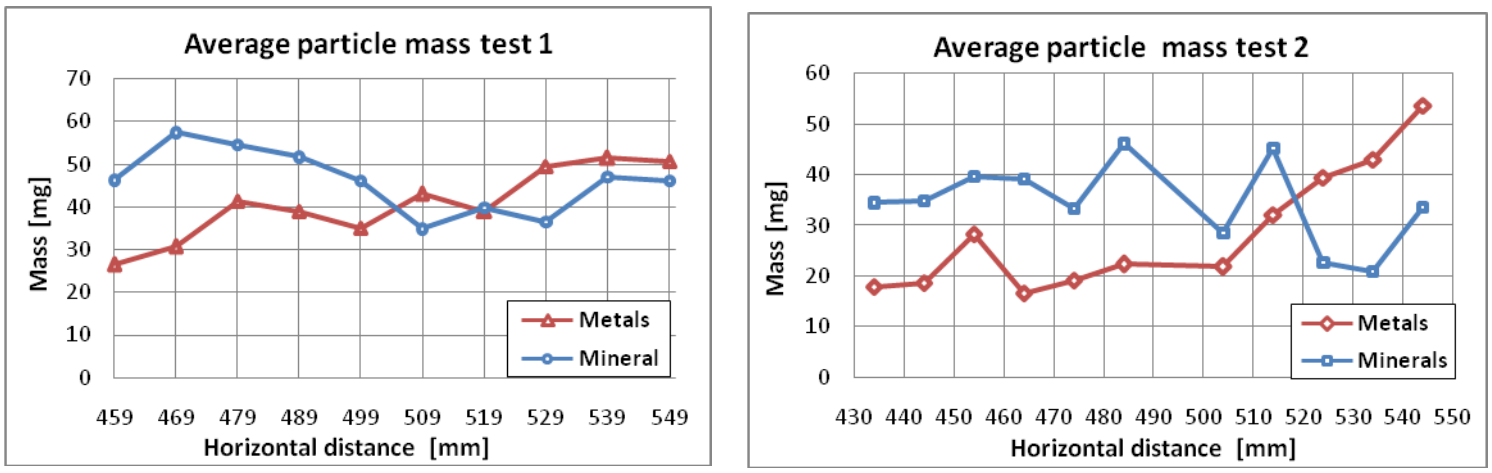


Figure 43: The average particle mass of metals and minerals. Left test 1 and right test 2.

**k-value**

For the control of the splitter with grade as criteria, the k-value a calibrated k-value is required. In this section the trend of the k-value and variation will be evaluated. Figure 44 shows the k-value as function of the horizontal distance of test 1 (12 % moisture) and test 2 (14% moisture). For test 2 in the range of 430-500 mm the average k-value was around 1.7 and for distances greater than 500 mm it was 0.6. For test 1 it was found that from 460-500 mm the k-value was 1.4 and 0.8 for distances greater than 500 mm. The k-value decreases with increasing horizontal distance. This decrease in k-value can be justified by the increase of the average metal particle mass with increasing horizontal distance. The k-value of the two tests differentiates at a certain horizontal position. This means that the k-value fluctuates as result of variations in feed such as varying moisture contents.

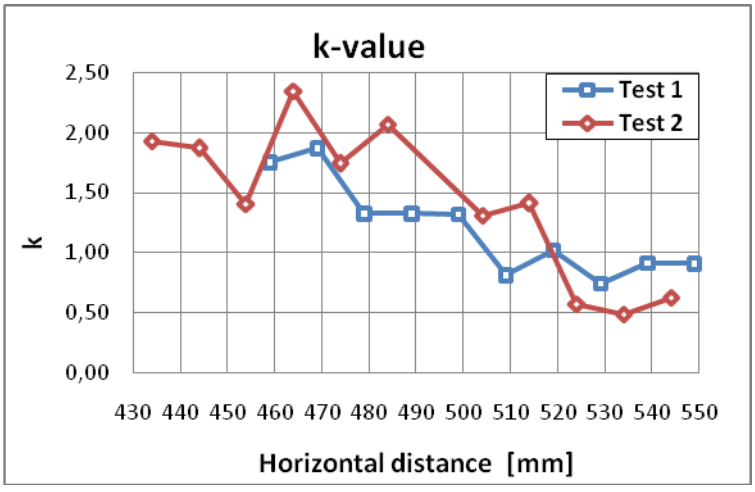


Figure 44: The k-value for test 1 (12 % moisture) and test 2 (14% moisture) BA feed.

The k-value was determined in the laboratory. Due to the acid treatment fines adhering to the particles may have been washed away which could have had an influence on the k-value as the fines add up to the average mass of a particle. In the work done by Rahman and Bakker (2013) the k-value was also investigated by doing in-situ experiments with the hybrid sensor. They found for Belgium BA feed containing 15% moisture a k-value of about 1.22 ±0.49, which is close to 1.3 found in this work. For quite dry feed (4.6% moisture) however they found a k-value of about k = 0.60 ± 0.20. This drop in k-value may have occurred as mineral particles may hold more moisture compared with metal particles as some of the mineral particles are porous. It also possible that at high moisture contents on during in-situ measurements, particles, mainly the mineral particles since they are in majority can stick to each other resulting in bigger (mineral) particles and thus a higher average mineral particle mass that will result in a higher k-value. It should also stressed that there methodology was different than the method for material analysis used in this work moreover the sources of BA was also different which may have a result on particle size distribution that will affect the average particle masses.

**Count ratio z**

Beside the option of controlling the splitter by using the criteria of the grade which is dependent on the k-value, another option to is to look at the count ratio z. Due to feed changes the particle trajectories may change and thus the amount of particles found at a certain distance. And as the z is count ratio of the metal and total particles, the z can change due to changes in the feed. The variation in z will be evaluated by comparing tests 1 and 2. Figure 45 shows the count ratio z as function of the horizontal distance. For test 1 the z is lower than test 2 at the same horizontal distance as a result of the difference in moisture content. This means that variations in moisture content cause a shift in the z as a result of the change in mineral particle trajectories. For example at a horizontal distance of 479 mm, z was 0.12 for a feed containing 12% moisture (test 1) and if the moisture content increases to 14% (test 2) the same z (0.12) is now found at 454 mm, so there is shift in distance of 25 mm.

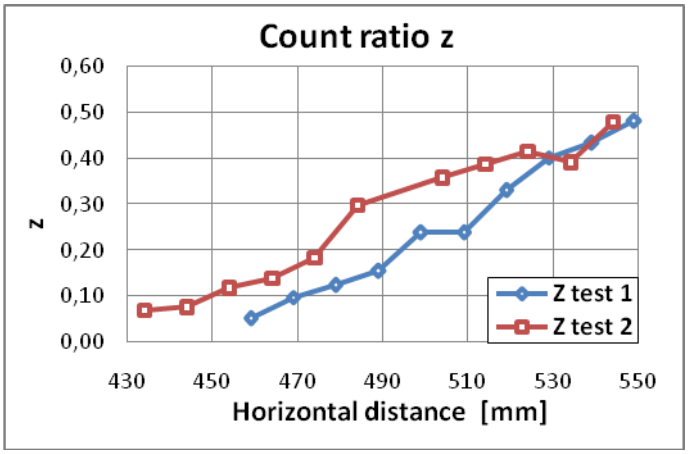


Figure 45: The count ratio z for tests 1 and 2

### 5.2.3 Sensor statistics and processing capacity

Estimated maximum measurement range for the sensor for both conditions of quite dry feed (assume <10% moisture no change) and very wet feed (assume >16% moisture no change) is 440-550 mm (*see Figure 46*), assuming the sensor tube of 30 mm diameter is 5 mm from the splitter. Maximum allowable physical feed rate without losing any particle is 5 metal particles per second for the EMS and 13 particles per second for the IRS. However, seeing that the number of metal particles is always quite small, the chance of missing particles is solely due to the total number of particles. In that view, the maximum physical feed rate for the sensor is estimated at 20 particles per second without significant errors. Above this count, a correction factor must be implemented as a function of splitter position (shows level of 14% moisture or 12 %moisture feed if splitter is at set-point) and number of IR counts.

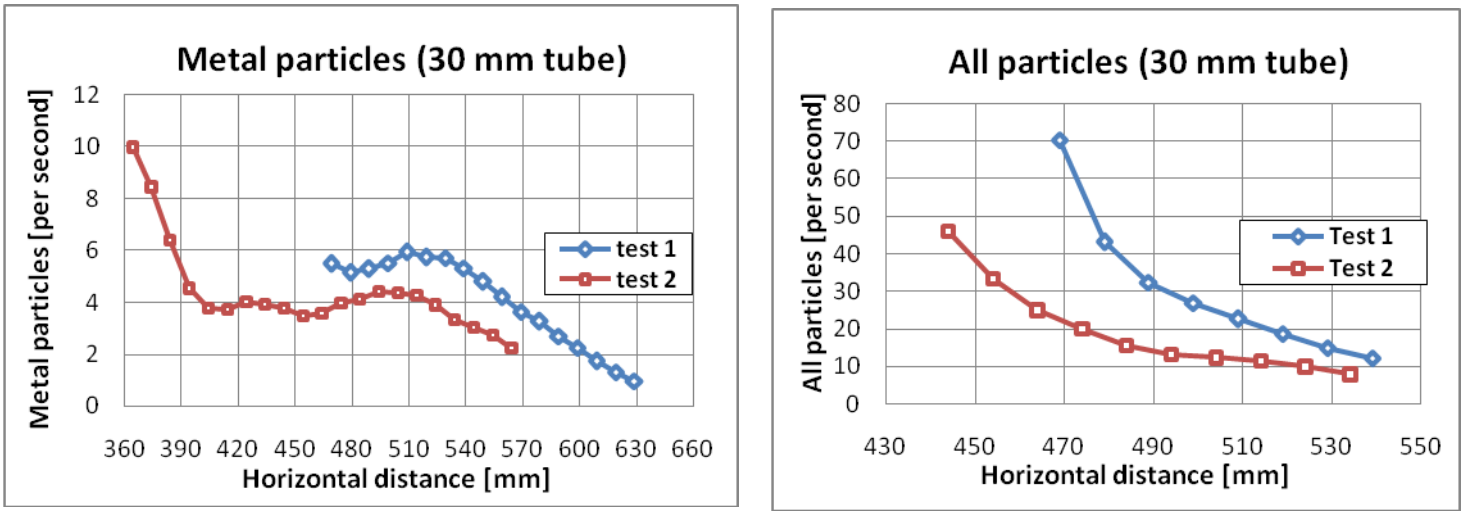


**Figure 46: Capacity requirements for: (a) EM sensor (metal particles) and (b) IR sensor (all particles). Taking a square shape opening of 30 mm in length**

**Integration time**

The required integration time can be estimated by looking at the measured particles per second. If the feeding rate for metal particles is around 4 particles per second, and a sampling error of 5% is acceptable the required number of metal particles according to the simplified Gy's formula is 400. This means that the integration time should be 100 seconds. However an integration time of 60 seconds is more practical and would result in a collection of 240 metal particles with 6.5% sampling error. Moreover the expected variation Δz as a result of feed fluctuations for 240 particles is 0.012 (see red line in Figure 47) and for 400 particles Δz is 0.01 if $z_{SET}$ =0.18. Also possible is to use interval measurements in which M samples are averaged with each $N^{metal}$ particles. Interval measurements reduce the effect of feed fluctuations.

$$z = \frac{N^{metal}}{N^{total}}$$

$$\Delta z = \sqrt{\left(\frac{\Delta N^{metal}}{N^{total}}\right)^2 + \left(\frac{N^{metal}}{N^{total^2}}\right)^2 \times (\Delta N^{total})^2}$$

$$\Delta N^{metal} = \sqrt{N^{metal}}$$

$$\Delta N^{total} = \sqrt{N^{total}}$$

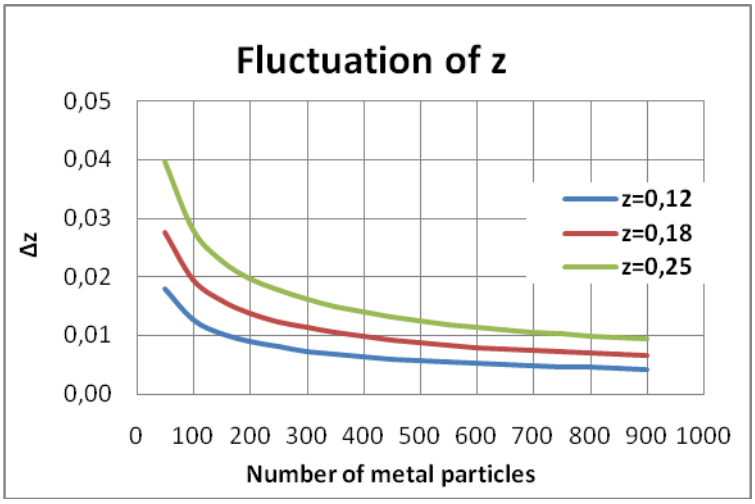


Figure 47: Number of particles and fluctuation in z-value.

# 6 ECONOMICAL OPTIMUM SPLITTER POSITION AND SIMULATION

In order to assess how the hybrid sensor should react on feed and what strategy for the control of the splitter results in the highest revenues fixed and moving splitter were simulated. In this chapter the results of these simulations are presented. However prior to the simulations, the optimal splitter position and set point were required. In *Section 6.1* the economical splitter position is presented based on the data from tests 1 and 2.

## 6.1 Economical optimum splitter position

The maximal value extraction will not only correspond with a splitter position but also with a product grade (quality). In this chapter the profit (revenues-costs) of the ECS metal as function of the metal grade will be calculated in order to determine the optimal product grade.

**Economic model**

The splitter plate of the ECS divides the ECS products in a mineral and a metal product. The metal product is then transported from the processing site to a central upgrading plant where it is separated in a LNF metal product mainly consisting of aluminium and a HNF metal product, high in copper concentration. After this separation, the minerals that were in the ECS metal product is land filled, for which a fee is paid. The ECS mineral product however stays on the ECS processing site and does not contribute to any kind of cost. In Figure 48 a schematic diagram of the ECS metal product flow from the treatment plant to the upgrading plant is shown. The correct splitter position is a balance between, the NF metals that goes with the ECS mineral product and thus is a loss, and the quality of the metal product. More mineral in the metal product means more land filling and thus higher costs. The same applies for transportation of the ECS metal product to the upgrading plant and more minerals in the metal product results in more mass to be transported unnecessary. The optimal cut point, splitter position is therefore determined by the maximal value extraction of the ECS NF metals product.

For the calculation three types of cost are taken into account, the cost of transporting the metal product from the ECS plant to the central upgrading plant, the cost of land filling the minerals that was in the metal product and the cost of further processing. For the revenues the HNF and the LNF products are considered separately. The prices of the two products were extracted from the LME website, for the HNF metal product the cupper price and for the LNF metal product the aluminium price. In practise just fraction of the LME price is paid by the smelter this fractions appears to be 64% for the HNF and 50% for the LNF. For the simplification of the calculations it was assumed that there is a perfect separation during the upgrading and that all the metals from that was in the ECS metal products is recovered. For the ECS machine on the processing plant it was assumed that the fraction NF metal lost in the ‘magnetic fraction ’is negligible, which is a reasonable assumption for this project. For the calculation of the revenues, aluminium and copper metal masses per slots were used. Since test 2 was measured close to the ECS belt, the data of test 2 was used.

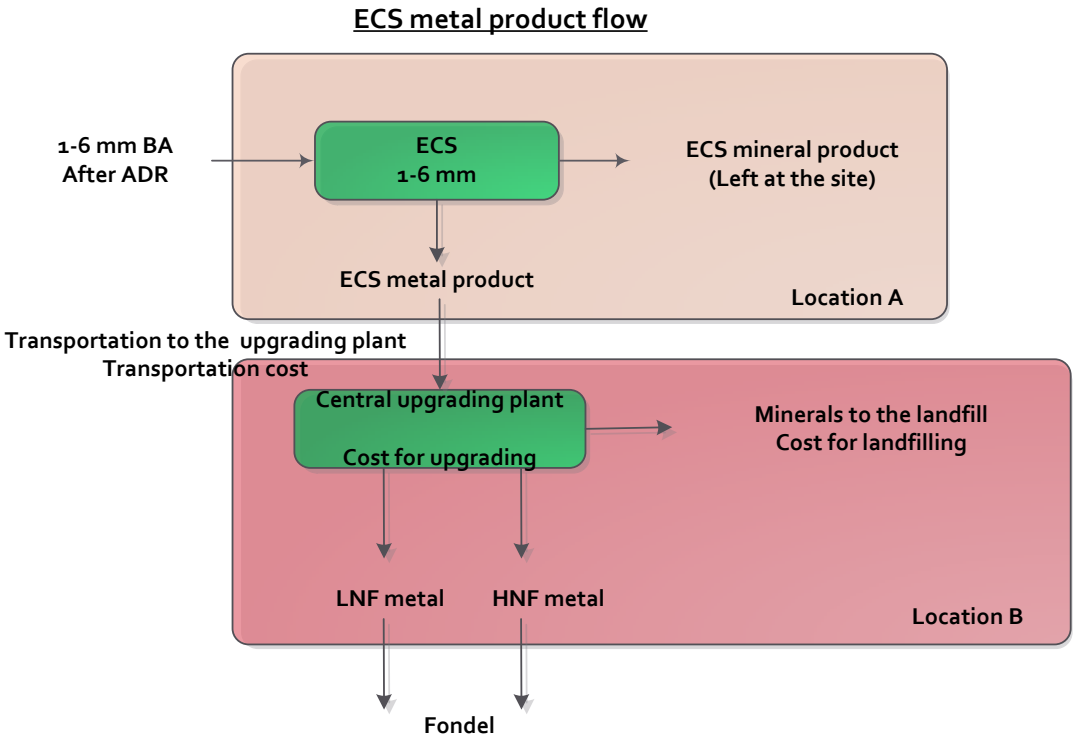


Figure 48: Illustration of ECS metal product flow.

$$revenue = Cu_{rev} + Al_{rev} - \sum costs$$
$$= (fract._{LME\ Cu\ price} \times Cu_{mass}) + (fract._{LME\ Al\ price} \times Al_{mass})$$
$$-(cost_{transportation} + cost_{processing} + cost_{landfilling}) \quad [4.12]$$

| | |
|---|---|
| Fraction of the LME Cu price (64%) | [euro/tonne] |
| Fraction of the LME Al price (50%) | [euro/tonne] |
| Cu mass | [tonne] |
| Al mass | [tonne] |
| Cost of transportation of the metal product to the upgrading plant | [euro/tonne] |
| Processing cost (upgrading cost) | [euro/tonne] |
| Cost for land filling of the minerals after the upgrading | [euro/tonne] |

Table 7: Costs per tonne for ECS metals product. Source: Inashco.

| Costs | €/tonne |
|---|---|
| **Transport of the ECS metal product** | 25 |
| **Upgrading of the ECS metal product** | 70 |
| **Disposal of residual minerals after upgrading** | 25 |
| | |

Table 8: Prices and percentage LME paid, source www.lme.com.

| Prices | €/tonne | | LME price 18-3-2013 |
|---|---|---|---|
| **HNF-metal** | 3894 | 64% of the LME price is paid | $ 7881 |
| **LNF-metal** | 750 | 50% of the LME price is paid | $ 1943 |

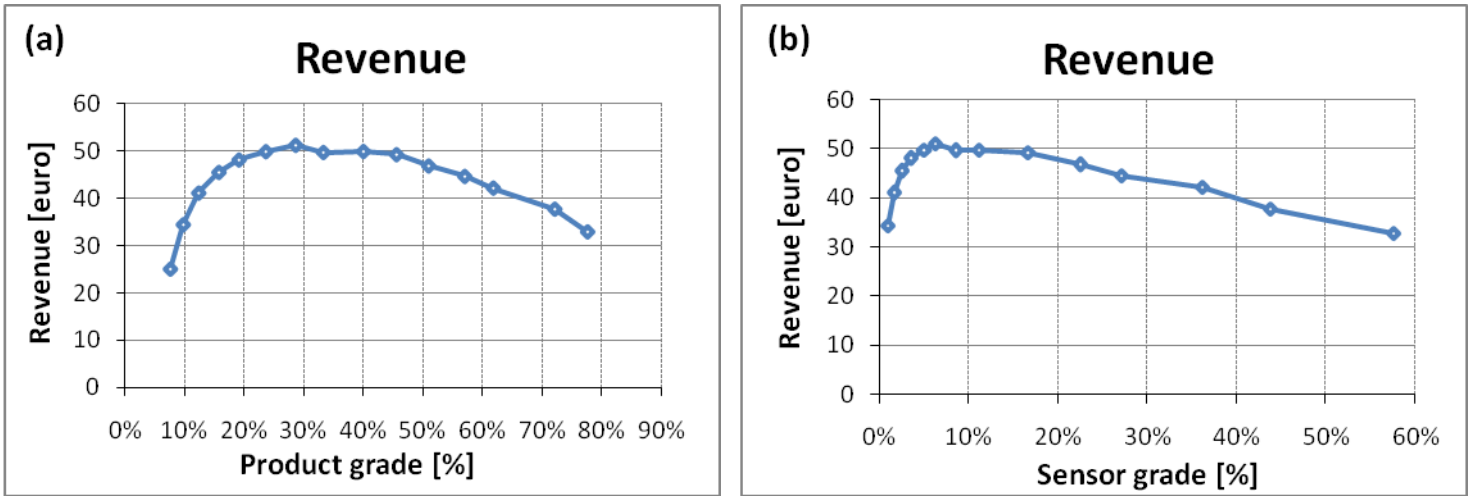


Figure 49: (a) Revenue plotted against ECS metals product grade. (b)Revenue plotted against sensor grade.

Figure 49a shows the revenue against the product grade and Figure 49b the revenue against the sensor grade. The sensor grade was calculated by averaging three slots. This was done to obtain an indicative set point for the grade for if the splitter would have been controlled based on the measured grade. The optimal product grade for the feed containing 14% moisture is around 29 % and for feed with 12% moisture it is 32 %. For feed containing 12% moisture the optimal splitter position is 480 mm and for the feed with 14% moisture 455 mm. This means that a difference of 2% moisture results in a shift of the optimal splitter position of 25 mm. In Figure 50a and 50b the optimal splitter positions are shown. The optimum product grade and splitter position will lead to the criteria (set point) for sensor based control of splitter.

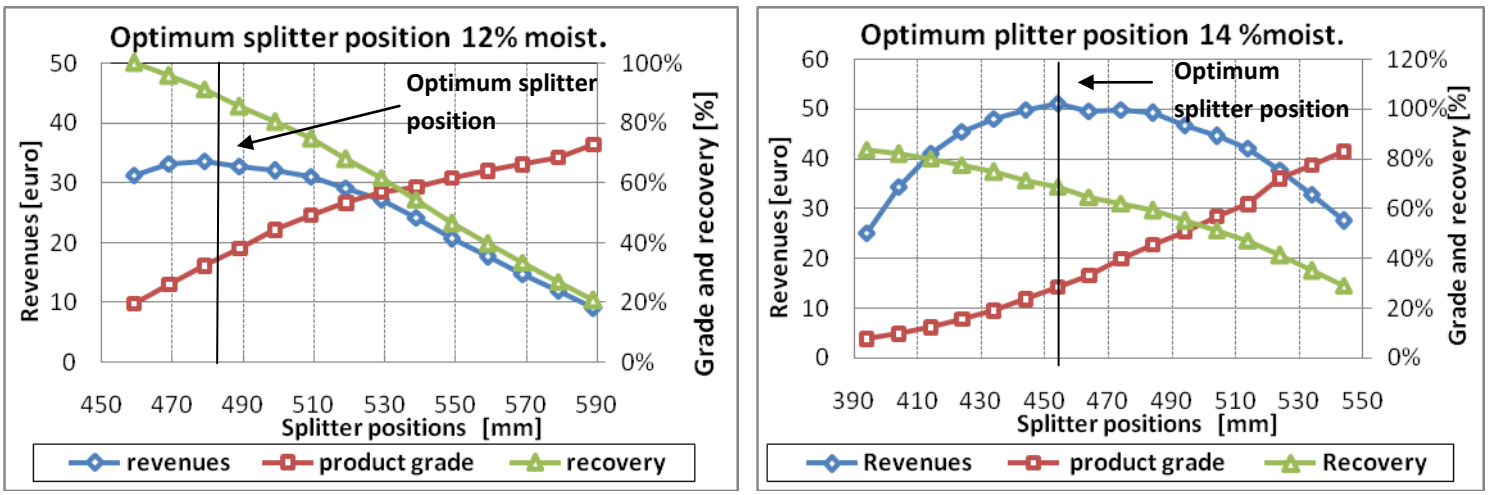


Figure 50: Optimal splitter positions for feed with 12 % moisture (left panel), and 14 % moisture (right panel)

**Set points**

In order to set the splitter at the optimal position by use of the sensor, the set point should be determined first. Possible set points based on grade and the count ratio will be presented in this section. It was found that a product grade of 30 % (optimal product grade) corresponds with a sensor grade of around 6 % and a count ratio z of 0.12, for the feed with 12% and 14% moisture, right on top of the splitter. However in practise set-points can be fine-tuned by an operator once the sensor is in place. The set-points shown in Figure 51 would have resulted in a movement of the splitter to the right or to the left depending on whether the feed material changes from 12% to 14% moisture or the other way around. From 14% to 12%, the splitter would have moved from 455 to 480 mm and from 12% to 14% the other way around. In Figure 51 the sensor grade and z values are shown. The sensor grade was calculated by assuming that the target sampling tube will be about 30 mm in diameter and therefore the sensor grade was calculated by averaging the metal and material masses of three slots.

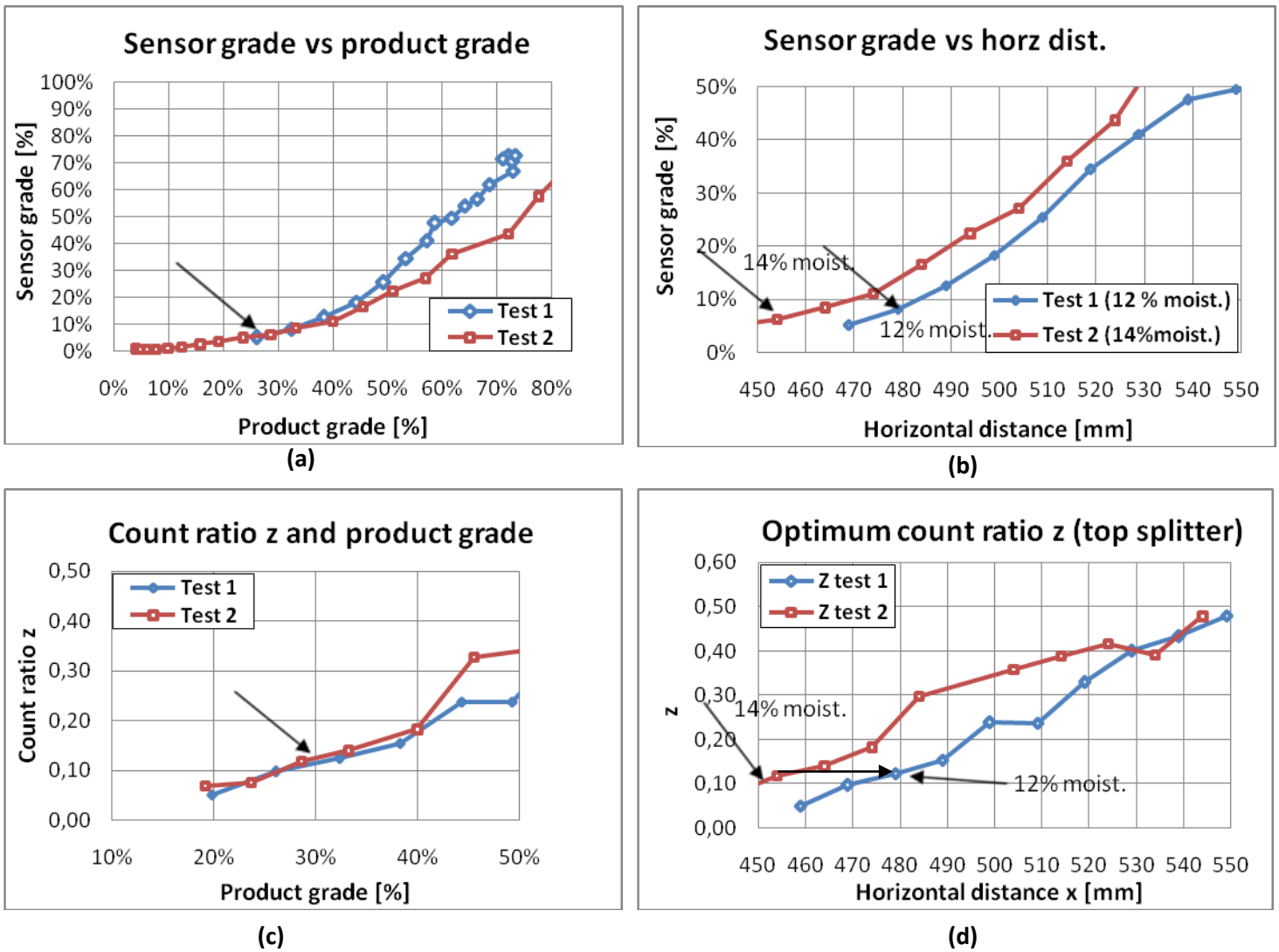


**Figure 51: (a) and (c) Sensor grade and count ratio vs product grade and (b) and (d) Sensor grade and count ratio vs horizontal distance. The set point for sensor grade and z is shown is indicated with an arrow.**

## 6.2 Simulation of fixed an moving splitter

The objective of the simulation was to evaluate how the hybrid sensor should react on feed changes and to evaluate the added value of the hybrid sensor. This chapter will present the results of the simulations. Prior to the results the input parameters will be explained.

**Input**

With the formulas for mass and particle estimation an ECS was simulated at different moisture contents and throughputs in order asses the added value of the sensor and to simulate how the sensor system (controller) should react on the variations the ECS feed. Two scenarios were simulated, one with a fixed splitter position (current situation) and second a splitter that is moving according based on the number of particles through the sensor. In each scenario the throughput and moisture content is varied in time. For the moisture again content two cases were distinguished, feed that is contains 12% moisture for 80% of the time and 14% moisture for 20 % of the time and the other way around. These moisture contents were chosen since the measured moisture content also contained 12 and 14 % moisture.

**Table 9: Input parameters for the model**

| **Input parameters model** | | | |
|---|---|---|---|
| | Integration time τ | 60 | [s] |
| **Starting splitter position** | $x_{ref}$ splitter position | 470 | [mm] |
| **Offset splitter sampling tube** | $dx_1$ (left boundary) | 5 | [mm] |
| | $dx_2$(right boundary) | 35 | [mm] |
| **Diameter sampling tube** | dx | 30 | [mm] |
| | Moisture content (t) | 12-14 | [%] |
| | Throughput G (t) | 9.2-12 | [t/h] |
| | Simulation time | 5 | [h] |
| **For moving splitter** | $z_{SET\ POINT}$ | 0.18 | |

The mineral particles were calculated with Eq. [4.2] and material mass with Eq. (4.3), the metal mass with Eq. [4.10] and the number of metal particles with Eq. [4.11]. With the metal only Al and Cu is meant as there was not enough data on the other NF metal particles. Beside a simulation with a fixed splitter position, a moving splitter was also simulated based on the count ratio z.

If z< 0.18, the splitter should move in steps of 5 mm away from the head pulley and if z > 0.18; x-5 mm, the splitter moves to the left closer to the head pulley. An exception was when if $N^{total}$< 5, the splitter should than remain at the reference position. Furthermore in order to simulate the fluctuations in metal and total particles per second the following formula was used;

$$N^{metal} = Norm.inv(rand, N_{calculated}^{\ metal}, \sqrt{N_{calculated}^{\ metal}})$$
$$N^{total} = Norm.inv(rand, N_{calculated}^{\ total}, \sqrt{N_{calculated}^{\ total}}) \quad [4.13]$$

In which the rand is a random number between 0 and 1, μ the number of particles per second (calculated) and σ the standard deviation for which, according to Gy's theory, the squire root of the number of particles was taken. In Figure 52 the results of the simulations are shown for the dry and

wet case without and with moving splitter based on the simulated sensor measurements. The average splitter position and movement is shown in Figure 52e and Figure 52f.

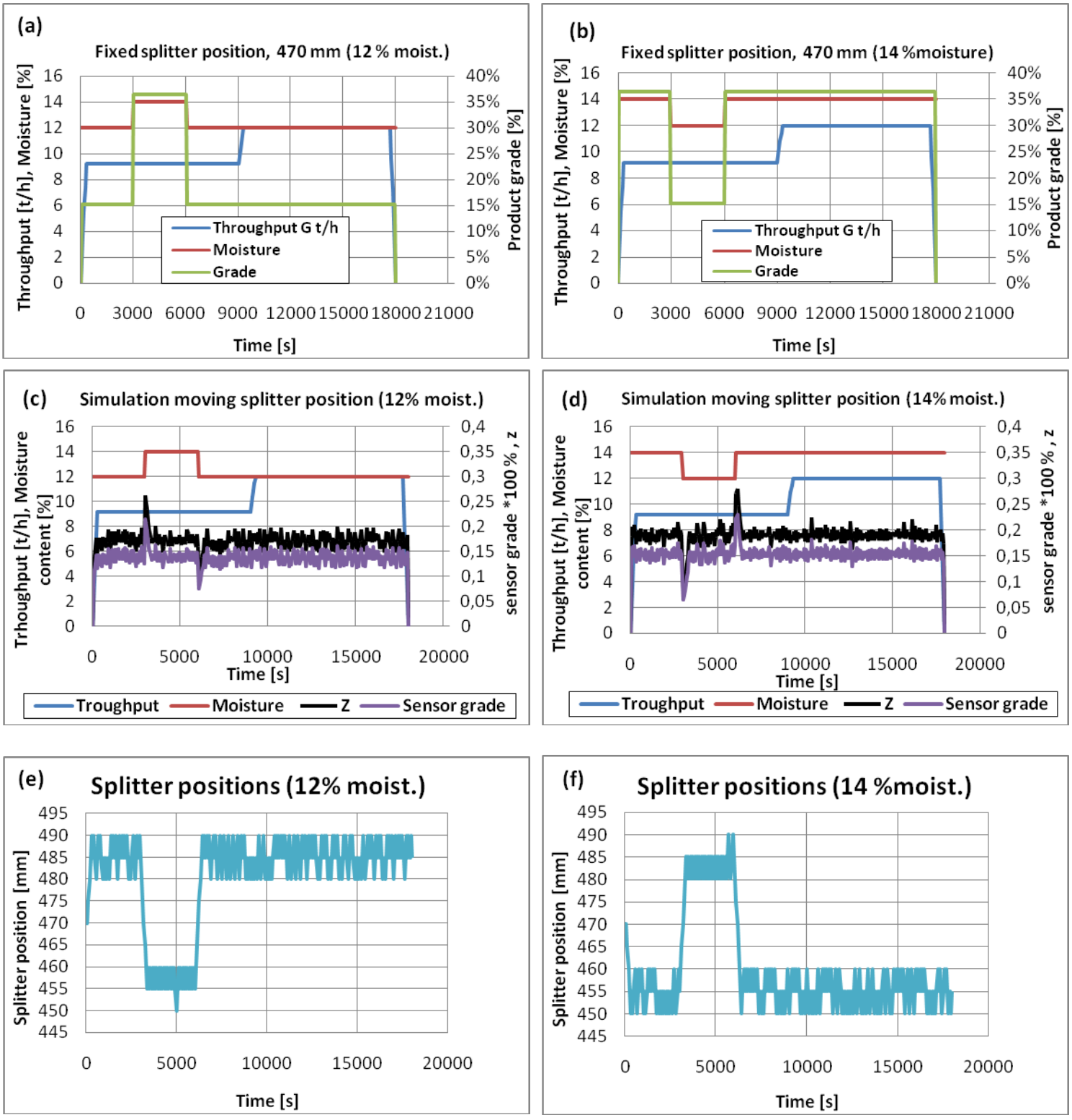


**Figure 52: (a) Fixed splitter position for feed with 12% moist., 80% of the time. (b) Fixed splitter position for feed with 14% moist., 80% of the time (c) and (d) moving splitter position, (e) and (f) movement of the splitter.**

**Results**

The average splitter position for the dry case was on average 485 mm and 455 mm for the wet case. It was found that moving the splitter by the count ratio z as criteria, resulted in an extra profit of four euro per ton ECS feed in the case with feed containing 14% moisture in comparison with same feed and a fixed splitter position. In the case where the feed contained 12% moisture the added value of the sensor is one euro per ton ECS feed. In case of the lower moisture content, the product grade is lower due to the longer particle trajectories of the mineral particles. Notice also that due to this affect the mass recovery is higher resulting in lower product grades. Moreover a higher metal recovery does not necessarily have to result in a higher profit. The idea behind the simulation was not to recover more metal, but to adjust the splitter in way that the maximal economic value of the ECS metal product could be achieved. Adjustment of the splitter is a balance between metal recovery and grade of the metal product. In Table 10 the grade and mass recoveries of are shown. Controlling the splitter based on sensor grade at two different k-values was also simulated. A difference of 0.4 in k-value results in deviation of 10 mm in splitter distance causing a small variation in the revenues. Table 11 shows the different cases that were simulated.

**Table 10: Fixed and moving splitter position.**

| Report | Fixed splitter (470mm) | | Moving splitter (z=0.18) | |
|---|---|---|---|---|
| | 12% moist. | 14% moist. | 12% moist. | 14% moist. |
| Time [hour] | 5.00 | 5.00 | 5.00 | 5.00 |
| Ton through ECS [ton] | 52.00 | 52.00 | 52.00 | 52.00 |
| Mass recovered [ton] | 5.53 | 3.16 | 4.29 | 3.84 |
| Mass recovered [%] | 11 | 6 | 8.0 | 7.4 |
| Grade [%] | 16 | 28 | 19.5 | 24.3 |
| Metal yield [ton] | 0.90 | 0.89 | 0.84 | 0.94 |
| Cu total [ton] | 0.29 | 0.27 | 0.28 | 0.28 |
| Al total [ton] | 0.61 | 0.61 | 0.56 | 0.65 |
| Profit [euro/ton] | **33.04** | **34.25** | **33.39** | **38.39** |

**Table 11: Simulation results for feed containing 12% and 14 % moisture for fixed and moving splitter positions.**

| Profit different cases | | | | | |
|---|---|---|---|---|---|
| | Fixed | Moving z=0.18 | Moving on sensor grade; 11% & k=1.3 | Moving on sensor grade; 11% & k=1.7 | Optimum splitter position |
| Dry case [euro/ton ] | 33.04 | 33.39 | 33.14 | 33.40 | 33.46 |
| Wet case [euro/ton] | 34.25 | 38.39 | 38.02 | 38.33 | 38.41 |

# 7 CONCLUSIONS

Application of the hybrid sensor unit in-situ, for real-time control of the splitter distance in order to maximize the value of the ECS metal was investigated.
Particle trajectories were experimentally determined and ECS and sensor measurements were modelled with the results from these in-situ experiments. The following conclusions can be drawn from this graduation work:

1. The ECS particle trajectory tests in the lab showed that the material was distributed according to a normal distribution with a mean of 465 mm (measured from the centre of the rotor to the middle of slot 15) and a variance of 40 mm. An increase in the metal particle trajectories was observed with increasing particle size for the same metal type. Moreover, it was found that Al particles had the shortest trajectories and Pb the longest while Cu and Zn trajectories were in between.
2. From the in-situ tests it was found that the material mass is distributed according to a power law function that increases in the direction of the head pulley.
3. For the mineral particles in the main mineral stream a difference of 1% in moisture content in the feed resulted in a trajectory shift of 15 mm. An increase in moisture content will cause a shift in the direction of the head pulley while a decrease in moisture of the feed material will result in a shift of the main mineral stream away from the head pulley.
4. In-situ ECS particle trajectories tests showed that the trajectories of metal particles become longer with increasing particle size, where Cu has longer trajectories than Al particles due to the higher conductivity.
5. The metal distribution can be subdivided into two populations, one population travels with the main material stream (jet stream) and the second population is clearly affected by the ECS, which we denote as ‘free metal’. The fraction of the metal particles that were dragged into the main material stream is dependent on particle size, moisture content and the type of NF metal. Increasing moisture content and a decreasing particle size resulted in an increase of the fraction of particles that were dragged in the main stream.
6. The sensor and product grade have a monotonic increasing trend with increasing distance from the head pulley. The sensor tests conducted in the lab showed that the count ratio z of metal and total number of particles increases with distance from the head pulley for both the dry case (12% moisture) and the wet case (14% moisture). Between the dry and wet case the same z can be found after a splitter shift of 25 mm.
7. The optimal economic value for the metal product is found at 29-32% metal product grade. This product grade was related to a sensor grade of 6 % for feed containing 12% and 14% moisture. The count ratio was z=0.12 and k = 1.3 for the feed with 12% moisture and k=1.7 for the feed with 14% moisture The optimum splitter position for the feed with 12% moisture was 480 mm and for the feed with 14% moisture it was 455 mm. Due to the 2% change in moisture content a splitter adjustment of 25 mm was required to regain the optimal product grade and thus the optimum economic value of the metal product.

8. Simulation of a fixed and a sensor-moved splitter, while using roughly estimated material market values and costs, showed that the value added by the sensor was about four euro per tonne ECS feed in the cased with feed containing 14% moisture and one euro in the case of 12% moisture, if the splitter was adjusted based on the count ratio z. For an ECS processing 36000 ton annually, the added value of the sensor is minimal 36000 euro. Adjustment of the splitter based on the count ratio showed that the optimal economic value can be achieved.

# 8 RECOMMENDATIONS FOR SENSOR INSTALLATION

## 8.1 Sensor installation

The sensor system should be placed in the falling particle stream of the ECS right behind the splitter, indicated with the arrow in Figure 53. Due to the inclination of the splitter, an offset between the splitter plate edge and the sensor tube will be present. The maximum allowable offset between the splitter and edge of the sampling tube is 5 mm. For a tube of 30 mm in diameter the offset between the splitter edge and centre of the tube is 20 mm.

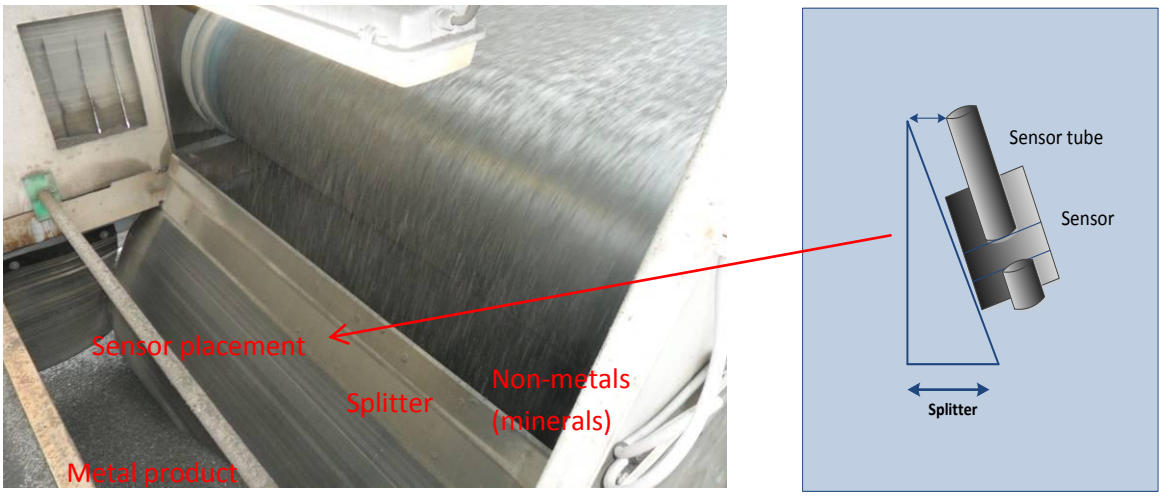


**Figure 53: (a) Splitter, height difference splitter edge and top belt 600 mm. (b) Sampling tube and proposed sensor setup. Offset splitter and sampling tube edge 5 mm. and 20 mm till the centre of the tube.**

## 8.2 Integration time

For a sampling tube of 30 mm in diameter an integration time of 60 s is recommend, resulting in 240 metal particles and a sampling error of 6.5%. Keeping the option to change the integration time is recommend if during testing to anticipate changes in bottom ash feed rate or composition.

## 8.3 Controlling aspects

The sensor system (controller) should continuously set the splitter at its economical optimal position. If the optimal position moves to the left, closer to the head pulley as a result of increase in moisture

content the splitter should also move to the left and vice versa. The control loop of the splitter movement is shown in Figure 54.

**Control over motion of the splitter**

- The ideal set point for a 30 mm diameter sampling tube right above the splitter would be z= 0.12 = $N^{EMS}$/ $N^{IRS}$. However, the tube is positioned with an extra offset of 5 mm as shown in Figure 53. Therefore, the practical set point is z=0.18, which occurs at the centre of the tube. 20 mm removed from the splitter in the metal product.

- If $z < z_{SET}$ the splitter moves away from the head pulley and if $z > z_{SET}$ it moves closer to the head pulley. The normal velocity is 1 mm/s and the duration of the motion is 2 seconds; then starts a new integration cycle.

- $|z - z_{SET}| > 0.06$ : the velocity is 1 mm/s and the duration of the motion is 10 seconds; then starts a new integration cycle.

The criterion for the control on slot grade should be G = 14 % if the offset between the edge sampling tube and splitter is 5 mm (20 mm from splitter to the centre of a 30 mm tube). The recommended k-value is 1.7 for wet feed (14% moisture) and 1.3 for feed (12% moisture).

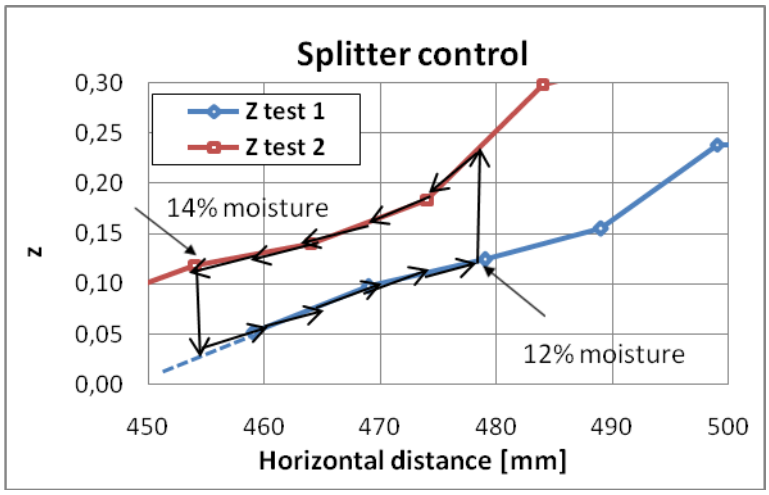


**Figure 54: The control loop when steering on the count ratio set point $Z_{SET}$ = 0.12 (indicated by arrows) and moving the splitter between the optimum positions for wetter (14% moisture) and dryer feed (12% moisture).**

## 8.4 Exceptions

- **Start-up or hardware reset**
  During the starting-up of the ECS the falling particle stream is irregular during a few minutes. The splitter should for example take its reference position during the start-up and move from this position towards the optimum position.
- **No sensor feed (low counts): IR counts < 5 particles/s (no feed or tube jamming)**
  The sensor should stay at its current position. If the belt feed is active the operator should unblock /clean the sensor tube. If the belt feed is not active then sensor waits for further activity.
- **Out of range: 420mm and 540 mm**
  If the sensor wants to move outside this range it should remain at the extreme position and possible give a signal that it is out of range (also visible from position data). This might occur during extreme wet conditions or abnormal feed.

## 8.5 Alternative placement of the sensor

Another possibility is to place the sensor in the falling stream of the metal product conveyor, where the metal product is discharged in the product container shown in Figure 55. The advantage of this option is that it allows for direct measurement of the product grade. The control of the splitter can be done directly based on the product quality (grade). A disadvantage is that the measurement is less sensitive to the changes in grade (noise limitation) and thus to changes in splitter position.


Figure 55: Discharge of the ECS metal product in the metal product container.

# 9 LIST OF ABBREVIATIONS AND NOMENCLATURE

| | |
|---|---|
| BA | Bottom ash |
| ECS | Eddy current separator |
| EMS | Electromagnetic sensor |
| HNF | Heavy Non-ferrous |
| IRS | Infrared sensor |
| LNF | Light Non-ferrous |
| MSWI | Municipal solid waste incinerator |
| MSW | Municipal solid waste |
| NF | Non-ferrous metals |
| PSD | Particle size distribution |

| | | |
|---|---|---|
| $B^a$ | amplitude of the magnetic flux density | [T] |
| $C^{IRS}$ | correction factor IRS | |
| $C^{EMS}$ | correction factor EMS | |
| k | number of magnetic pole pairs | |
| k-value | ratio of the average mineral and metal particle mass | |
| R | radius of the particle | [m] |
| s | shape and orientation factor | |
| T | throughput eddy current separator | [t/h] |
| V | particle volume | [$m^3$] |
| w | width of a pole pair | [m] |
| z | count ratio of metal and total particles | |
| $\omega_{drum}$ | angular velocity of the magnetic drum/rotor | [rad/s] |
| Ω | rolling of the particle | [rad/s] |
| σ | electrical conductivity | [S] |
| ρ | mass density | [kg/$m^3$] |
| $\mu_0$ | magnetic permeability of vacuum | [H/m] |

# 10 REFERENCES

Berkhout, S. P. M., Oudenhoven B. P. M., Rem, P., 2011. Optimising non-ferrous metal value from MSWI bottom ashes, Journal *of Environmental Protection*, no.2, pp. 564-570.

Bird, R.B., Stewart, W.E. and Lightfoot, E.N., 2001(Second edition), *Transport Phenomena*. John Wiley & Sons.

CBS, PBL, Wageningen UR, 2012. *Afvalproductie en wijze van verwerking, 1985-2010*. [Online] (indicator 0204, version 10, 10 September 2012)
Available at:http://www.compendiumvoordeleefomgeving.nl/indicatoren/nl0204-Afvalproductie-en-wijze-van-verwerking.html?i=1-4> [Accessed 26 October 2012]

European Commission, Joint Research Centre, 2006*. Reference Document on the Best Available Techniques for Waste Incineration*. [Online] Seville: European Commission, Joint Research Centre. Available at: <http://eippcb.jrc.ec.europa.eu/reference/wi.html> [Accessed 23 October 2012].

Inashco, 2013. *About*. [online] Available at: <http://www.inashco.com/en/about> [Accessed 13 May 2013].

Maraspin, F., Bevilacqua, P., Rem, P., 2004. Modelling the throw of metals and non-metals in eddy current separations*. International Journal of Mineral Processing*, Vol. 73(1), pp. 1–11.

Muchova, L., 2010. *Wet physical separation of MSWI bottom ash*, Ph.D. Delft University of Technology.

Rahman A.M.D. and Bakker, M.C.M., 2012. Hybrid sensor for metal grade measurement of a falling stream of solid waste particles, *Waste Management,*Vol. 32, pp. 1316-1323.

Rahman A.M.D. and Bakker, M.C.M., (in press). Sensor-based control in eddy current separation of incinerator bottom ash, *Waste Management.* (Accepted for publication March 2013).

Rem, P. 1999, *Eddy Current Separation*, Delft: Eburon.

Pretz, Th., 2012, Processing of WEEE, Practical test EMEC 2011-2012. Department of Processing and Recycling, RWTH Aachen University.

Settimo, F., Bevilacqua, P., Rem, P., 2004. Eddy current separation of fine non-ferrous particles from bulk streams. *Physical Separation in Science and Engineering*, Vol. 13(1), pp. 15–23.

Vereniging afvalbedrijven, 2012. *AVI-bodemas*. [Online] Available at: <http://www.avi-bodemas.nl/> [Accessed 26 October 2012]

Zhang, S., Rem. P, Forssberg, E., 1998.The investigation of separability of particles smaller than 5 mm by eddy current separation technology, part 1: rotating type eddy current separators. *Magnetic and Electrical Separation*, Vol. 9, pp. 233-251.

Zhang, S., Rem. P, Forssberg, E., 1999. Particle trajectory simulation of two-drum eddy current separators. *Resources, Conservation and Recycling*, Vol.26, pp. 71–90.

Zhang, S., Rem. P, Forssberg, E., Jong, T., 2000. The investigation of separability of particles smaller than 5 mm by eddy current separation technology, part 2: novel design concepts, *Magnetic and Electrical Separation*, Vol. 10, pp. 85-105.

Steinert, 2012. *Steinert NES (Eddy Current Separator).* [Online] Available at: <http://www.steinert.de/home/products/steinert-nes-eddy-current-separator> [Accessed 25 November 2012].

**Personal communication**

Rahman, A., 2012. Ph.D student. Development of hybrid sensor. [conversation October 2012].

# 11 APPENDICES

## Appendix A: Eddy current forces

In this appendix a more detailed version of the eddy currents forces is shown based on (Rem,1999). Moreover in Table 12 the ratio of the electrical conductivities and mass densities of Al, Cu, Pb and Zn is shown.

In the figure below the forces acting on a NF metal particle is shown for a concentric system.

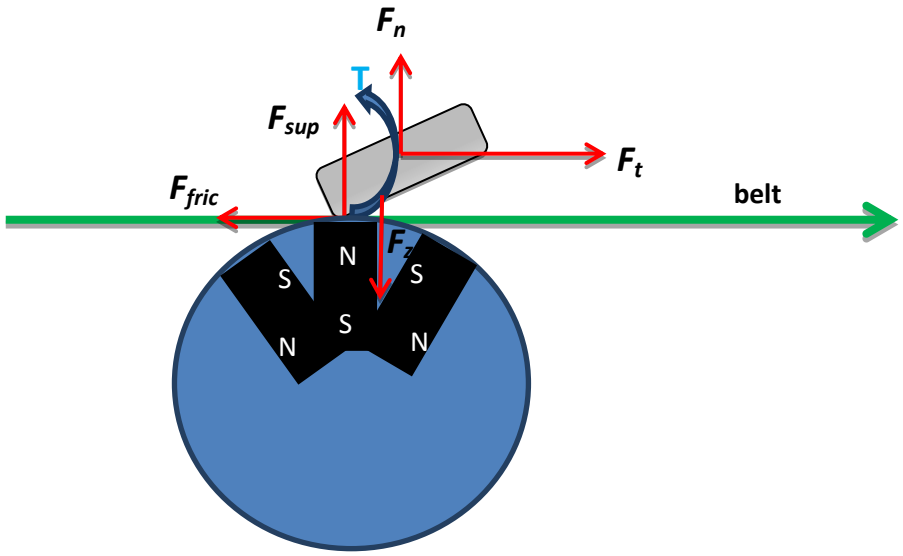


| | | |
|---|---|---|
| $F_n$ or $F_r$ | : Normal force (radial force) | [N] |
| $F_z$ | : Gravity force | [N] |
| $F_t$ | : Tangential force | [N] |
| $F_{sup}$ | : Support force | [N] |
| $F_{fric}$ | : Frictional force | [N] |
| T | : Torque | [Nm] |

The radial force $F_r$ also called the normal force lifts the particle upwards and increases with the particle size. The force that accelerates the NF metal particles forward is the tangential eddy current force $F_t$. Another force that is acting on a conductive particle is the electromagnetic torque T. The torque causes the conducting particles to spin and increases with particle size (see Figure 7b). The eddy current forces acting on a metal particle can be expressed as:

$$F_r = M_{||}\frac{2\pi sB^a}{w} = \frac{2\pi s(B^a)^2 V}{\mu_0 w}\frac{(k\omega_{rotor}-\Omega)^2\tau^2}{1+(k\omega_{rotor}-\Omega)^2\tau^2}$$

K factor

$$F_t = M_{\perp}\frac{2\pi sB^a}{w} = \frac{2\pi s(B^a)^2 V}{\mu_0 w}\frac{(k\omega_{rotor}-\Omega)\tau}{1+(k\omega_{rotor}-\Omega)^2\tau^2}$$

$$T = M_{\perp}\times B^a = \frac{s(B^a)^2 V}{\mu_0}\frac{(k\omega_{rotor}-\Omega)\tau^2}{1+(k\omega_{rotor}-\Omega)^2\tau^2}$$

$$\tau = s\mu_0\sigma R$$

| | | |
|---|---|---|
| M | : magnetic moment | [A m$^2$] *(derivation in Rem, 1999)* |
| s | : shape and orientation factor | |
| $B^a$ | : amplitude of the magnetic flux density | [T] |
| V | : volume of the particle | [m$^3$] |
| w | : width of a pole pair | [m] |
| $\mu_0$ | : magnetic permeability of vacuum | [H/m] |
| k | : number of magnetic pole pairs | |
| $\omega_{drum}$ | : angular velocity of the of the rotor | [rad/s] |
| Ω | : rolling of the particle | [rad/s] |
| R | : radius of the particle | [m] |
| σ | : electrical conductivity | [S] |
| ρ | : mass density of the particle | [kg/m$^3$] |

The derivation of the forces is beyond the scope of this work however interested readers may want to read the book on eddy current separation by *(Rem, 1999).*
For particles < 5 mm which is the case in this work, the contribution of $F_r$ on the particle trajectory is so small that it can be neglected *(Zhang et al., 1998).* The relevant eddy forces for small particles are the tangential forces and the electromagnetic torque.

**Table 12: The electrical conductivity and mass density for pure metals**

| Metal | Density (ρ) [kg/m$^3$] | Conductivity (σ) [S] | σ/ρ |
|---|---|---|---|
| **Aluminium** | 2700 | 36000000 | 13333 |
| **Copper** | 8900 | 59000000 | 6629 |
| **Lead** | 11400 | 5000000 | 439 |
| **Zinc** | 7100 | 16000000 | 2254 |

## Appendix B: The parameters alpha, mean, sigma and free for the metal particle distribution.

| Test 1 | Alpha | Mean [mm] | Sigma [mm] | Free | Total particles |
|---|---|---|---|---|---|
| **Cu 1-2 mm** | 1.110 | 511 | 44.41 | 0.89 | 417 |
| **Cu 2-4 mm** | 1.068 | 537 | 49.85 | 0.95 | 651 |
| **Cu 4-5.6 mm** | 1.295 | 579 | 62.14 | 1 | 76 |
| **Al 1-2 mm** | 1.04 | 500 | 41.06 | 0.6 | 438 |
| **Al 2-4 mm** | 1.203 | 515 | 58.63 | 0.83 | 1959 |
| **Al 4-5.6 mm** | 1.355 | 543 | 82.03 | 1 | 383 |

| Test 2 | Alpha | Mean [mm] | Sigma [mm] | Free |
|---|---|---|---|---|
| **Cu 1-2 mm** | 1.03 | 481 | 48.37 | 0.49 |
| **Cu 2-4 mm** | 1.11 | 516 | 50 | 0.83 |
| **Al 1-2 mm** | 1.01 | 449 | 38.7 | 0.22 |
| **Al 2-4 mm** | 1.1 | 495 | 61 | 0.63 |

## Appendix C: Principle IR and EM sensor

In this section the individual sensors that are mounted in the hybrid sensor will be explained.

**Principle of the infrared sensor (IRS)**

The principle of the IRS is based on the detection of the shadow that a particle produces in a light fan beam. The IRS counts all the particles irrespective of the material type. Figure 57 shows the layout of the IRS. The IRS is capable of detecting particles bigger than 2 mm. Particles smaller than 2 mm are not detected due to the arrangement of the spacing between the diodes. However, if particles are shiny enough, e.g. glass or metal, the light scatters to some degree which increases the chance of detection. The electronics of the sensor is arranged in way that signal interpretation is simple and when particles fall together, which is the case in BA application, a single count would be produced. The higher the feed rate, the more particles will be undetected or detected as one single particle which in reality is not the case. So at higher feed rates a count error occurs. The vertical dimension of the diode and the feeding method are also of importance for the count error. The limitation of the sensor at higher feed rates was solved by applying a count correction factor which was determined by calibration with artificial samples and BA *(Rahman and Bakker, 2012)*

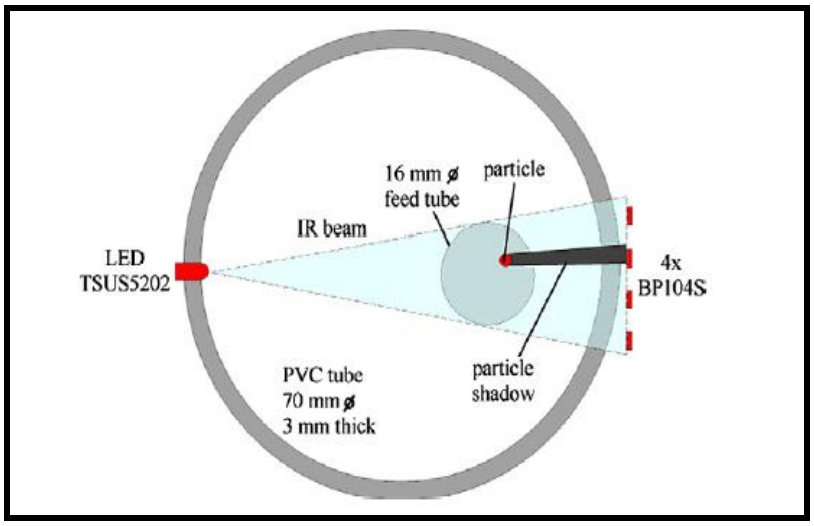


Figure 56: Layout Infrared sensor *(Rahman and Bakker, 2012)*

**Principle of the electromagnetic sensor (EMS)**

The principle of the EMS is based on a balanced, tuned transformer circuit in which the falling metal particles cause a disturbance resulting in amplitude modulated signals. In simple terms, a metal particle causes a disturbance in the applied field resulting in a signal that is amplified and further processed. The EMS consists of three coils, two bias coils (L1, L2) and a detection coil Ld. In Figure 58 the layout of the EMS including the data processing steps is given. An alternating bias current is supplied to the bias coils that produce two opposing magnetic fields B1 and B2. If conductive non-magnetic particle falls between the two coils it produces an induction current which out-of phase magnetic response causes an unbalance detected by the detection coil. If however a ferromagnetic falls through the coils it produces a strengthening of the magnetic flux and is in-phase with the applied field. The detected signal of a ferromagnetic particle and non-magnetic particle are different in term of phases and therefore can be distinguished. With the help of signal processing and computer software the metal particles count are obtained. EMS was specially designed for the detection of small particles with low conductivities and to cope with noise and interference since these conditions are typically found in the ECS bottom ash application. At high feed rates not all the metal particles are detected. The EMS is capable of detecting metal particles > 1 mm with the current settings. Detecting particles < 1 mm was considered as unimportant for the purpose of the sensor *(Rahman and Bakker, 2012)*

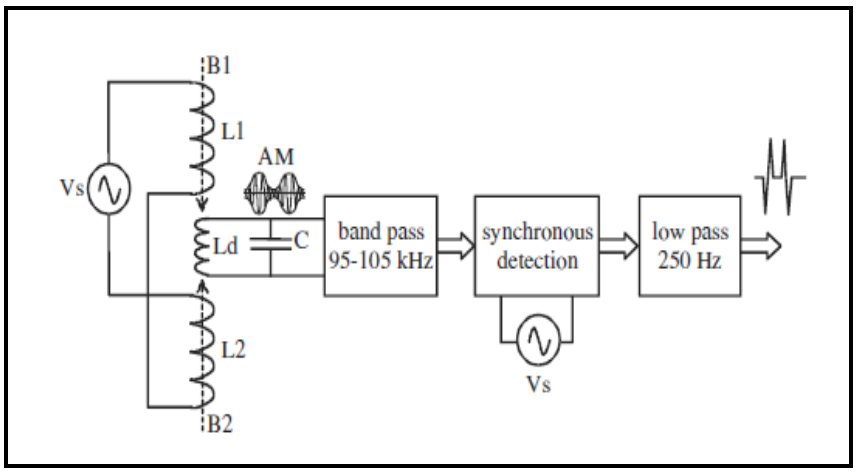


Figure 57: Layout EMS and data processing units for signal processing *(Rahman and Bakker, 2012).*

**Calibration curves for correction factors of the sensors**

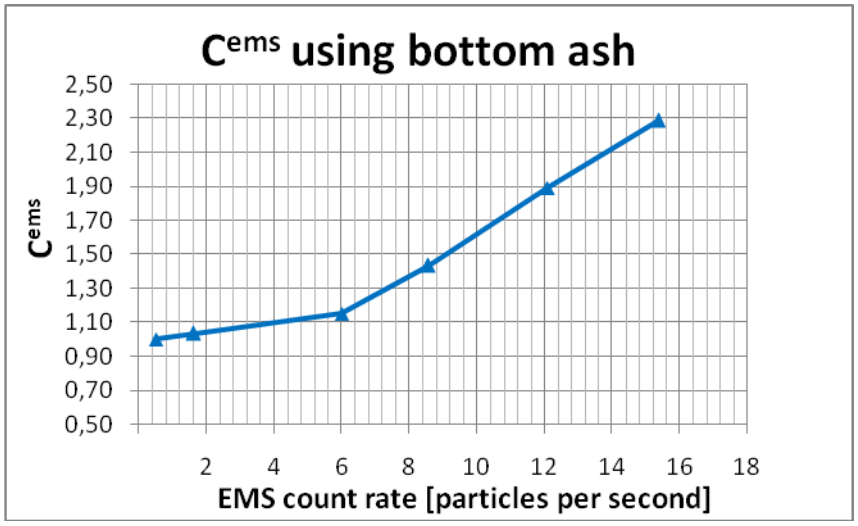

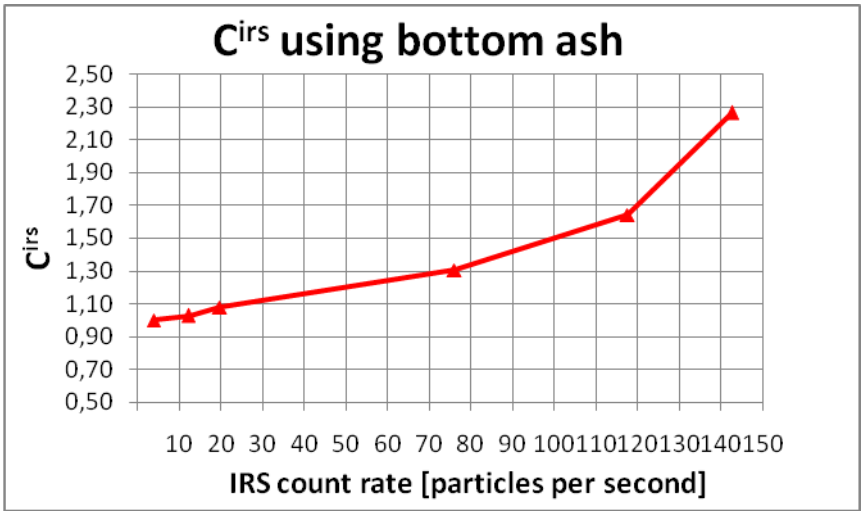


**Figure 58: Top: Calibration curve for the EMS determined in the lab by Rahman. Bottom: Calibration curve for the IRS. Source: *(Rahman and Bakker, 2012)***

## Appendix D: Sensor count data

| Test 1 | | | | | | | | | | |
|---|---|---|---|---|---|---|---|---|---|---|
| **Slot no** | **Horizontal distance** | **Mineral mass** | **Metal mass** | **Average mineral particle mass** | **Average metal particle mass** | **k-value** | **Total mineral particles** | **Total metal particles** | **z** | **Grade by k-value** |
| | **[mm]** | **[g]** | **[g]** | **[g]** | **[g]** | | | | | **[wt%]** |
| 1 | 459 | 263.55 | 8.17 | 0.05 | 0.03 | 1.75 | **5692** | 309 | 0.64 | 3.0 |
| 2 | 46 | 159.70 | 9.20 | 0.06 | 0.03 | 1.87 | **2783** | 300 | 0.65 | 5.4 |
| 3 | 479 | 103.35 | 11.05 | 0.05 | 0.04 | 1.32 | **1892** | 268 | 0.57 | 9.7 |
| 4 | 489 | 72.42 | 9.98 | 0.05 | 0.09 | 1.33 | **1400** | 256 | 0.57 | 12.1 |
| 5 | 499 | 47.34 | 11.24 | 0.05 | 0.03 | 1.32 | **1028** | 322 | 0.57 | 19.2 |
| 6 | 509 | 34.10 | 13.15 | 0.03 | 0.04 | 0.81 | **978** | 306 | 0.45 | 27.8 |
| 7 | 519 | 25.92 | 12.48 | 0.04 | 0.04 | 1.02 | **652** | 321 | 0.51 | 32.5 |
| 8 | 529 | 15.88 | 14.32 | 0.04 | 0.05 | 0.74 | **434** | 290 | 0.43 | 47.4 |
| 9 | 539 | 18.57 | 15.53 | 0.05 | 0.05 | 0.91 | **395** | 302 | 0.48 | 45.5 |
| 10 | 549 | 12..91 | 13.14 | 0.05 | 0.05 | 0.91 | **280** | 259 | 0.48 | 50.4 |

| Test 2 | | | | | | | | | | |
|---|---|---|---|---|---|---|---|---|---|---|
| **Slot no** | **Horizontal distance** | **Mineral mass** | **Metal mass** | **Average mineral particle mass** | **Average metal particle mass** | **k-value** | **Total mineral particles** | **Total metal particles** | **z** | **Grade by k-value** |
| | **[mm]** | **[g]** | **[g]** | **[g]** | **[g]** | | | | | **[wt%]** |
| 9 | 434 | 41.44 | 1.61 | 0.04 | 0.02 | 1.93 | **1202** | 90 | 0.07 | 3.74 |
| 10 | 444 | 28.77 | 1.27 | 0.05 | 0.02 | 1.87 | **824** | 68 | 0.08 | 4.23 |
| 11 | 454 | 20.14 | 1.92 | 0.04 | 0.03 | 1.41 | **507** | 68 | 0.12 | 8.70 |
| 12 | 464 | 17.78 | 1.24 | 0.04 | 0.02 | 2.35 | **454** | 74 | 0.14 | 6.50 |
| 13 | 474 | 10.88 | 1.40 | 0.05 | 0.02 | 1.74 | **326** | 73 | 0.18 | 11.39 |
| 14 | 484 | 8.68 | 2.05 | 0.05 | 0.03 | 2.07 | **188** | 92 | 0.33 | 19.12 |
| 15 | 494 | - | - | 0.04 | 0.02 | - | **-** | - | - | - |
| 16 | 504 | 4.61 | 1.96 | 0.05 | 0.03 | 1.31 | **161** | 90 | 0.36 | 29.88 |
| 17 | 514 | 6.44 | 2.89 | 0.02 | 0.04 | 1.41 | **142** | 90 | 0.39 | 31.01 |
| 18 | 524 | 2.84 | 3.00 | 0.04 | 0.06 | 0.58 | **125** | 76 | 0.38 | 51.37 |
| 19 | 534 | 2.05 | 2.92 | 0.05 | 0.10 | 0.49 | **98** | 68 | 0.41 | 58.75 |
| 20 | 544 | 1.65 | 2.95 | 0.04 | 0.02 | 0.63 | **49** | 55 | 0.53 | 64.13 |

**Appendix E:** Excel file with raw data from the laboratory and in-situ tests